

**DIRECTED EVOLUTION OF PHOSPHOTRIESTERASE:  
TOWARDS THE EFFICIENT DETOXIFICATION OF SARIN AND SOMAN**

A Dissertation

by

KARIN T. LUM

Submitted to the Office of Graduate Studies of  
Texas A&M University  
in partial fulfillment of the requirements for the degree of

DOCTOR OF PHILOSOPHY

May 2004

Major Subject: Toxicology

© 2004

KARIN T. LUM

ALL RIGHTS RESERVED

**DIRECTED EVOLUTION OF PHOSPHOTRIESTERASE:  
TOWARDS THE EFFICIENT DETOXIFICATION OF SARIN AND SOMAN**

A Dissertation

by

KARIN T. LUM

Submitted to Texas A&M University  
in partial fulfillment of the requirements  
for the degree of

DOCTOR OF PHILOSOPHY

Approved as to style and content by:

---

Frank M. Raushel  
(Chair of Committee)

---

Stephen H. Safe  
(Member)

---

Timothy D. Phillips  
(Member)

---

James R. Wild  
(Member)

---

Timothy D. Phillips  
(Chair of Toxicology Faculty)

---

Emile A. Schweikert  
(Head of Department)

May 2004

Major Subject: Toxicology

## ABSTRACT

Directed Evolution of Phosphotriesterase:

Towards the Efficient Detoxification of Sarin and Soman. (May 2004)

Karin T. Lum, A.B., Smith College

Chair of Advisory Committee: Dr. Frank M. Raushel

Directed evolution studies were done with PTE for the enhancement of hydrolysis of both sarin and soman analogs. Particular attention was focused on the toxic  $S_pR_c$  and  $S_pS_c$  isomers of the soman analog, and the  $S_p$  isomer of the sarin analog. Double substitution libraries yielded several mutants that had enhanced activity for the substrates. Among them was the double mutant, H257Y-L303T, which displayed a 462-fold increase in activity for hydrolysis of the most toxic  $S_pS_c$  isomer of the GD analog in comparison to the wild type. Several other mutants such as the triple mutants H254R-H257A-L303T and H254R-H257S-L303T had enhancements of between 150- and 200-fold, and had also displayed a different order of stereoselectivity relative to the wild type. For these mutants, the order of preferential hydrolysis was such that the  $S_pR_c$  isomer was preferentially hydrolyzed first. In contrast, the order of preferential hydrolysis for the wild type was that the  $R_pR_c$  was hydrolyzed first, followed by the  $R_pS_c$ ,  $S_pR_c$ , and then the  $S_pS_c$  isomer.

The reversal of stereoselective preference was also seen with the double substitution library members for hydrolysis of the sarin analog isomers. However, there were no significant improvements for sarin analog hydrolysis in these libraries. Among the best mutants obtained were H254G-H257W, H254G-H257R, and H257Y, all of which had catalytic efficiencies on the order of  $10^6 \text{ M}^{-1} \text{ s}^{-1}$  for hydrolysis of the  $S_p$  isomer.

The toxicity for analogs of sarin, soman, and VX was evaluated using *Hydra attenuata* as a model organism. The toxicity of each compound was assessed quantitatively by measuring the minimal effective concentration within 92 h in *H. attenuata*. There was a positive correlation between the molecular hydrophobicity of the compound and its ability to cause toxicity. Results from this study indicate the potential for application of this assay in the field of organophosphate nerve agent detection, as well as for the prediction of toxicity of structurally similar organophosphate compounds. The minimal effective concentration for two of the VX analogs was 2 orders of magnitude more toxic than the analog for soman and four orders of magnitude more toxic than the analog for sarin.

## **ACKNOWLEDGEMENTS**

I would like to express my sincere appreciation and gratitude to all of my mentors, past and present, as well as to my family and friends.

## TABLE OF CONTENTS

	Page
ABSTRACT.....	iii
ACKNOWLEDGEMENTS.....	v
TABLE OF CONTENTS .....	vi
LIST OF TABLES .....	viii
LIST OF FIGURES.....	ix
 CHAPTER	
I INTRODUCTION.....	1
Background.....	1
II STEREOSELECTIVE DETOXIFICATION OF SARIN AND SOMAN ANALOGS .....	28
Introduction.....	28
Materials and Methods .....	32
Results .....	35
Discussion.....	52
III EVOLUTION OF PTE TOWARDS EFFICIENT SOMAN HYDROLYSIS .....	57
Introduction.....	57
Materials and Methods .....	59
Results .....	67
Discussion.....	98
IV DIRECTED EVOLUTION STUDIES AND STEREOSPECIFICITY INVESTIGATIONS ON SARIN HYDROLYSIS .....	106
Introduction.....	106
Materials and Methods .....	108
Results .....	112
Discussion.....	141

CHAPTER	Page
V	ORGANOPHOSPHATE NERVE AGENT ANALOG TOXICITY
	IN HYDRA ATTENUATA..... 146
	Introduction..... 146
	Materials and Methods ..... 148
	Results ..... 151
	Discussion..... 164
VI	SUMMARY AND CONCLUSIONS ..... 168
	REFERENCES..... 174
	VITA..... 182



## LIST OF TABLES

TABLE		Page
1.1	The toxicity of the most common organophosphate nerve agents .....	19
2.1	The kinetic constants for hydrolysis of the sarin and soman isomers and racemate, as catalyzed by wild type PTE, G60A, and I106A-F132A-H257Y .....	42
3.1	The primers used for the single and double substitution libraries.....	62
3.2	The identities of 5 colony forming units isolated from each single substitution library .....	68
3.3	The identities of 5 colony forming units isolated from each double substitution library .....	82
3.4	The kinetic constants for the individual GD analog isomer.....	90
3.5	The comparison of ratios obtained from kinetic and time course data.....	92
3.6	Maximal velocity for PTE catalyzed hydrolysis of the nerve agent GD .....	97
4.1	The identities of the codons from 5 random colony forming units of the H254X-H257X library made in both wild type and L303T .....	113
4.2	The kinetic constants for the individual R <sub>p</sub> and S <sub>p</sub> isomers of GB, along with the ratios determined from the catalytic efficiency and the ratios determined from the time course .....	126
5.1	The MEC <sub>92h</sub> (mg/L) for each of the compounds administered are listed with the corresponding calculated log partition coefficient.....	153

## LIST OF FIGURES

FIGURE	Page
1.1	Phosphotriesterase is a homodimer protein, that contains an $(\beta/\alpha)_8$ TIM barrel fold ..... 4
1.2	The zinc binuclear metal center of PTE is shown with the ligated amino acids ..... 5
1.3	The structures of S <sub>p</sub> -(I) and R <sub>p</sub> -(I) methyl ethyl <i>p</i> -nitrophenyl phosphate, and the structures of S <sub>p</sub> -(II) and R <sub>p</sub> -(II) methyl phenyl <i>p</i> -nitrophenyl phosphate ..... 6
1.4	The residues of the <i>large</i> and <i>small</i> subsites, and the leaving group pocket within the active site of PTE ..... 8
1.5	The chemical structures are shown for each of the stereoisomers of sarin, soman, VX, and Soviet V-gas ..... 11
1.6	The structure of DFPase from <i>Loligo vulgaris</i> , depicting a 6-fold b propeller motif..... 14
1.7	A signal travels down the axon to initiate the release of ACh from synaptic vesicles into the neuromuscular junction ..... 22
1.8	The structures of a prophylaxis agent, an antidote, and a regenerator..... 25
2.1	Time course for the hydrolysis of the racemic sarin analog using the mutant forms of PTE ..... 38
2.2	Time course for the hydrolysis of the racemic sarin analog using the mutant forms of PTE ..... 39

FIGURE	Page
2.3 The turnover rate for racemic GB analog, R <sub>p</sub> -isomer, and S <sub>p</sub> -isomer hydrolysis for wild type protein, and the mutants, G60A and I106A-F132A-H257Y .....	40
2.4 The value of $k_{cat}/K_m$ of racemic GB analog, R <sub>p</sub> -isomer, and S <sub>p</sub> -isomer hydrolysis for wild type protein, and the mutants, G60A and I106A-F132A-H257Y .....	41
2.5 The preferential hydrolysis of one isomer within the racemic soman mixture containing 4 isomers, as exhibited by the wild type PTE .....	44
2.6 Time course for the hydrolysis of the diastereomeric mixture of the soman analog S <sub>p</sub> R <sub>c</sub> -(IV) and R <sub>p</sub> R <sub>c</sub> -(IV) using G60A as the first enzyme .....	45
2.7 Time course for the hydrolysis of the diastereomeric mixture of the soman analog S <sub>p</sub> R <sub>c</sub> -(IV) and R <sub>p</sub> R <sub>c</sub> -(IV) using I106A-F132A-H257Y as the first enzyme .....	46
2.8 Time course for the hydrolysis of the diastereomeric mixture of the soman analog S <sub>p</sub> S <sub>c</sub> -(IV) and R <sub>p</sub> S <sub>c</sub> -(IV) using G60A as the first enzyme .....	47
2.9 Time course for the hydrolysis of the diastereomeric mixture of the soman analog S <sub>p</sub> S <sub>c</sub> -(IV) and R <sub>p</sub> S <sub>c</sub> -(IV) using I106A-F132A-H257Y as the first enzyme .....	48
2.10 The turnover rate of the individual stereoisomers of the GD analog for wild type protein, and the mutants, G60A and I106A-F132A-H257Y as expressed in the log plot of the $k_{cat}$ .....	50

FIGURE	Page
2.11 The catalytic efficiency of the individual stereoisomers of the GD analog (IV) for wild type protein, and the mutants, G60A and I106A-F132A-H257Y .....	51
2.12 The active site residues and ligand binding residues of PTE.....	54
3.1 A map of the plasmid, <i>pJW01</i> , shows a multiple cloning site similar to that of pUC 18, as well as ampicillin resistance, and the <i>lacZ</i> gene .....	60
3.2 The results from the GD analog hydrolysis assays for the H254X single substitution library .....	70
3.3 The results from the crude culture screen for the H257X single substitution library .....	72
3.4 The results from the crude culture screen for the L271X single substitution library .....	73
3.5 The results from the crude culture screen for the S308X single substitution library .....	75
3.6 The results from the crude culture screen for the Y309X single substitution library .....	77
3.7 The results from the crude culture screen for the M317X single substitution library .....	78
3.8 The results from the crude culture screen for the G60X and I106X single substitution library .....	80
3.9 The results from the GD analog hydrolysis assays for plate 3 of the H254X-H257X double substitution library.....	84

FIGURE	Page
3.10 The results from the GD analog hydrolysis assays for plate 6 of the H254X-H257X double substitution library.....	85
3.11 The results from the GD analog hydrolysis assays for the G60A-[H254X-H257X] double substitution library .....	87
3.12 The results from the GD analog hydrolysis assays for the [H254X-H257X]-L303T double substitution library .....	89
3.13 Wild type-catalyzed hydrolysis of the first two isomers within the racemic GD analog .....	94
3.14 Wild type-catalyzed hydrolysis of the second and the third isomers within the racemic GD analog.....	95
3.15 Wild type-catalyzed hydrolysis of the third and fourth isomers within the racemic GD analog .....	96
4.1 The results from the GB analog hydrolysis assays for plate B1 of the H254X-H257X library .....	115
4.2 The results from the GB analog hydrolysis assays for plate B2 of the H254X-H257X library .....	116
4.3 The results from the GB analog hydrolysis assays for plate B3 of the H254X-H257X library .....	118
4.4 The results from the GB analog hydrolysis assays for plate B4 of the H254X-H257X library .....	119
4.5 The results from the GB analog hydrolysis assays for plate 4 of the H254X-H257X library .....	121

FIGURE	Page
4.6 The results from the GB analog hydrolysis assays for plate 6 of the H254X-H257X library .....	122
4.7 The results from the GB analog hydrolysis assays for the [H254X-H257X]-L303T library .....	124
4.8 The catalytic efficiency of the purified mutants for the hydrolysis of the S <sub>p</sub> isomer of the GB analog .....	138
4.9 Two time courses from wild type catalyzed hydrolysis of the racemic GB analog .....	130
4.10 Two time courses from I106A-F132A-H257W-catalyzed hydrolysis of the racemic GB analog .....	132
4.11 The non-enzymatic hydrolysis of 0.5 mM GB at pH 7.72 at 25 °C .....	133
4.12 Wild type catalyzed hydrolysis of 0.5 mM GB at pH 7.72 at 25 °C .....	134
4.13 G60A catalyzed hydrolysis of 0.5 mM GB at pH 7.72 at 25 °C .....	135
4.14 I106A-H257Y catalyzed hydrolysis of 0.5 mM GB at pH 7.72 at 25 °C .....	136
4.15 I106A-H257Y-S308A catalyzed hydrolysis of 0.5 mM GB at pH 7.72 at 25 °C .....	137
4.16 I106A-F132A-H257Y catalyzed hydrolysis of 0.5 mM GB at pH 7.72 at 25 °C .....	138
4.17 The double enzyme plot of GB hydrolysis .....	140
5.1 The physical stages of adult <i>Hydra attenuata</i> .....	154
5.2 The time course for the toxic effect of various concentrations of paraoxon on <i>Hydra attenuata</i> .....	155

FIGURE	Page
5.3 Comparison of the $MEC_{92h}$ for the organophosphate nerve agent analogs IV, V, and VII determined in this investigation versus the reference dose for the chemical warfare agents sarin, soman and VX .....	157
5.4 The lowest and highest energy of the compounds as determined by the Boltzmann Conformer Search Method for each of the test compounds .....	159
5.5 The physical properties of volume, surface area, and mass for each of the test compounds .....	160
5.6 The polarizability for each of the compounds tested is expressed in $\text{\AA}^3$ .....	161
5.7 The molecular hydrophobicity is expressed as $\log P$ , the partition coefficient of octanol:water, for each test compound .....	162
5.8 Correlation between the log of the partition coefficient for a mixture of octanol/water and the $MEC_{92h}$ for the compounds assayed in this investigation .....	163

## CHAPTER I

### INTRODUCTION

#### **Background**

##### *Background Information on Phosphotriesterase (PTE)*

Phosphotriesterase (PTE) is an enzyme that was found in two different soil bacteria, *Pseudomonas diminuta* MG and *Flavobacterium* sp. strain ATCC 27551 during the 1970's (Mulbry et al., 1986). While the *Pseudomonas diminuta* protein was first discovered in the United States, and the *Flavobacterium* sp. protein was found in the Philippines, cell-free extracts from both bacteria were capable of hydrolyzing several organophosphorus insecticides such as methyl parathion and paraoxon faster than base-catalyzed hydrolysis (Chaudry et al., 1988). Sequence analysis via restriction digest patterns of the both genes revealed that the 1693 bp *opd* gene was virtually identical (Mulbry et al., 1986).

The *opd* gene was subcloned into *Escherichia coli*, and the protein was over expressed and purified to homogeneity (Omburo et al., 1992). It was determined that the protein exists as a homodimer, with each monomer weighing approximately 36 kD (Donarski et al., 1989). Within each monomer is a binuclear metal center that is essential for catalysis. In Nature, PTE exists as a zinc metalloprotein. However, the zinc may be replaced with divalent cations such as  $Mn^{2+}$ ,  $Co^{2+}$ ,  $Cd^{2+}$ , and  $Ni^{2+}$  while still maintaining catalytic activity (Omburo et al., 1992). Removal of the metal ions with chelators such as EDTA, and 1,10-phenanthroline produces the apoenzyme form of the protein, which is essentially inactive (Omburo et al., 1992).

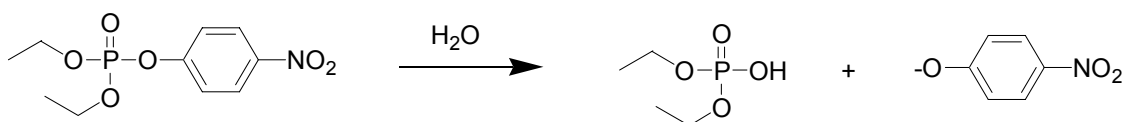
---

This dissertation follows the style of *Protein Science*.



Titration experiments also implicated the requirement of two metals for catalytic activity. The highest activity for the hydrolysis of paraoxon has been reported with the use of  $\text{Co}^{2+}/\text{Co}^{2+}$  PTE, which has a  $k_{\text{cat}}/K_{\text{m}}$  of  $3.8 \times 10^7 \text{ M}^{-1}\text{s}^{-1}$  (Omburo et al., 1992). The activities reported for other metal ions are lower than that of  $\text{Co}^{2+}$ , in the following order of  $\text{Zn}^{2+}$ ,  $\text{Mn}^{2+}$ ,  $\text{Ni}^{2+}$ , and  $\text{Cd}^{2+}$ . The  $k_{\text{cat}}/K_{\text{m}}$  for the  $\text{Zn}^{2+}/\text{Zn}^{2+}$  PTE enzyme and the  $\text{Cd}^{2+}/\text{Cd}^{2+}$  PTE enzyme is  $3.4 \times 10^7 \text{ M}^{-1}\text{s}^{-1}$  and  $7.0 \times 10^6 \text{ M}^{-1}\text{s}^{-1}$ , respectively (Omburo et al., 1992).

PTE catalyzes the hydrolysis of many organophosphates and their related phosphonates with high catalytic efficiency and broad substrate specificity (Chen-Goodspeed et al., 2001a). Of particular interest are the organophosphate nerve agents, which have shown to be hydrolyzed, and thus detoxified, by this enzyme. The best rates for hydrolysis have been shown with the insecticidal agent, paraoxon. The PTE-catalyzed reaction occurs with a rate constant ( $k_{\text{cat}}/K_{\text{m}}$ ) of  $4 \times 10^7 \text{ M}^{-1}\text{s}^{-1}$  and a turnover rate of approximately  $2200 \text{ s}^{-1}$  (Shim and Raushel, 2000). It has been determined that the hydrolysis of phosphotriesters occurs via a  $\text{S}_{\text{N}}2$ -like process, in which an activated hydroxyl group displaces the leaving group of the substrate resulting in an inversion of configuration at the phosphorus center (Lewis et al., 1988).



Scheme 1. The hydrolysis of paraoxon results in p-nitrophenol and diethylphosphate.

In terms of tertiary folding, each monomer consists of eight parallel  $\beta$  sheets ( $\beta/\alpha$ )<sub>8</sub>, similar to the classic example that is seen in triose phosphate isomerase (TIM). The TIM-barrel fold is maintained in other amidohydrolase superfamily members such as urease,

adenosine deaminase, and dihydroorotase, implying a direct relationship via divergent evolution (Holm and Sander, 1997). Similar to these proteins, PTE contains the  $(\beta/\alpha)_8$  fold as seen in Figure 1.1.

As with most of the other TIM-barrel containing proteins, the active site of PTE is located at the C-terminal end of the  $\beta$ -barrel of the  $(\beta/\alpha)_8$  motif (Nagano et al., 2002). Within the active site, there is a binuclear metal center, in which the more buried metal, known as the  $\alpha$  metal, is ligated to His55, His57, and Asp301 (Figure 1.2). The more solvent-exposed metal, known as the  $\beta$  metal, is ligated to His201, His230, and two water molecules. The carboxylated K169 residue bridges the two metal ions, in addition to a hydroxide which is believed to be the nucleophile during the hydrolysis of the substrate (Benning et al., 2001).

It has been determined that the space available within the binding pockets dictates the stereospecificity of the enzyme. This is observed in previous studies in which both the substituent size and the binding pocket size were varied (Chen-Goodspeed et al., 2001a,b). The effects of substrates containing either methyl, ethyl, isopropyl, and or phenyl substituents at the phosphorus center were probed. It was determined that the wild type protein preferentially catalyzed the hydrolysis of the  $S_p$  enantiomers over the  $R_p$  enantiomers, with a factor ranging from 1 for the methyl ethyl p-nitrophenyl phosphate substrate (I) to 90 for the methyl phenyl p-nitrophenyl phosphate substrate (II) as shown in Figure 1.4 (Chen-Goodspeed et al., 2001a).

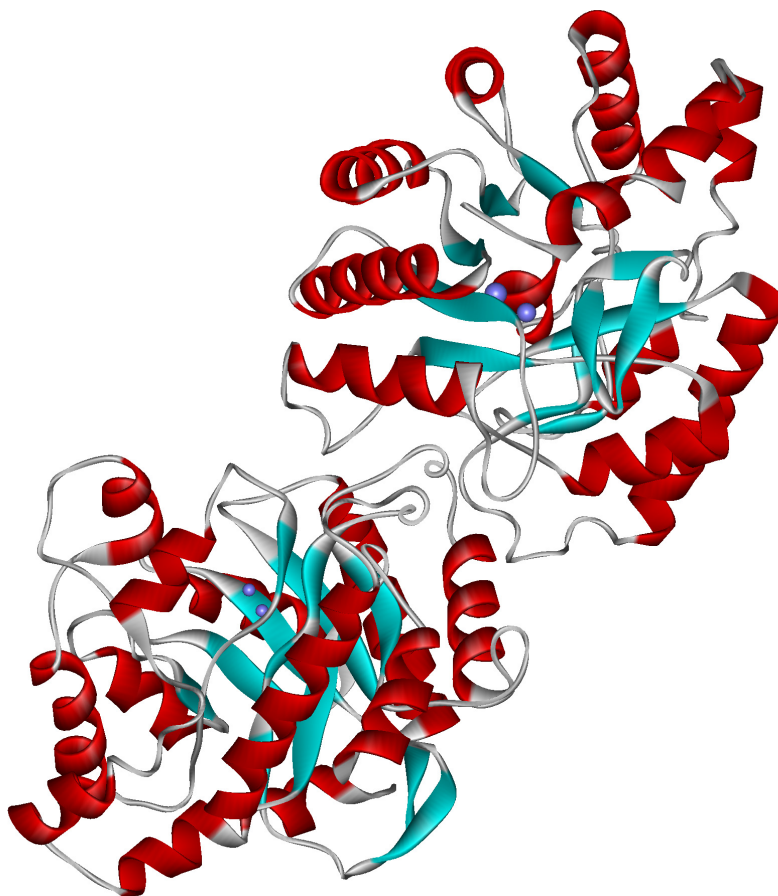


Figure 1.1. Phosphotriesterase is a homodimer protein, that contains an  $(\beta/\alpha)_8$  TIM barrel fold (IPTA pdf file from Benning et al., 1994).

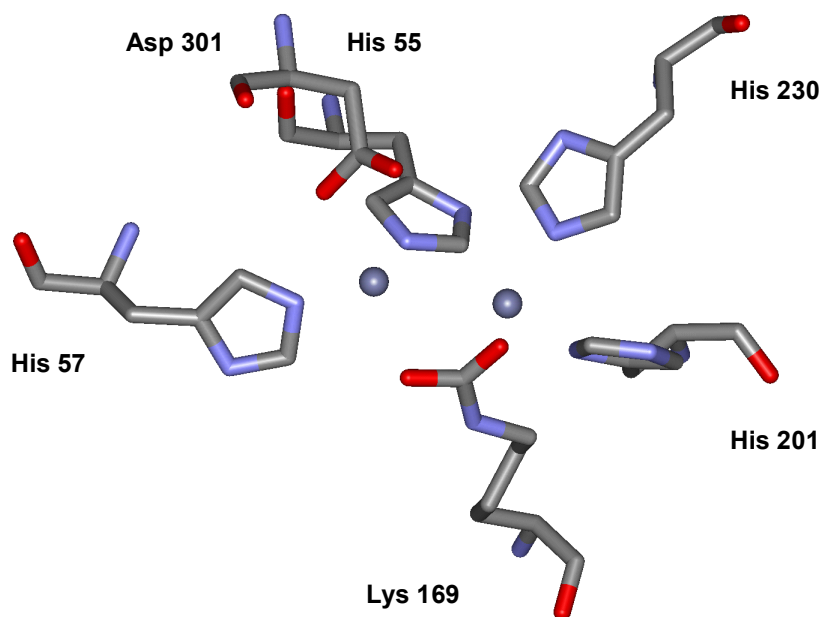


Figure 1.2. The zinc binuclear metal center of PTE is shown with the ligated amino acids.

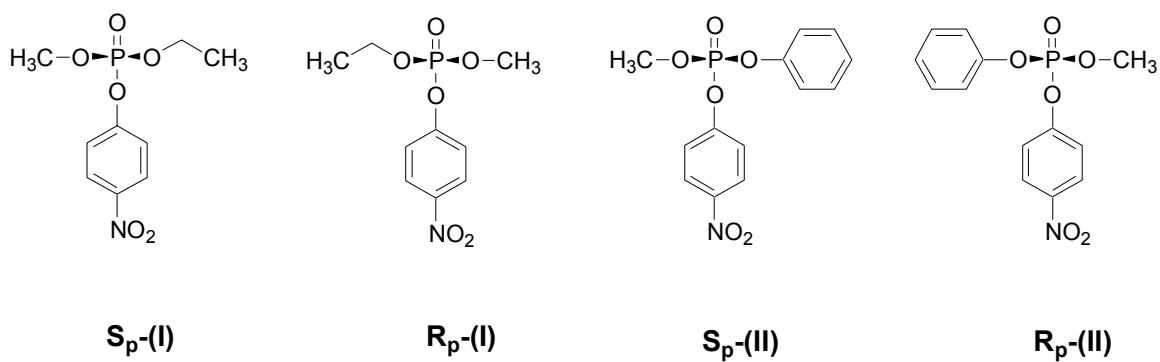


Figure 1.3. The structures of S<sub>p</sub>-(I) and R<sub>p</sub>-(I) methyl ethyl p-nitrophenyl phosphate, and the structures of S<sub>p</sub>-(II) and R<sub>p</sub>-(II) methyl phenyl p-nitrophenyl phosphate.

This observation, in conjunction with structural information of PTE with a bound substrate analogue, has implied that the  $S_p$  enantiomer fits in a way such that the larger substituent is in the large subsite, and the smaller substituent is in the small subsite of the active site.

From the crystal structure of  $Zn^{2+}/Zn^{2+}$  PTE, it is apparent that there are three binding subsites: a large pocket, a small pocket, and the leaving group subsite (Benning et al., 2001). As illustrated in Figure 1.3, the residues that define the small pocket are Gly60, Ile106, and Ser308. Residues that line the large pocket are His254, His257, Leu271, and Met317. In the leaving group pocket, there are the hydrophobic residues Trp131, Phe132, and Tyr309.

In addition to effects from variation of substituent size, it was determined that modification of the small and large subsite residues also contributed to the stereoselectivity. The residue Gly60 was modified to an Ala, thereby decreasing the space available within the small subsite. The mutation resulted in a significant decrease for the catalytic constants for hydrolysis of the  $R_p$  enantiomer, leading to a subsequent increase in the ratio of rates for hydrolysis of the  $S_p$  over the  $R_p$ -enantiomer.

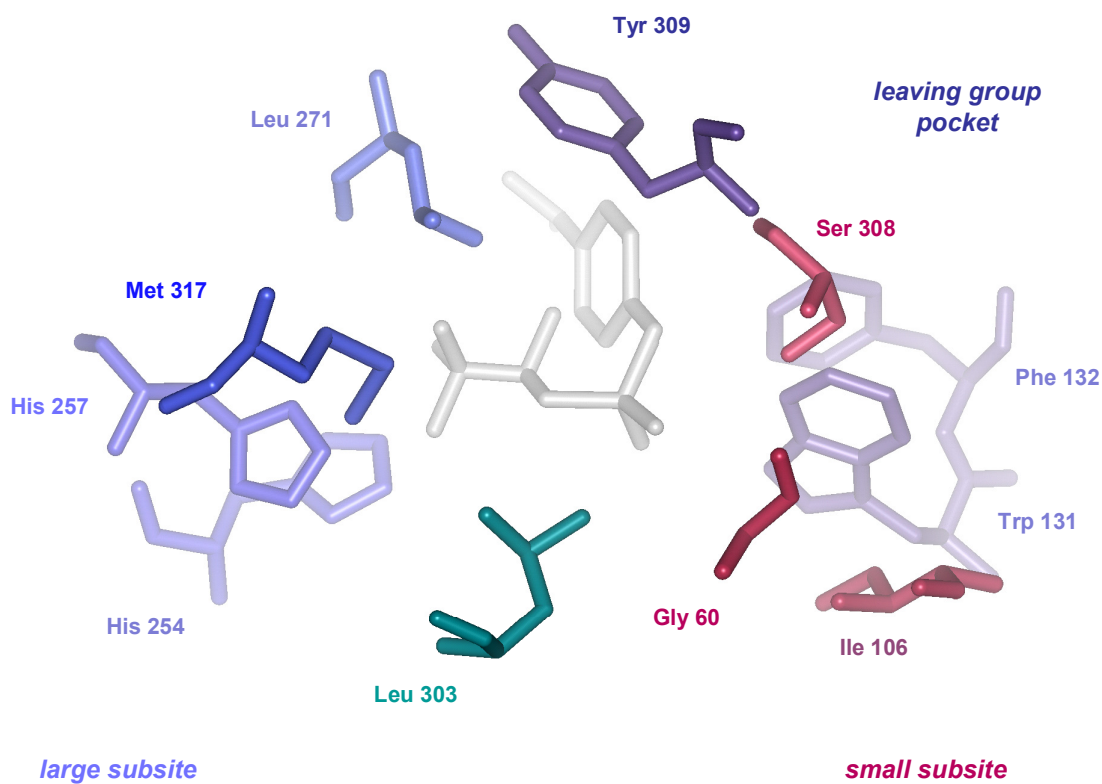


Figure 1.4. The residues of the large and small subsites, and the leaving group pocket within the active site of PTE. The substrate modeled in the active site is the R<sub>p</sub>S<sub>c</sub> isomer of the soman analog, pinacolyl p-nitrophenyl methyl phosphonate. The figure has been modified based upon the 3-D structural information from zinc-containing PTE (Vanhook et al., 1996).

In contrast, a reduction in the physical size of the large subsite resulted in a reversal of the preference that was observed with the wild type protein. As in the case with the H257Y mutant, a Tyr residue was used to replace His in the 257 position causing there to be less space available within the large subsite. The His to Tyr mutation led to a decrease in the catalytic efficiency for the  $S_p$  enantiomers, and an overall preference for the  $R_p$  enantiomers. For the  $R_p$  enantiomer, the larger substituent is in the small subsite and the smaller substituent is in the large subsite.

Similar perturbations in the large subsite were also studied by the Wild laboratory. In particular, the H254R, H257L, and H254R-H257L mutants were tested with VX and soman analogs (Di Sioudi et al., 1999). There was enhanced substrate specificity with each of the mutants for the VX analog, demeton-S. In addition, there was a 11- and 18-fold increase in the catalytic efficiency for soman analog hydrolysis for the H257L and H254R-H257L, respectively. Results from this study indicated that modification in the large subsite led to increased structure flexibility, allowing for larger substrates to fit better within the active site.

The importance of both large subsite residues 254 and 257 was also mentioned in a study comparing PTE with the OpdA protein obtained from *Agrobacterium radiobacter* P230 (Yang et al., 2003). Comparison of both proteins revealed a 90% identity at the amino acid level. The active sites of both proteins were also extremely similar. In the same study, directed evolution studies with the *opd* gene, combined with screening, resulted in the finding of H254R in all third generation mutants identified as having enhanced activity for a coumaphos substrate. It was also noted that there is a Arg in position 254 and a Tyr at



position 257 for the opdA protein, instead of His that is found in both positions in PTE (Yang et al., 2003).

#### *PTE-catalyzed Detoxification of Nerve Agents*

The potential use of PTE for the detoxification of organophosphate nerve agents and pesticides appears to be promising. In animal studies, it has been shown that mice pretreated with PTE before organophosphate exposure have a significant increase in resistance when given doses that are higher than the expected LD<sub>50</sub> (Tuovinen et al., 1999). In the Tuovinen study, the result is quite dramatic for protection against intraperitoneally injected paraoxon. Pre-treated mice showed no sign of adverse affect up to fifty times the dose tolerated by the untreated mice (Tuovinen et al., 1994).

PTE has been shown to hydrolyze the nerve agents, sarin (GB), soman (GD), and VX but the rate constants for the enzymatic hydrolysis of these substrates is significantly lower than other substrates such as paraoxon (Di Sioudi et al., 1999). In considering the potential application of PTE, one must also account for the differential toxicities that each isomer of these agents elicits (Benschop et al., 1984). As shown in Figure 1.5, there is one chiral center for both GB and VX, resulting in two isomers, and for GD there are two chiral centers and four isomers.

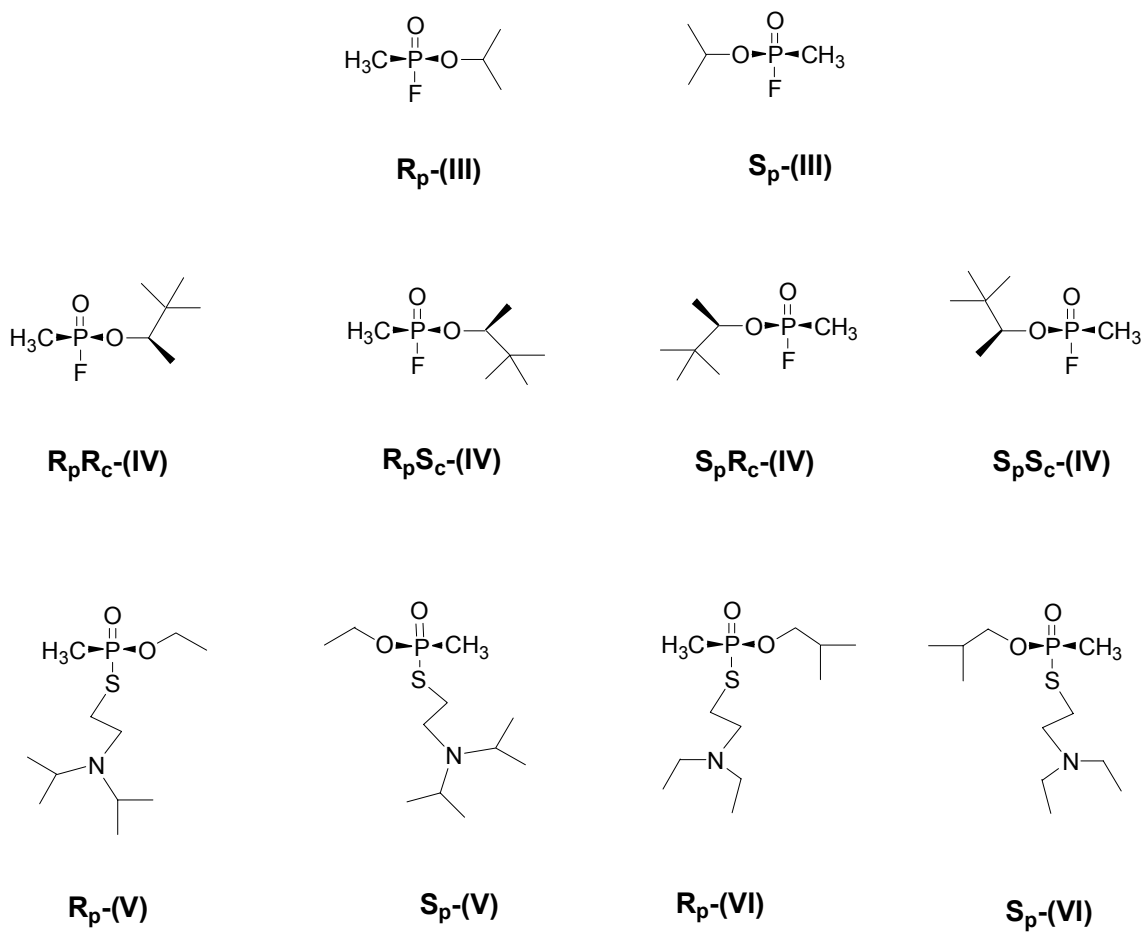


Figure 1.5. The chemical structures are shown for each of the stereoisomers of sarin (III), soman (IV), VX (V), and Soviet V-gas (VI).

As observed in previous in vitro mouse studies conducted with GB and GD, the S<sub>p</sub> enantiomer of sarin is more toxic (Spruit et al., 2000). The two S<sub>p</sub> diastereomers of soman have been shown to be at least 50 times more toxic than the two R<sub>p</sub> diastereomers (Benschop et al., 1984). Inhibition rate constants of the individual isomers on AChE reveal that the S<sub>p</sub> isomer of GB is approximately 4000 times more reactive than the R<sub>p</sub> isomer (De Jong et al., 1988). The rate constant (M<sup>-1</sup> min<sup>-1</sup>) for inhibition of AChE by the individual R<sub>p</sub> and S<sub>p</sub> isomer of GB is 3 x 10<sup>3</sup> and 1.4 x 10<sup>7</sup>, respectively (De Jong et al., 1988). For inhibition elicited by the stereoisomers of GD, the rate constant is less than 5 x 10<sup>3</sup> for both the R<sub>p</sub> diastereomers, 2.8 x 10<sup>8</sup> for the S<sub>p</sub>R<sub>c</sub>, and 1.8 x 10<sup>8</sup> for the S<sub>p</sub>S<sub>c</sub> isomer (De Jong et al., 1988).

Both the toxicity and inhibition data provide distinct results, indicating that the individual isomers elicit differential effects which appear to be determined more by the chirality at the phosphorous center than the chirality of the alkoxy center of anti-cholinesterase inhibitor such as GD (De Jong et al., 1988).

#### *Other Organophosphate Hydrolyzing Protein and Applications*

DFPase has also been identified as an enzyme capable of hydrolyzing nerve agents, specifically tabun, sarin, cyclosarin, diisopropyl fluorophosphate (DFP), and soman. Although it is an organophosphate hydrolyzing protein, it shares no similarity to other proteins such as butyrylcholinesterase, organophosphorus acid anhydrolase, and PTE. It was isolated from the head ganglion of *Loligo vulgaris*, and exists as a monomer of 314 amino acids. The protein has excellent activity against DFP, with a k<sub>cat</sub> of 526 s<sup>-1</sup> and a k<sub>cat</sub>/K<sub>m</sub> of 1.3 x 10<sup>6</sup> M<sup>-1</sup> s<sup>-1</sup> (Hartleib and Rüterjans, 2001). However, the activity for both sarin and

soman are lower than PTE, and unlike PTE, DFPase is not capable of hydrolyzing the most toxic nerve agent, VX. The structure of the enzyme is shown in Figure 1.6.

The main advantage of all organophosphate hydrolyzing enzymes is their non-corrosive nature. Currently, the method for decontamination of chemical warfare agents involves the use of bleach, which is harsh, corrosive, and bad for the environment (U.S. Congress, 1993). Protein is easily obtainable in substantial amounts, and is cost efficient. Applications of enzyme use include the use of polyurethane foams, and various types of sensors.

Polyurethane foams have been found to have a high binding affinity to nerve agents, and have been able to successfully shield PTE from environmental factors such as pH and temperature, that detrimentally affect catalytic activity (LeJeune et al., 1998). The enzyme-polyurethanes are readily formed within minutes, and have proven to be effective in decontamination exercises (LeJeune et al., 1998). The lifetime of catalytic activity has been shown to be substantially increased with the use of foam. The enzyme within the foam retains 100% activity for 25 days, whereas the enzyme alone rapidly decreases in catalytic activity just after the first day (LeJeune et al., 1998).

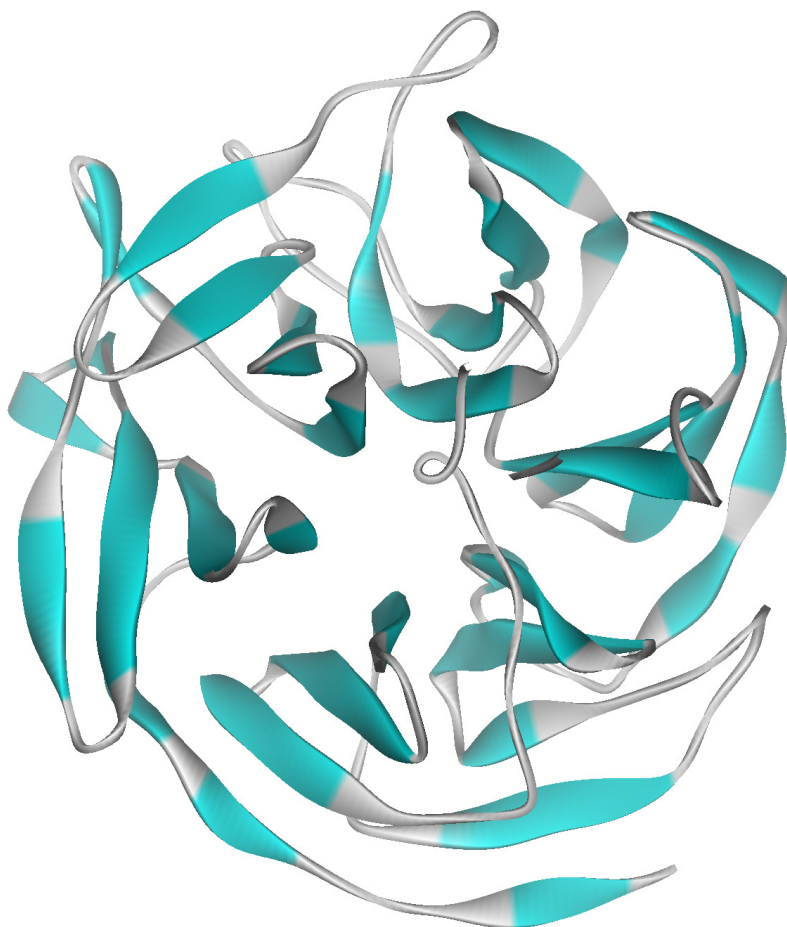
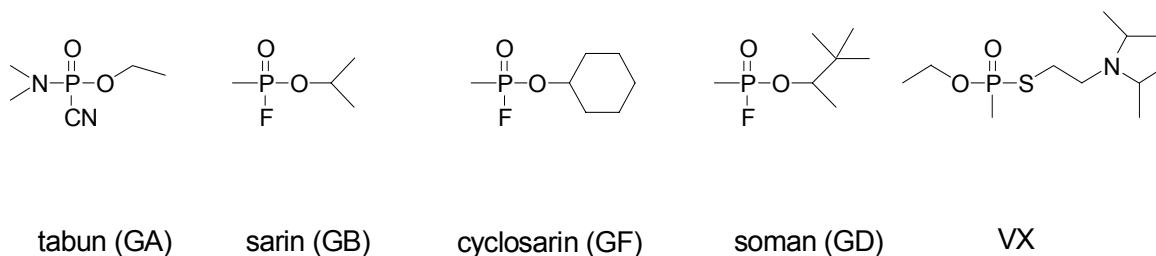


Figure 1.6. The structure of DFPase from *Loligo vulgaris*, depicting a 6-fold  $\beta$  propeller motif. The Protein Data Bank ID of this structure is 1E1A (Scharff et al., 2001).

Amperometric sensors have been constructed using PTE, where the enzyme is co-immobilized with albumin on a nylon net. Together, they are attached to a carbon paste electrode, and are capable of detecting organophosphate insecticides such as parathion and paraoxon within the nM range (Chough et al., 2002).

### History of Organophosphate Nerve Agents

The German pharmaceutical company, Bayer, developed the first organophosphate insecticides (U.S. Department of Defense, 1998). Upon the discovery of their anti-acetylcholine esterase (AChE) activity, the newly developed insecticides were used as nerve agents. Other compounds were synthesized within a period of 30 years. Among them were the organophosphate nerve agents tabun (GA), sarin (GB), cyclosarin (GF), soman (GD), and VX (U.S. Department of Defense, 1998). As seen in scheme 2, GA has a cyanide leaving group. The three remaining G agents, GB, GF, and GD, each have



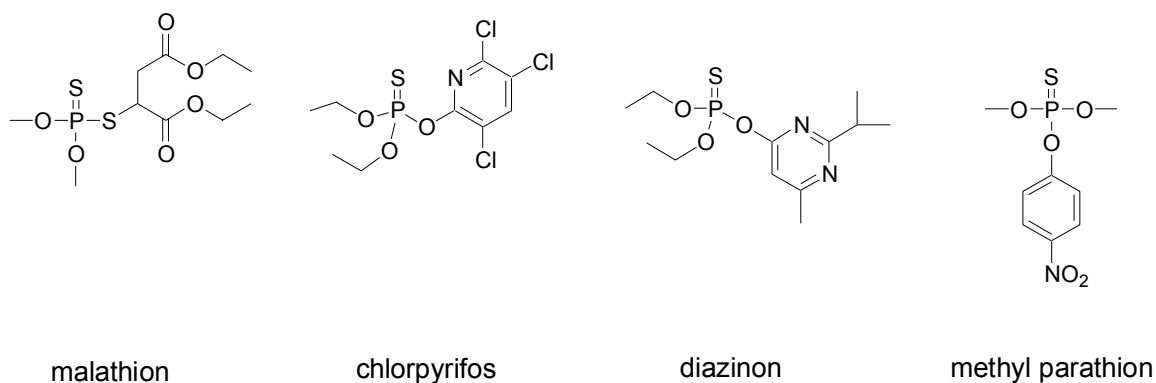
Scheme 2. The chemical structures of the 5 most common organophosphate nerve agents; tabun (GA), sarin (GB), cyclosarin (GF), and VX.

a fluorine leaving group, and VX has a thiolate leaving group. The G agents are considerably volatile, implying that toxicity occurs readily via inhalation exposure routes. Toxicity

resulting from the V agents is far greater in terms of dose required for lethality. However, V agents such as VX are not volatile, but are far more persistent. Toxicity occurs primarily via a percutaneous route (i.e. droplets on skin) (Munro, 1994). In general, the organophosphate nerve agents share the characteristics of being highly toxic and stable (Munro, 1994).

### *Organophosphate Compounds and Toxicity*

The organophosphates were first recognized as a distinct class of compounds in 1854, but the toxicity associated with this class of compounds was not discovered until the 1930's (Moseley and Snead, 1953). The first organophosphate insecticide synthesized was tetraethyl pyrophosphate (TEPP) (Minton and Murray, 1988). As of the late 1980's, there have been over 100,000 compounds screened for insecticidal use, and over a hundred are available for commercial use (Minton and Murray, 1988). The effect of organophosphate compounds on the environment has been, and continues to be, very critically analyzed by the U.S. Environmental Protection Agency (EPA). Although the usage of organophosphate pesticides has declined approximately 30% from 1980 to 1999, this particular class of compounds still accounted for 72% of the 126 million pounds of active ingredients within pesticides for 1999 (Donaldson et al., 2002). Malathion, chlorpyrifos, diazinon, and methyl parathion are among the top ten active ingredients used annually by the pesticide industry. The structures are depicted in Scheme 3. Each of these compounds has been shown to cause toxicity, and have resulted in a number of exposure-toxicity case studies (Donaldson et al., 2002).



Scheme 3. The chemical structures are shown for the pesticidal agents, malathion, chlorpyrifos, diazinon, and methyl parathion.

As a class, the organophosphates are structurally characterized as compounds containing a pentavalent phosphorus. Typically, one substituent is double bond bonded to oxygen, sometimes a sulfur is used instead, and the three remaining substituents are varied. This variation leads to the broad range of structures within this class, and the complexity in determining their differential targets. Direct targets of organophosphates include acetylcholine esterase (AChE), the muscarinic acetylcholine receptor (mAChR) and the nicotinic acetylcholine receptor (nAChR) (Marrs et al., 1996). Other enzymes that have detoxifying capabilities are phosphotriesterase (PTE), paraoxonase (PON), as well as squid enzyme and organophosphate acid anhydrolases (Tuovinen et al., 1994)(Veronesi et al., 1997)(Hartleib and Rüterjans, 2001)(Cheng et al., 1999).

The mechanism of toxicity of these nerve agents is similar to that of organophosphate insecticides such as paraoxon and chlorpyrifos, and many of the details of organophosphate toxicity have been determined by using paraoxon and chlorpyrifos as model substrates because they are considerably less dangerous (Mileson et al., 1998). The toxicity occurs



primarily by inhalation and percutaneous absorption, as seen with the toxicity data reported in Table 1. Exposure through these routes results in the inhibition of AChE and affects the AChR and ionic channels (i.e. a more direct route than AChE) thereby causing cholinergic excess (Tuovinen et al., 1994). While there has been considerable attention directed towards dealing with the toxicity of these compounds (Mileson, 1998), other complexities involving the mechanism of action have yet to be elucidated. One such complexity is the occurrence of compartmentalization of soman into depots within the skin, muscles, and lungs, which has been observed in some studies (Kadar et al., 1985). Although a small fraction is contained in the depot, only 1-3% of the dose administered elicits the toxic effects, so that the quantity within the depot may prove to be significant in determining toxicity (Bajgar, 1996).

For the testing of nerve agents in living systems, there has been significant toxicological data compiled on the effects of the nerve agents in their racemic mixture. However, several studies indicate that there are substantial differences in the toxicological properties between different stereoisomers of the same compound due to stereospecific interactions involved in AChE-OP binding (Ordentlich et al., 1999) (Benschop et al., 1984). In such studies, it has been determined that for soman, the two  $R_p$  enantiomers are relatively non-toxic, whereas the  $S_pS_c$  enantiomer is extremely toxic and the  $S_pR_c$  contributes somewhat to this toxicity (Benschop et al., 1984). The structures of the individual isomers are shown in Figure 1.5.

Table 1.1. The toxicity of the most common organophosphate nerve agents (USAMRICD, 1995). Vapor toxicity is expressed as LC<sub>50</sub>, IC<sub>50</sub>, and MC<sub>50</sub> and reported in terms of mg min m<sup>3</sup>, whereas the LD<sub>50</sub> represents toxicity via percutaneous absorption, and it is reported in terms of mg quantity. The terms, LC<sub>50</sub>, IC<sub>50</sub>, and MC<sub>50</sub>, are lethal concentration, incapacitating concentration, and miosis concentration, respectively, for 50 percent of the population. The LD<sub>50</sub> represents the dose that causes lethality to 50 percent of the population.

<b>Agent</b>	<b>LC<sub>50</sub></b>	<b>IC<sub>50</sub></b>	<b>MC<sub>50</sub></b>	<b>LD<sub>50</sub></b>
<b>GA</b>	<b>400</b>	<b>300</b>	<b>2-3</b>	<b>1000</b>
<b>GB</b>	<b>100</b>	<b>75</b>	<b>3</b>	<b>1700</b>
<b>GD</b>	<b>70</b>	<b>n/a</b>	<b>&lt;1</b>	<b>50</b>
<b>GF</b>	<b>n/a</b>	<b>n/a</b>	<b>&lt;1</b>	<b>30</b>
<b>VX</b>	<b>50</b>	<b>35</b>	<b>0.04</b>	<b>10</b>

Although all avenues of organophosphate toxicity have yet to be fully elucidated, it is clear that cholinergic effects are primary and there is inhibition of AChE (e.g. anti-AChE). In terms of anti-AChE activity, the reactivity of each organophosphate is derived from the intrinsic electrophilicity of the phosphorus, which is determined by how electron withdrawing the leaving group is, in addition to how well the substituents fit into the target active site (Milesion et al., 1998). Secondary effects of organophosphate toxicity are mediated by hormones, and symptoms such as hyperglycemia, hyperlipidemia (Somani, 1992).

#### *AChE: The Primary Target of Organophosphate Nerve Agents*

Transmission at a chemical synapse is initiated by an action potential. As an action potential arrives at the presynaptic membrane, there is depolarization of the synaptic terminus, which triggers the opening of voltage-gated  $\text{Ca}^{2+}$  channels. The subsequent influx of extracellular  $\text{Ca}^{2+}$  into the presynaptic terminals results in the exocytosis of synaptic vesicles containing AChE (Dan and Poo, 1992). As illustrated in Figure 1.7, the acetylcholine (ACh) packets are released into the synaptic cleft where they may bind to receptors on the postsynaptic membrane. The binding of ACh at the receptor causes a change in ion permeability, leading to the subsequent change in membrane potential of the postsynaptic membrane (Matthews, 1991).

AChE is a serine esterase that resides at the sites of mAChR and nAChR (Somani, 1992). It catalyzes the degradation of ACh into acetate and choline, which ends the nerve transmission. Within the active site of AChE, there is a catalytic triad similar to that of serine proteases, which is comprised of Ser200, His440, and Glu237. Without the presence

of AChE inhibitors, this enzyme maintains a  $k_{cat}$  on the order of  $10^5 \text{ min}^{-1}$ , which is considered to be a turnover rate close to perfection (Froede and Wilson, 1984). However, if organophosphate nerve agents are present, there is phosphorylation at the catalytic serine, resulting in dead enzyme (Marrs et al., 1996). In addition, the inhibition of AChE activity results in an increased concentration of ACh in the synapses and neuromuscular junctions, leading to the over stimulation of the cholinergic receptors, nAChR and mAChR (Veronesi et al., 1997). As overstimulation occurs, symptoms that typically manifest are miosis, bronchial constriction, sweating, and increased secretion within the trachial-bronchial tract. Other symptoms such as tremors, seizures, and death may occur if the administered dose is high enough (Hartmann, 2002).

#### *nAChR and mAChR: The Secondary Targets of Nerve Agents*

The secondary effect of AChE inhibition is the sustained activation of the cholinergic receptors. Although this is considered a secondary effect, direct binding of ACh, as well as organophosphates, has been well documented (Veronesi et al., 1997) (Katz et al., 1997). In a study by Katz et al., the nAChR agonist carbamoylcholine and the non-competitive allosteric antagonist [ $^3\text{H}$ ] thienyl-cyclohexyl-piperidine (TCP) were used to determine the binding of ACh and the organophosphates, chlorpyrifos and parathion (Katz et al., 1997). Because the organophosphates were able to bind while ACh (active site) and TCP (allosteric site) were bound, it was determined that the organophosphates used were bound to a separate site, distinguishable from both the active and labeled allosteric sites.

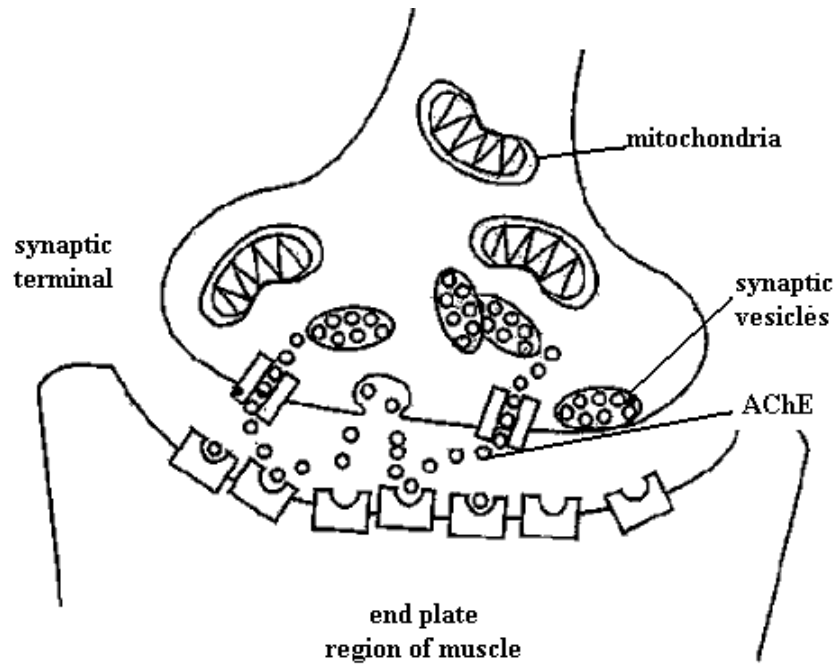


Figure 1.7. A signal travels down the axon to initiate the release of ACh from synaptic vesicles into the neuromuscular junction.

The details of the binding states, such as conformation and ligand affinity, were also examined by several related experiments. There were three different conformations of nAChR described; a resting state with little affinity for ACh, a desensitized state characterized by very high affinity for ACh or carbamylcholine while remaining inactivated, and an active state marked by very high affinity. A desensitized state could result from two possible outcomes. One of which could be a general increase in ACh levels leading to subsequent activation of nAChR, triggering conformational changes leading to the state and possible “receptor plasticity,” whereby repeated OP exposure resulted in down regulation of both types of cholinergic receptors. The other possibility entails the activation of mAChR in the heart and blood vessels, leading to symptoms such as bradycardia, hypertension, and asphyxiation (Katz et al., 1997).

Similar experiments were done using mAChR. The main differences between the two receptors are location and structure. The nAChRs which contain 5 subunits ( $\alpha_1\alpha_2\beta_1\beta_2$ ), are located in the autonomic nervous system, neuromuscular junctions and the brain. The binding of ACh occurs at the  $\alpha$  subunit (Somani, 1992). Each mAChR consists of 7 transmembrane domains, and they are G-protein-coupled receptors found within the parasympathetic nervous system (Huff and Abou-Donia., 1995).

The five subtypes of mAChR are classified according to which G protein family they are coupled to. When activated by ACh,  $M_1$ ,  $M_3$ , and  $M_5$  stimulate phosphatidylinositol phosphate hydrolysis through the  $G_p$  family whereas  $M_2$  and  $M_4$  trigger the inhibition of adenylate cyclase through the  $G_i$  family when activated (Huff and Abou-Donia, 1995).

In a study by Silveira et al., [ $^3H$ ]cis-methyl dioxolane was used as an agonist competing against the organophosphate nerve agents, GA, GB, GD, and VX to determine the

location of organophosphate binding on M<sub>2</sub>AChRs (Silveira et al., 1990). It was determined that both the nerve agents and ACh bind to the active site. Other organophosphates, such as chlorpyrifos were found to be less competitive, and less toxic. Thus, a correlation between competitive inhibition and toxicity was established for the target mAChR (Silveira et al., 1990).

#### *Current Treatment of Organophosphate-induced Toxicity*

The methods available for treating toxicity induced by organophosphate compounds are prophylaxis, antidote, regenerators, and anticonvulsants. Prophylaxis involves the reversible binding of a carbamate, which acts as a competitive AChE inhibitor with the nerve agent. Toxicity is prevented by constant release of active enzyme from binding with carbamates such as the stigamines. However, a limitation associated with prophylaxis agents is timing. They must be administered before exposure in order to be effective. An example of a carbamate prophylaxis agent is pyridostigmine, as shown in Figure 1.8.

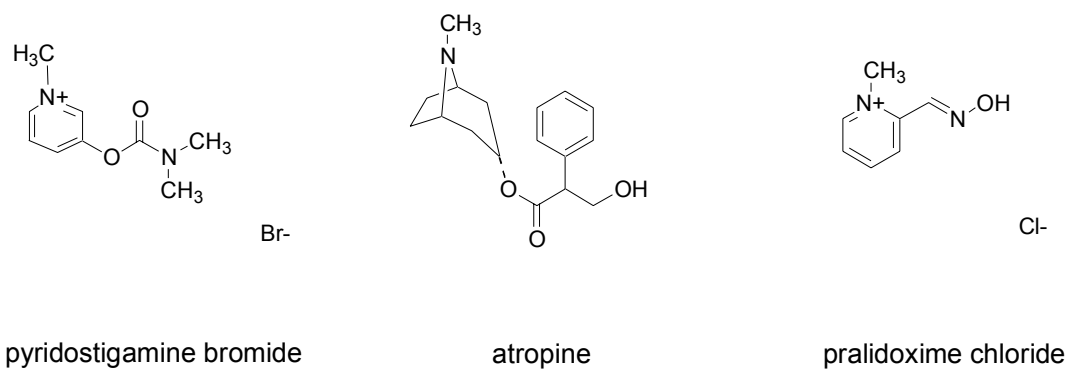


Figure 1.8. The structures of a prophylaxis agent (i.e. pyridostigmine), an antidote (i.e. atropine), and a regenerator (i.e. pralidoxime).



In the event that exposure has occurred, antidotes, regenerators, or anticonvulsants may be used. An antidote such as atropine is used as a cholinergic antagonist, to titrate against symptoms of cholinergic excess. Regenerators, such as oximes (i.e. pralidoxime) block the binding of organophosphates to AChE, and reactivate the enzyme of nerve endings (Sidell, 1994). These, however, must be administered early after exposure due to a post inhibitory reaction known as aging. After the nerve agent has phosphorylated the active site serine, the compound is still susceptible to dealkylation of its branched alkyl groups, otherwise known as aging, which leads to irreversible enzyme inhibition (Millard et al., 1999).

Anticonvulsants act to counter the central nervous system effects, so that cardio-respiratory function can be normalized. The anticonvulsant agent is most effective if it can penetrate the blood-brain barrier to prevent resulting brain damage (Mileson, et al., 1998).

### *Conclusions*

The potential use for phosphotriesterase as an agent to combat chemical warfare agents has been demonstrated in a number of studies (Tuovinen et al., 1994)(Tuovinen et al., 1999). Phosphotriesterase (PTE) is the only protein that has been found thus far to hydrolyze, and thereby detoxify, both the G- and V-series of nerve agents (Raushel, 2002). Data from both in vitro and in vivo experiments indicate the promise that this protein has for use in bio-remediation types of applications. However, a formidable obstacle impeding the advancement of its use in such applications is the characteristic stereoselectivity that the enzyme exhibits, as well as the rates of hydrolysis. From previous studies, it is clear that the wild-type enzyme naturally prefers the isomer that corresponds to the least toxic isomer of

the nerve agent (Li et al., 2001). This is true in the case of both the sarin and soman analogs that have been used as substrates for PTE.

There have been several strategies used to modify the stereoselectivity of the enzyme, as well as enhance the rates of hydrolysis. Among them, the methodology of directed evolution and random mutagenesis has been employed targeting residues within the active site of PTE. This thesis describes efforts towards the goal of improving phosphotriesterase for enhanced hydrolysis against the individual toxic isomer of sarin and soman.

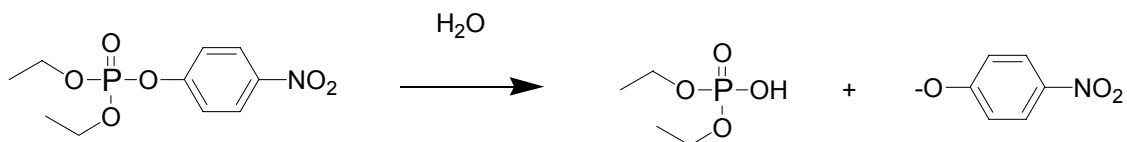
## CHAPTER II

### STEREOSELECTIVE DETOXIFICATION OF SARIN AND SOMAN ANALOGS

#### Introduction

Activated organophosphate triesters and organophosphonate diesters are very toxic materials because of their inherent ability to inhibit the enzyme acetylcholinesterase (AChE). This property has been exploited over the last half century through the development of numerous commercial insecticides for agricultural and household uses. For example, in the USA today, there are approximately 40 organophosphate insecticides registered for use by the Environmental Protection Agency. Each year approximately 100 million pounds of insecticides, including acephate, malathion, and chlorpyrifos are applied to the environment for the control of a variety of insects and other pests (Aspelin and Grube, 1999). The organophosphate insecticides inactivate AChE through the irreversible phosphorylation of an active site serine residue. The persistence of organophosphate insecticides in the soil is significantly diminished through microbial degradation. One of the primary bacterial detoxification mechanisms for organophosphate esters is enzymatic hydrolysis.

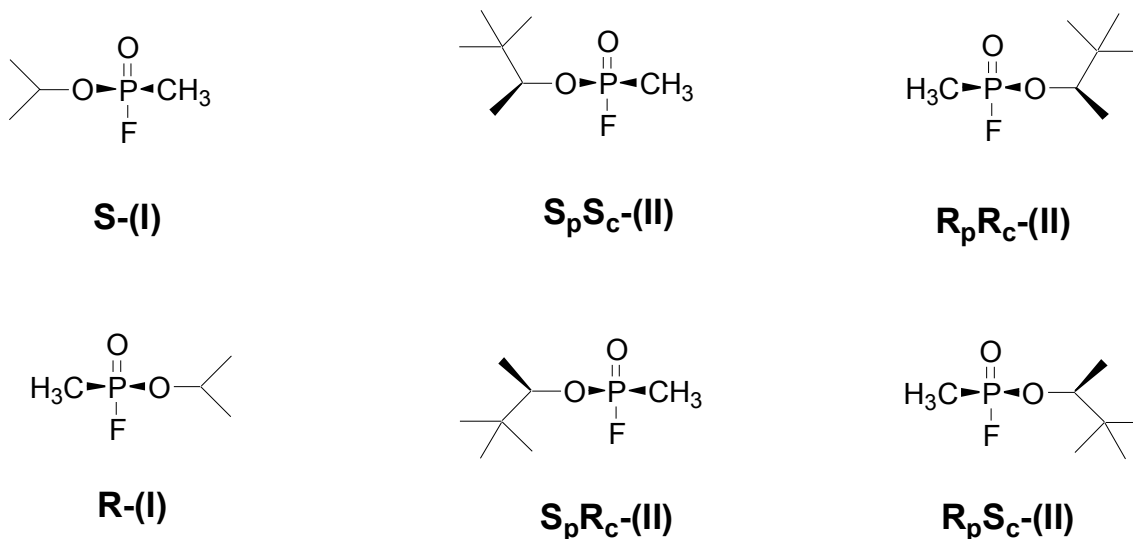
The phosphotriesterase (PTE) from *Pseudomonas diminuta* is the best-characterized enzyme for the hydrolytic detoxification of organophosphate nerve agents (Raushel and Holden, 2000). This enzyme is a zinc metalloprotein, which catalyzes the hydrolysis of a wide variety of organophosphates and related phosphonates with a high catalytic turnover and broad substrate specificity (Omburo et al., 1992). For example, the  $k_{\text{cat}}$  and  $k_{\text{cat}}/K_m$  values for the insecticide paraoxon are approximately  $10^4 \text{ s}^{-1}$  and  $10^8 \text{ M}^{-1}\text{s}^{-1}$ , respectively (Omburo et al, 1993). The hydrolysis of paraoxon is illustrated in Scheme 1.



Scheme 1. The hydrolysis of paraoxon results in *para*-nitrophenol and diethyl phosphoric acid.

The x-ray crystal structure of PTE, determined by the Holden laboratory, has shown that the protein folds in a ‘TIM-barrel’ motif that is embedded with a binuclear zinc center at the active site (Benning et al., 1995)(Vanhook et al., 1996). The zinc metallo-center of PTE is homologous to the binuclear  $Ni^{2+}$ -center found in urease (Jabri et al., 1995). These enzymes are members of the amidohydrolase superfamily (Holm and Sander., 1997).

It has previously been demonstrated that the bacterial PTE will hydrolyze, and thus detoxify, the military organophosphate nerve agents sarin and soman, although the turnover numbers for these compounds do not rival the rate constants for the enzymatic hydrolysis of insecticides such as paraoxon (Dumas et al., 1989)(Di Sioudi et al., 1999).

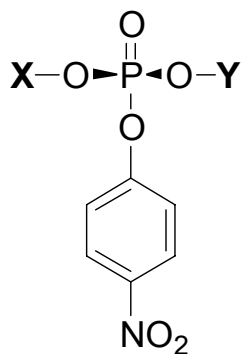


Scheme 2. The chemical structures of the individual stereoisomers of the nerve agents, sarin (I) and soman (II).

Nevertheless, the catalytic properties of the wild type PTE make it the leading candidate for the enzymatic detoxification of organophosphate nerve agents under a variety of field conditions. However, of particular concern is the differential toxicity for the stereoisomers of the nerve agents, sarin and soman. Sarin has a single chiral center at phosphorus while soman possesses an additional center of asymmetry within the pinacolyl substituent. The structures of these stereoisomers are illustrated in Scheme 4. It has been determined that the  $S_p$ -enantiomer of sarin inactivates AChE approximately  $10^4$  times faster than the  $R_p$ -enantiomer (Benschop and De Jong, 1988). For soman, the two  $S_p$ -diastereomers inactivate AChE approximately  $10^5$  times faster than the two  $R_p$ -diastereomers (Benschop et al., 1984).

The wild type PTE is moderately stereoselective for the hydrolysis of chiral organophosphate triesters. All possible combinations of the substituents methyl, ethyl,

isopropyl, and phenyl have been synthesized and characterized as substrates for PTE using the template depicted in Scheme 3 (Hong and Raushel, 1999).



Scheme 3. The general skeleton of phosphate substrates for PTE, in which *X* and *Y* represent different alkyl groups.

In every case the preferred stereoisomer is the one where the substituent *Y* is bulkier than the substituent *X*. The ratios of the experimental  $k_{\text{cat}}/K_m$  values for the  $S_p$ - and  $R_p$ -enantiomers in this series of stereoisomers ranged from 1 to 90 (Hong and Raushel, 1999). These results have been shown to be consistent with the physical dimensions of the subsites within the active site of PTE.

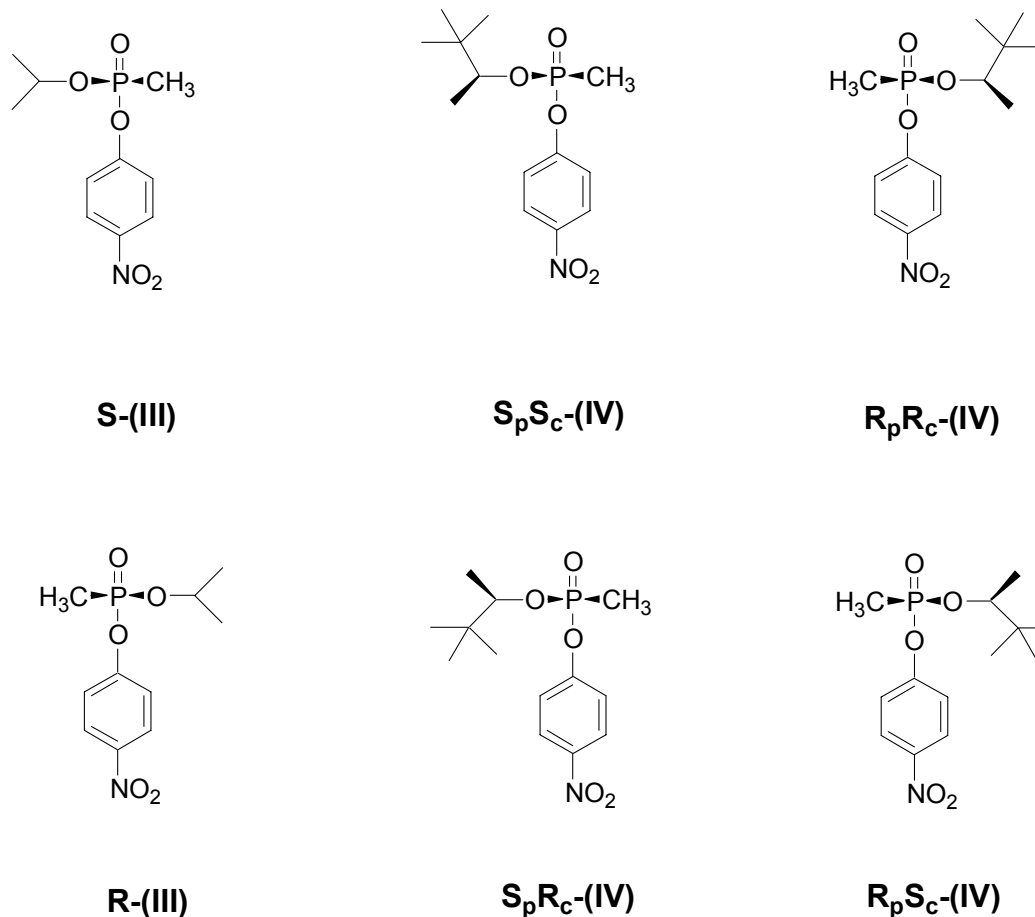
In this chapter, the stereoselective properties of the wild type PTE toward chiral analogs of sarin and soman were examined. Since the individual stereoisomers for these nerve agents were not readily available, novel chemo-enzymatic syntheses of chiral analogs, where the leaving group fluoride has been replaced with *p*-nitrophenol, were developed by Dr. Wen-Shan Li. This substitution provides for a convenient optical signal of the cleavage event. For the sarin analog the relative rates of hydrolysis for the two enantiomers varied by

an order of magnitude when the wild type PTE was used as a catalyst. With the soman analog, the relative rates of hydrolysis differed by nearly four orders of magnitude. A small number of mutations within the active site of PTE were able to reverse the stereoselectivity exhibited by the wild type enzyme.

## **Materials and Methods**

### *Materials*

Restriction enzymes and T4 DNA ligase were obtained from Promega or New England Biolabs. Wizard Miniprep DNA Purification System was purchased from Promega. Gene Clean DNA purification kit was purchased from Bio 101. Oligonucleotide synthesis and DNA sequencing reactions were conducted by the Gene Technology Laboratory of Texas A&M University. All of the substrates used in the following experiments, with the exception of paraoxon, were synthesized by Wen-Shan Li (Li et al., 2001). The chemical structures of the individual stereoisomers of the sarin analog (III) and the soman analog (IV) are shown in Scheme 4.



Scheme 4. The structures of the individual stereoisomers are shown for the GB analog (III) and GD analog (IV).

#### *Site Directed Mutagenesis*

Changes to the amino acid sequence of the phosphotriesterase enzyme were initiated by cassette mutagenesis of the *opd* gene within the plasmid pJW01 (Chen-Goodspeed et al., 2001a,b). Unique restriction sites on either side of the codon to be mutated were identified and the targeted site was excised with the appropriate enzymes. The digested fragment was purified by agarose gel electrophoresis. The two mutagenic primers were annealed by



incubating 20  $\mu\text{L}$  of 1-2  $\mu\text{M}$  of each oligonucleotide with 2  $\mu\text{L}$  of T4 DNA ligase buffer at 72  $^{\circ}\text{C}$  for five minutes, and then incubated at 25  $^{\circ}\text{C}$  for one hour. The annealed oligonucleotides and restricted pJW01 plasmid were ligated with T4 DNA ligase at 16  $^{\circ}\text{C}$  overnight and then transformed into *E. coli* BL-21 cells. The mutated plasmids were sequenced to ensure that no other alterations were introduced during the mutagenic protocols.

### *Purification of Enzymes*

The mutants and the wild type PTE were expressed in *E. coli* BL-21 cells as previously described (Kuo and Raushel, 1994). PTE and the mutant enzymes were purified according to the protocol of Omburo et al. (Omburo et al., 1992). SDS-PAGE indicated that the purified mutants were the same size as the wild type PTE and were at least 95% pure. Apoenzyme was prepared according to an established procedure and then reconstituted with 5 equivalents of  $\text{CoCl}_2$  (Omburo et al., 1992).

### *Kinetic Measurements and Data Analysis*

The enzymatic hydrolysis of paraoxon, and the sarin (isopropyl *p*-nitrophenyl methyl phosphonate) and soman (*p*-nitrophenyl pinacolyl methyl phosphonate) analogs, were measured by monitoring the formation of *p*-nitrophenol at 400 nm ( $\epsilon = 17,000 \text{ M}^{-1} \text{ cm}^{-1}$ ) and 25  $^{\circ}\text{C}$  using a Gilford Model 260 spectrophotometer. The reactions were conducted in 50 mM CHES buffer, pH 9.0, for paraoxon and the sarin analogs, while 10% methanol was added to improve the solubility of the soman analogs. The kinetic constants were obtained by fitting the data to Equation 2.1, in which  $v$  is the initial velocity,  $V_m$  is the maximal velocity,  $A$  is the concentration of substrate, and  $K_m$  is the Michaelis constant.

$$v = V_m A / (K_m + A) \quad (2.1)$$

### *Substrate Specificity*

The substrate specificity for the racemic sarin (III) and soman (IV) analogs was conducted at a total concentration of 35  $\mu$ M in 50 mM CHES, pH 9.0 at 25  $^{\circ}$ C. The addition of potassium hydroxide was used to confirm the total concentration of the substrate analog. The hydrolysis of substrate was monitored spectrophotometrically by the appearance of *p*-nitrophenol at 400 nm. The temperature was kept constant by the use of a circulating water bath.

The PTE mutants, G60A and I106A-F132A-H257Y were used in the stereoselectivity experiments. The mutant G60A was the first enzyme added, and allowed to hydrolyze half of the total substrate within 15 minutes, as determined spectrophotometrically. After half of the substrate was hydrolyzed, the second enzyme, I106A-F132A-H257Y, was added and allowed to hydrolyze the remaining substrate. The entire reaction was over in 30 minutes. The reaction was also done with the enzymes in reverse order such that I106A-F132A-H257Y was added first, and then G60A was added second.

## **Results**

### *Selection of G60A and I106A-F132A-H257Y and Kinetic Analysis of the Chiral Sarin*

#### *Analogs*

A library of active site mutants of PTE was surveyed in order to identify enzymes that were more stereoselective for the  $R_p$ -enantiomer than the wild-type enzyme. This same library was also probed for mutant enzymes that would prefer the  $S_p$ -enantiomer relative to

the  $R_p$ -enantiomer. The two mutants, G60A and I106A-F132A-H257Y, were selected for these experiments on the basis of previous results using similar compounds as substrates.

Chen-Goodspeed et al. determined that G60A shared the same order or stereoselectivity as wild type, and had higher rates for almost all of the substrates tested. In every case, the mutant G60A preferred the  $S_p$  isomer over the  $R_p$  isomer (Chen-Goodspeed et al., 2001a). The preference varied from a  $k_{cat}/K_m$  ratio of 12:1 for  $S_p$ : $R_p$  methyl ethyl *p*-nitrophenyl phosphate to 15,000:1 for  $S_p$ : $R_p$  phenyl isopropyl *p*-nitrophenyl phosphate. As a note, the  $S_p$  isomer of the phosphate substrates described in Chen-Goodspeed et al. corresponds to the  $R_p$  isomer of the phosphonates described in this study.

In contrast, the stereoselectivity of I106A-F132A-H257Y is reversed relative to the wild type PTE as described by another investigation done by Chen-Goodspeed et al. (Chen-Goodspeed et al., 2001b). In general, the triple mutant had a higher catalytic efficiency for the  $R_p$  isomer than for the  $S_p$  isomer of the chiral substrates tested. However, the ratio of preference was more modest than those described for G60A, with the highest  $k_{cat}/K_m$  ratio of hydrolysis of 10:1 reported for  $R_p$ : $S_p$  phenyl methyl *p*-nitrophenyl phosphate. The I106A-F132A-H257Y mutant was found to have an enhanced stereoselectivity for the  $S_p$  isomer of the sarin analog while the mutant G60A possessed a preference for the  $R_p$  isomer.

The differing chiral preferences for these two mutants are graphically shown in Figures 2.1 and 2.2. In this experiment, G60A was able to hydrolyze only one stereoisomer at a significant rate of the racemic mixture while I106A-F132A-H257Y was able to hydrolyze the remaining stereoisomer (Figure 2.1). This discovery permitted the utilization of these two isomers in the kinetic resolution of either stereoisomer from the racemic mixture. When the G60A mutant was used as the hydrolytic catalyst, the  $S_p$  isomer was

isolated in high yield with a very low contamination by the  $R_p$  isomer. The  $R_p$  isomer was isolated in high yield and excellent enantiomeric excess using the mutant I106A-F132A-H257Y (Figure 2.2). However, the I106A-F132A-H257Y mutant exhibits less stereoselectivity than the G60A mutant, as seen when both Figures 2.1 and 2.2 are compared.

The purified enantiomers of the sarin analogs,  $S_p$  and  $R_p$ , in addition to the racemic mixture, were tested as substrates for the wild-type enzyme and the two mutant enzymes, G60A and I106A-F132A-H257Y. For the wild-type enzyme the  $k_{cat}$  for the  $R_p$  isomer is approximately 9 times faster than the  $S_p$  isomer, as graphically depicted in Figure 2.3. The  $k_{cat}/K_m$  is 20 times more favorable in the direction of  $R_p$  to  $S_p$  isomer, as shown in Figure 2.4. For the mutant G60A, the chiral preference for the  $R_p$  isomer of the sarin analog is enhanced relative to the wild-type enzyme. Thus, the ratios of  $k_{cat}$  and  $k_{cat}/K_m$  for G60A are 50- and 140-fold more favorable, respectively, for the  $R_p$  stereoisomer. In contrast, the  $k_{cat}$  for the triple mutant is 10 times greater for the  $S_p$  isomer than the  $R_p$  isomer while  $k_{cat}/K_m$  is 30-fold higher for the same isomer. The kinetic constants are presented in Table 2.1.

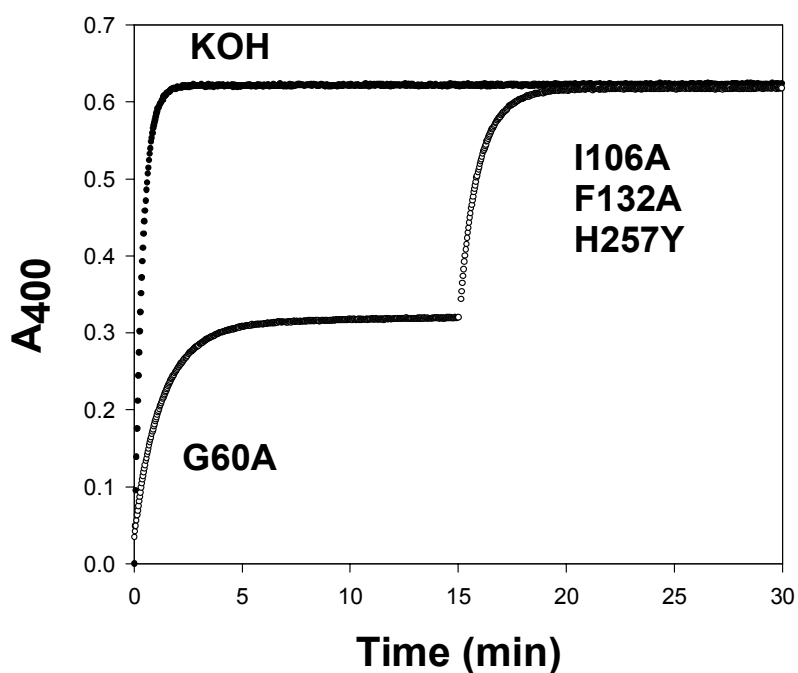


Figure 2.1. Time course for the hydrolysis of the racemic sarin analog (III) using the mutant forms of PTE. The total concentration of the sarin analog ( $36 \mu\text{M}$ ) was determined by the addition of KOH. The PTE mutant G60A was added at time zero to hydrolyze the  $R_p$  enantiomer to completion. After 15 min., the I106A-F132A-H257Y mutant form of PTE was added to hydrolyze the  $S_p$  enantiomer.

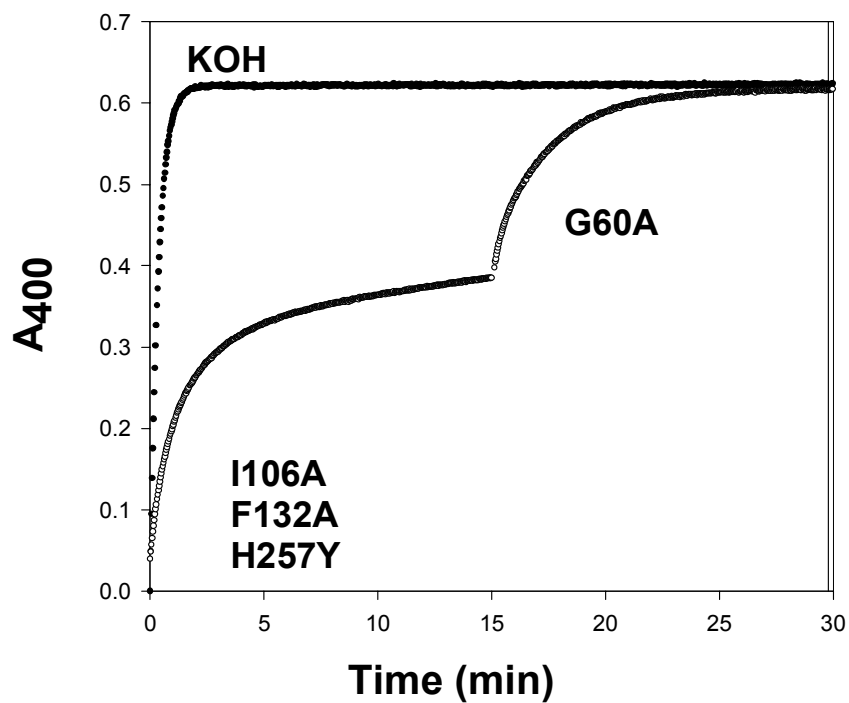


Figure 2.2. Time course for the hydrolysis of the racemic sarin analog (III) using the mutant forms of PTE. The total concentration of the sarin analog ( $36 \mu\text{M}$ ) was determined by the addition of KOH. The PTE mutant I106A-F1332A-H257Y was added at time zero to hydrolyze the  $S_p$  enantiomer to completion. After 15 min., the G60A mutant form of PTE was added to hydrolyze the  $R_p$  enantiomer.

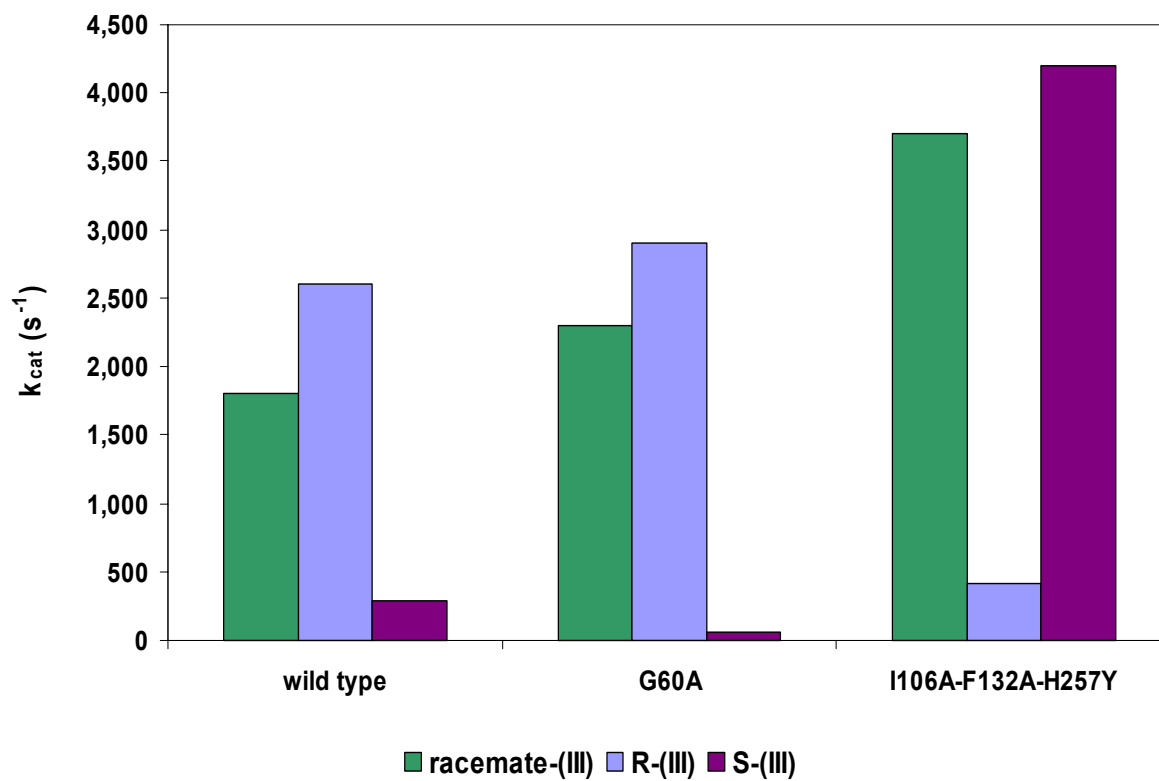


Figure 2.3. The turnover rate for racemic GB analog (III),  $R_p$ -isomer, and  $S_p$ -isomer hydrolysis for wild type protein, and the mutants, G60A and I106A-F132A-H257Y.

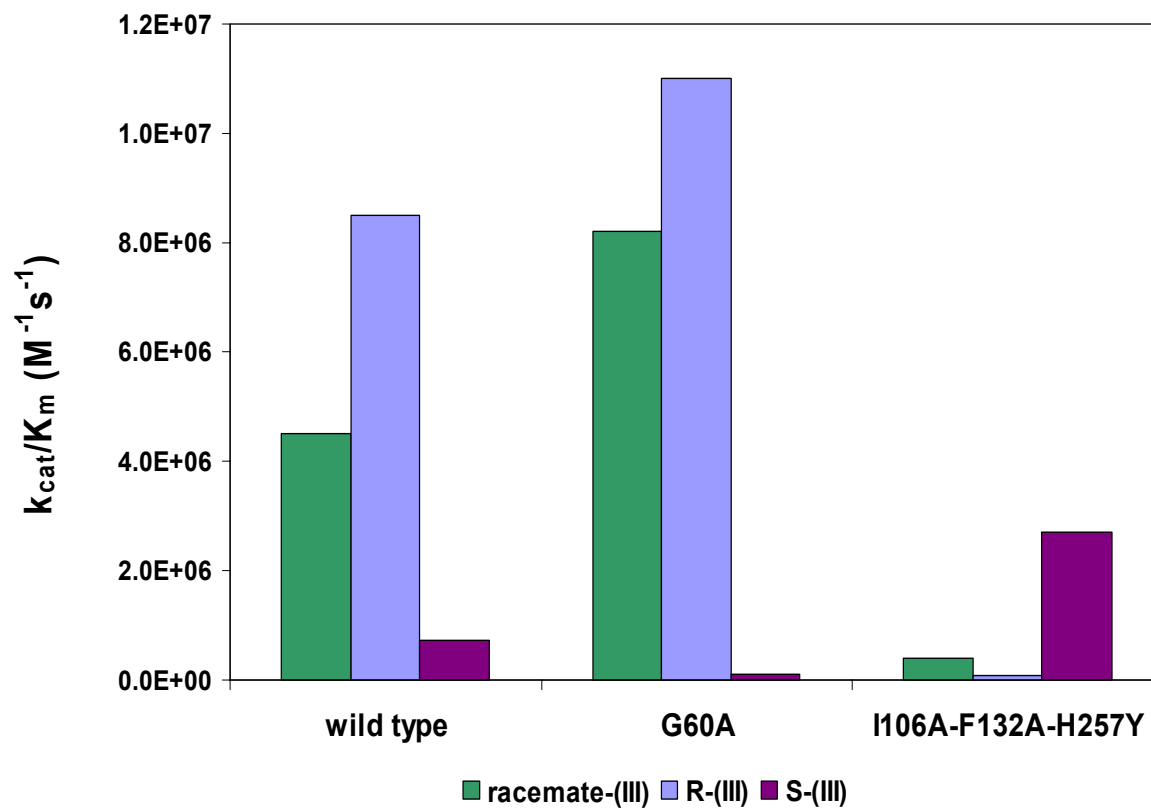


Figure 2.4. The value of  $k_{cat}/K_m$  of racemic GB analog (III),  $R_p$ -isomer, and  $S_p$ -isomer hydrolysis for wild type protein, and the mutants, G60A and I106A-F132A-H257Y.



Table 2.1. The kinetic constants for hydrolysis of the sarin and soman isomers and racemate, as catalyzed by the wild type PTE, G60A, and I106A-F132A-H257Y.

	$K_m$ (mM)			$k_{cat}$ ( $s^{-1}$ )			$k_{cat}/K_m$ ( $M^{-1}s^{-1}$ )		
	WT	G60A	I106A F132A H257Y	WT	G60A	I106A F132A H257Y	WT	G60A	I106A F132A H257Y
racemic sarin analog	0.44±0.01	0.28±0.03	5.1±0.59	1800±15	2300±110	3700±370	4.5x10 <sup>6</sup>	8.5 x10 <sup>6</sup>	7.3 x10 <sup>5</sup>
<b>R<sub>p</sub></b> sarin analog	0.31±0.02	0.27±0.02	4.6±0.37	2600±69	2900±200	410±17	8.2x10 <sup>6</sup>	1.1 x10 <sup>7</sup>	9.0 x10 <sup>4</sup>
<b>S<sub>p</sub></b> sarin analog	0.72±0.01	0.80±0.05	1.6±100	290±2.2	58±1.7	4200±130	4.1 x10 <sup>5</sup>	7.2 x10 <sup>4</sup>	2.7 x10 <sup>6</sup>
racemic soman analog	1.1±0.01	1.0±0.27	1.6±0.37	44±2.0	93±13	4.6±0.56	4.0 x10 <sup>4</sup>	9.3 x10 <sup>4</sup>	2.9 x10 <sup>3</sup>
<b>R<sub>c</sub></b> diastereomers	1.1±0.34	0.75±0.23	0.98±0.27	40±6.6	92±13	5.6±0.63	3.6 x10 <sup>4</sup>	1.2 x10 <sup>5</sup>	5.6 x10 <sup>3</sup>
<b>S<sub>c</sub></b> diastereomers	1.0±0.09	0.29±0.06	0.93±0.29	9.6±0.44	16±0.99	1.1±0.14	9.6 x10 <sup>3</sup>	5.3 x10 <sup>4</sup>	1.2 x10 <sup>3</sup>
<b>R<sub>p</sub>R<sub>c</sub></b> soman analog	0.34±0.07	0.82±0.18	1.1±0.31	48±2.4	120±11	0.28±0.03	1.6 x10 <sup>5</sup>	1.5 x10 <sup>5</sup>	2.8 x10 <sup>2</sup>
<b>R<sub>p</sub>S<sub>c</sub></b> soman analog	0.42±0.02	0.59±0.12	4.5±1.1	4.8±0.06	33±3.0	0.25±0.05	1.2 x10 <sup>4</sup>	5.6 x10 <sup>4</sup>	5.6 x10 <sup>1</sup>
<b>S<sub>p</sub>R<sub>c</sub></b> soman analog	0.78±0.17	10±2.3	1.2±0.07	0.30±0.03	0.07±0.01	11±0.39	3.8 x10 <sup>2</sup>	7.0 x10 <sup>0</sup>	9.2 x10 <sup>3</sup>
<b>S<sub>p</sub>S<sub>c</sub></b> soman analog	2.4±0.49	2.8±0.41	1.7±0.23	0.04±0.01	0.02±0.00	2.1±0.16	1.6 x10 <sup>1</sup>	7.1 x10 <sup>0</sup>	1.2 x10 <sup>3</sup>

*Preparation and Kinetic Analysis of the Chiral Soman Analogs*

Two sets of diastereomers were constructed and obtained from Dr. Wen-Shan Li (Li et al., 2001). They were of a single configuration at the chiral carbon center, but racemic at the phosphorus center  $R_pR_c/S_pR_c$  and  $R_pS_c/S_pS_c$ . For the fully racemic mixture, the wild-type PTE hydrolyzed one of the stereoisomers at a significantly faster rate than the others (Figure 2.5). By analogy with the known stereoselectivity exhibited by the wild-type enzyme for the sarin analogs and other phosphotriester substrates, the more rapidly hydrolyzed stereoisomer within each pair of diastereomers was concluded to be of the  $R_p$  configuration (Hong and Raushel, 1999). This conclusion was supported by the preference for the same isomer when the mutant G60A was tested with these two pairs of diastereomers.

The differential rates of hydrolysis exhibited by G60A and I106A-F132A-H257Y for the two stereoisomers contained within the  $S_pR_c/R_pR_c$  mixture of diastereomers are graphically presented in Figures 2.6 and 2.7, and the same is shown for the differential rates of hydrolysis within the  $S_pS_c/R_pS_c$  mixture of diastereomers in Figures 2.8 and 2.9. It is assumed in both cases that G60A is preferentially hydrolyzing the  $R_p$  isomers while I106A-F132A-H257Y is preferentially hydrolyzing the  $S_p$  isomers. These contrasting stereoselectivities made it technically feasible to use these two mutants as catalysts for the kinetic resolution of the two pairs of diastereomers into the four individual stereoisomers.

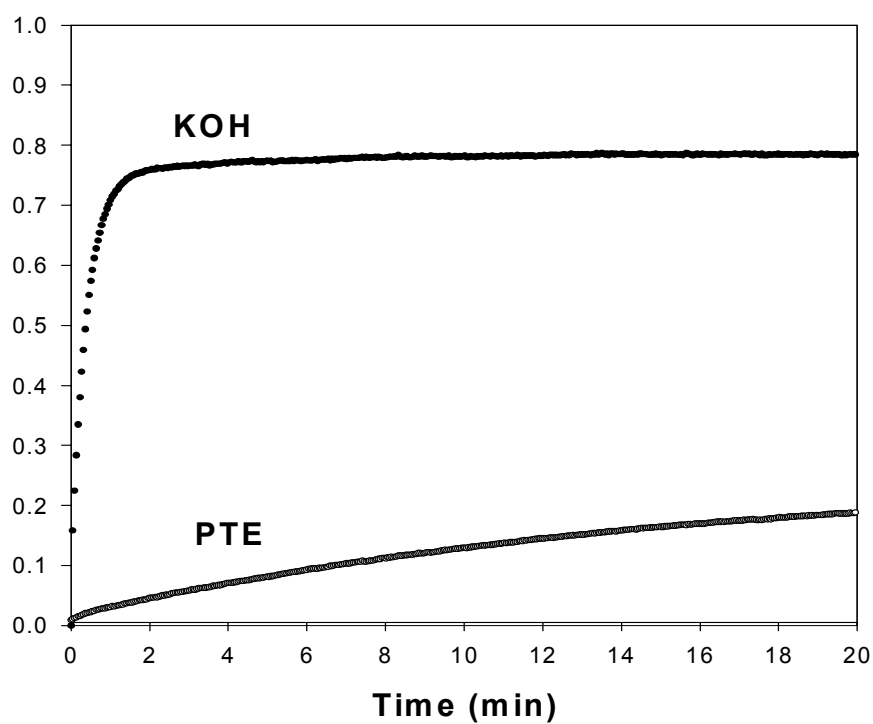


Figure 2.5. The preferential hydrolysis of one isomer within the racemic soman mixture (IV) containing 4 isomers, as exhibited by the wild type PTE. The total concentration of the soman analog was  $45 \mu\text{M}$ , as determined by the addition of KOH.

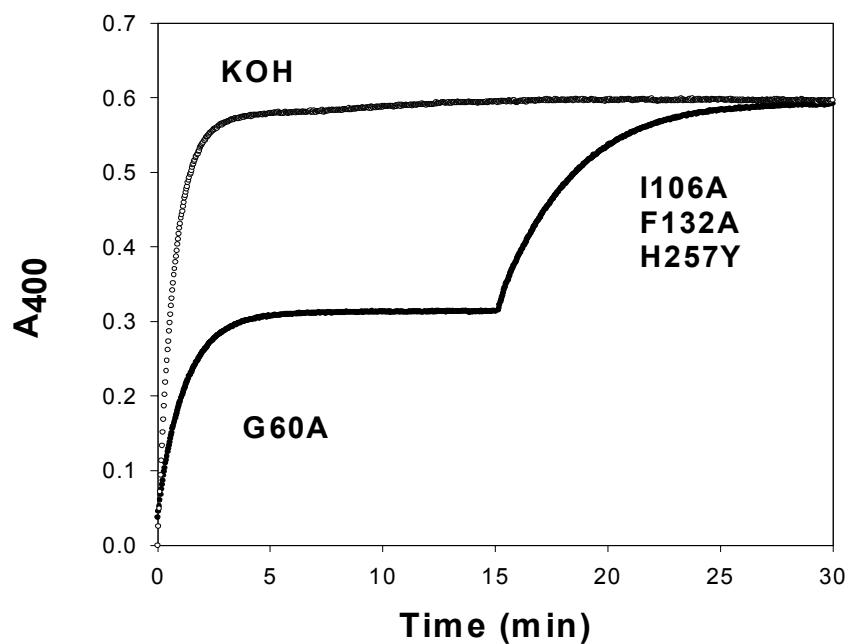


Figure 2.6. Time course for the hydrolysis of the diastereomeric mixture of the soman analog  $S_pR_c-(IV)$  and  $R_pR_c-(IV)$  using G60A as the first enzyme. The total concentration of the soman analog ( $35 \mu\text{M}$ ) was determined by the addition of KOH. The PTE mutant G60A was added at time zero to hydrolyze the  $R_pR_c$  enantiomer. After 15 min., the I106A-F132A-H257Y mutant form of PTE was added to hydrolyze the  $S_pR_c$  enantiomer.

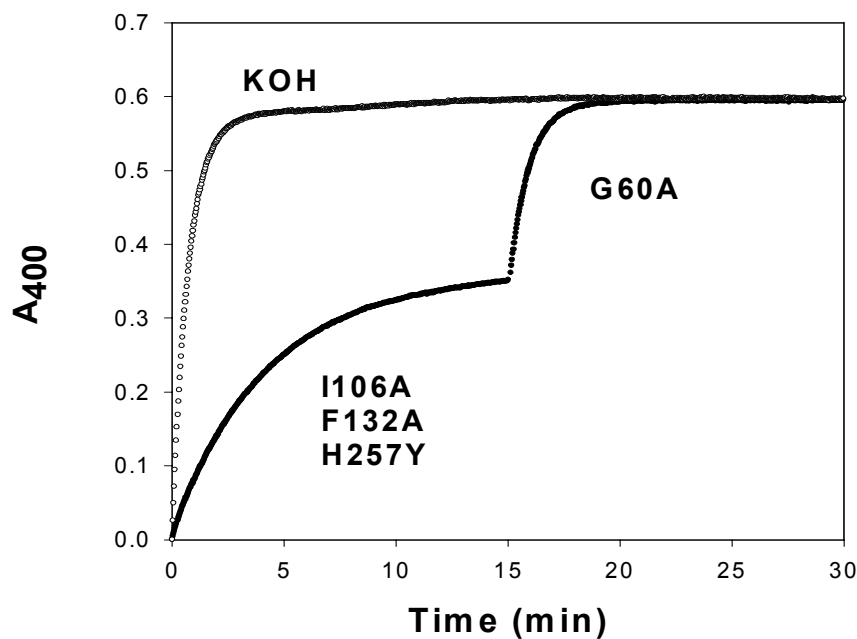


Figure 2.7. Time course for the hydrolysis of the diastereomeric mixture of the soman analog  $S_pR_c$ -(IV) and  $R_pR_c$ -(IV) using I106A-F132A-H257Y as the first enzyme. The total concentration of the soman analog ( $35 \mu\text{M}$ ) was determined by the addition of KOH. The PTE mutant I106A-F132A-H257Y was added at time zero to hydrolyze the  $S_pR_c$  enantiomer. After 15 min., the G60A mutant form of PTE was added to hydrolyze the  $R_pR_c$  enantiomer.

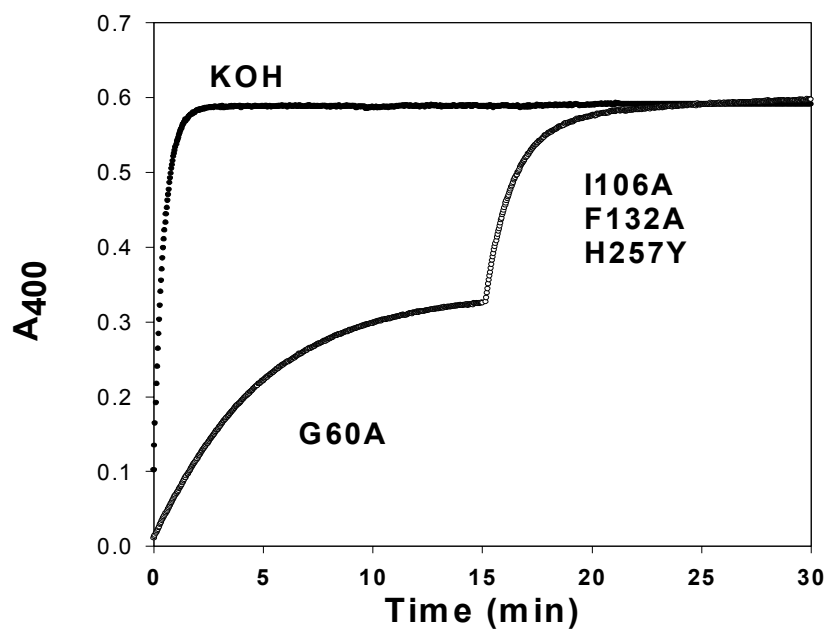


Figure 2.8. Time course for the hydrolysis of the diastereomeric mixture of the soman analog  $S_pS_c$ -(IV) and  $R_pS_c$ -(IV) using G60A as the first enzyme. The total concentration of the soman analog ( $35 \mu\text{M}$ ) was determined by the addition of KOH. The PTE mutant G60A was added at time zero to hydrolyze the  $R_pS_c$  enantiomer. After 15 min., the I106A-F132A-H257Y mutant form of PTE was added to hydrolyze the  $S_pS_c$  enantiomer.

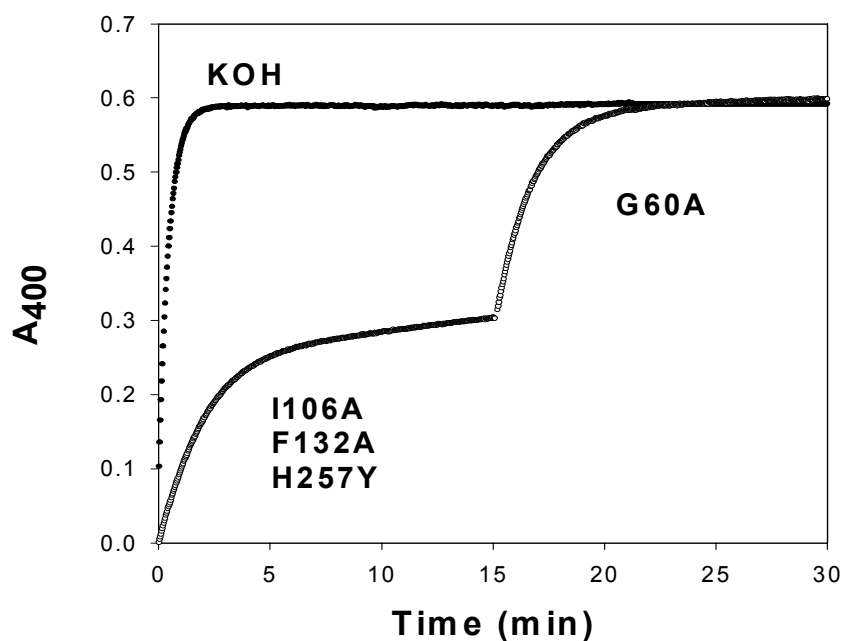


Figure 2.9. Time course for the hydrolysis of the diastereomeric mixture of the soman analog  $S_pS_c$ -(IV) and  $R_pS_c$ -(IV) using I106A-F132A-H257Y as the first enzyme. The total concentration of the soman analog ( $35 \mu\text{M}$ ) was determined by the addition of KOH. The PTE mutant I106A-F132A-H257Y was added at time zero to hydrolyze the  $S_pS_c$  enantiomer. After 15 min., the G60A mutant form of PTE was added to hydrolyze the  $R_pS_c$  enantiomer.

*Stereoselectivity of Wild Type PTE, G60A, and I106A-F132A-H257Y for the Soman Analog*

The four soman analog stereoisomers were characterized as substrates for the wild-type PTE and the two mutant enzymes, G60A and I106A-F132A-H257Y. The  $k_{\text{cat}}$  for each individual stereoisomer of the GD analog is graphically represented on a log scale in Figure 2.10, while the  $k_{\text{cat}}/K_m$  for each stereoisomer of the GD analog is shown in Figure 2.11. For the wild-type enzyme the catalytic selectivity as measure by  $k_{\text{cat}}/K_m$  is  $R_pR_c : R_pS_c : S_pR_c : S_pS_c$  of 10,000:750:23:1. The same relative order of isomeric preferences was found for G60A as in the wild type. With the G60A, the relative rates were greater than wild type and were determined to be 21,000:8000:1:1. In contrast, the triple mutant preferred the isomers in the following order;  $S_p R_c$ ,  $S_p S_c$ ,  $R_p R_c$ , and then  $R_p S_c$ . The stereoselectivity was determined to be reversed with the triple mutant. The  $k_{\text{cat}}/K_m$  ratio of rates for hydrolysis was also substantially smaller, and was reported as 5:1:164:21 for the corresponding isomers. The kinetic parameters are listed in Table 2.1.



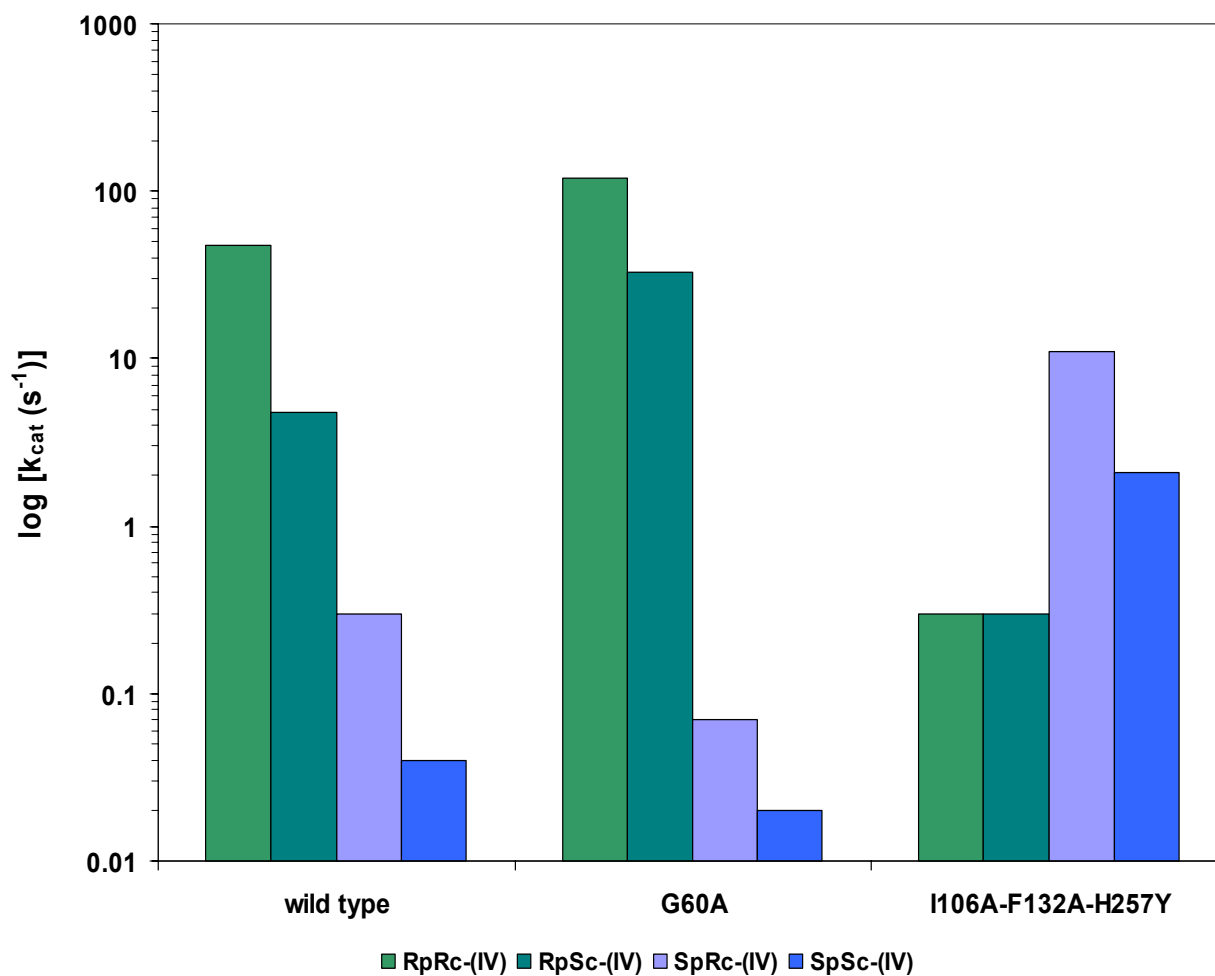


Figure 2.10. The turnover rate of the individual stereoisomers of the GD analog (IV) for wild type protein, and the mutants, G60A and I106A-F132A-H257Y, as expressed in the log plot of the  $k_{\text{cat}}$ .

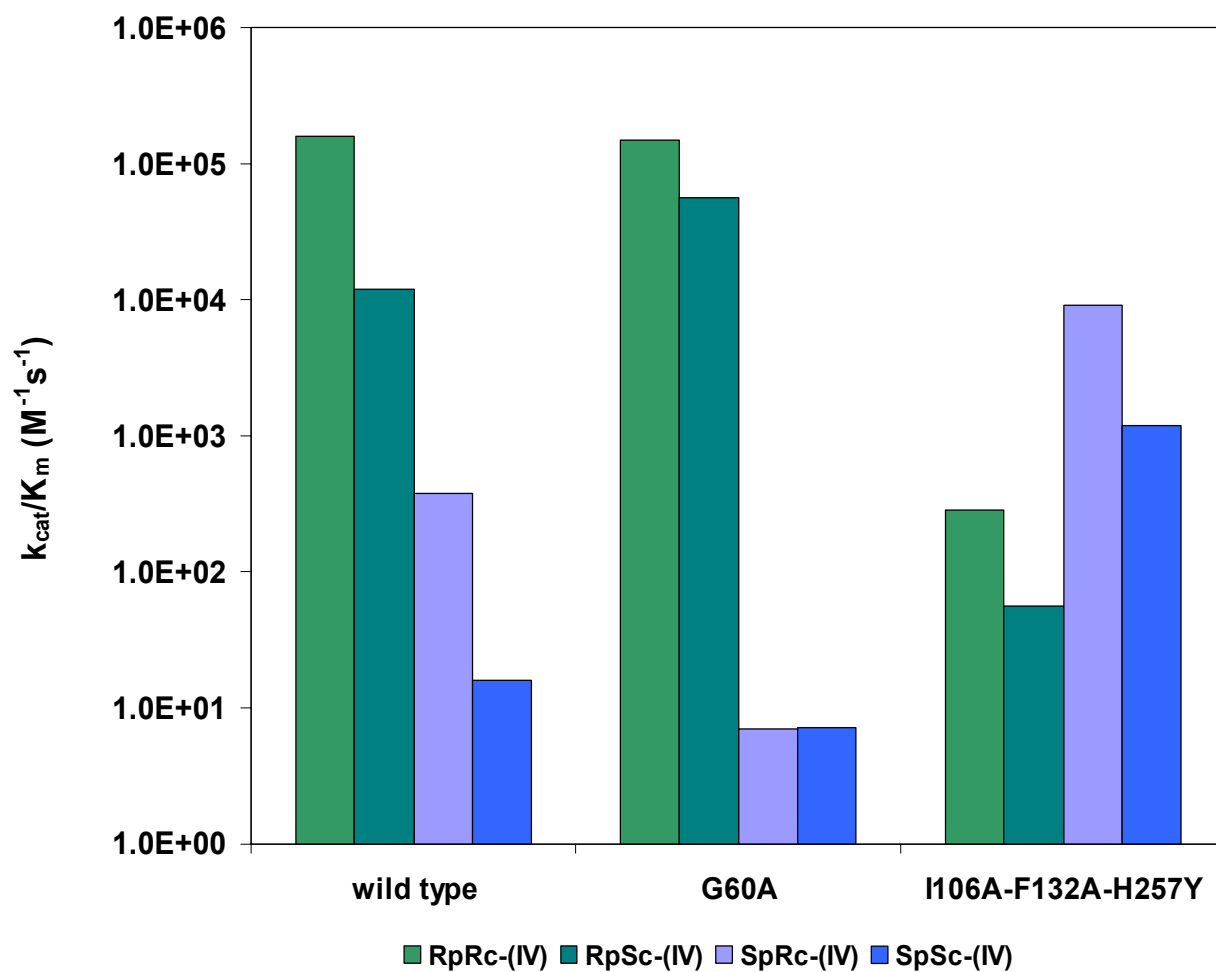


Figure 2.11. The catalytic efficiency of the individual stereoisomers of the GD analog (IV) for wild type protein, and the mutants, G60A and I106A-F132A-H257Y.

## Discussion

### *Enzymatic Hydrolysis of Sarin Analogs*

The wild type PTE and the selected mutants were able to catalyze the hydrolysis of both stereoisomers of the sarin analog (III). For the R<sub>p</sub>-isomer, the  $k_{\text{cat}}$  and  $k_{\text{cat}}/K_{\text{m}}$  with the wild type enzyme was  $2600 \text{ s}^{-1}$  and  $8.2 \times 10^6 \text{ M}^{-1} \text{ s}^{-1}$ , respectively. The magnitude of these values was approximately one third the size of the kinetic constants obtained for the insecticide paraoxon. Thus, a substantial fraction of the inherent catalytic power within the native PTE was available for the hydrolysis of the R<sub>p</sub>-isomer of the sarin analog. For the S<sub>p</sub>-enantiomer of the sarin analog, the values of  $k_{\text{cat}}$  and  $k_{\text{cat}}/K_{\text{m}}$  were approximately an order of magnitude smaller. The stereoselectivity towards the R<sub>p</sub>-enantiomer of the sarin analog was consistent with the previously determined substrate specificity of PTE using a small library of organophosphate triesters (Hong and Raushel, 1999). The catalytic preference for the hydrolysis of the sarin analog R<sub>p</sub> over S<sub>p</sub> can also be rationalized structurally on the basis of the optimized size of the subsites for the binding of the *i*-propyl substituent relative to that for the methyl substituent of the two enantiomers (Benning et al., 2000).

The wild type PTE was able to hydrolyze the analog for the most toxic stereoisomer of the nerve agent sarin. However, the rate of hydrolysis of this substrate was significantly slower than the turnover rate with the less toxic R<sub>p</sub>-enantiomer of the sarin analog. If PTE is going to achieve its full potential as an agent for the catalytic destruction of toxic nerve agents, then derivatives of this protein with altered kinetic properties must be constructed and more fully characterized. The catalytic properties of the triple mutant of PTE, I106A-F132A-H257Y, effectively demonstrated that structural

variants of PTE can be readily constructed with significant enhancements to both  $k_{\text{cat}}$  and  $k_{\text{cat}}/K_m$  for the initially slower  $S_p$ -isomer of the sarin analog. This objective was met through a subtle alteration of the two binding subsites within the active site of PTE that dictate the catalytic and substrate specificity of this enzyme.

Prior x-ray crystallographic analysis of PTE in the presence of a bound inhibitor by the Holden laboratory has localized those residues that dictate the structural dimensions of these binding subsites (Benning et al., 2000). In the example presented here, the *small subsite* was slightly enlarged through the mutation of Ile106 and Phe132 to alanine residues while the *large subsite* was diminished in size by the conversion of His257 to a phenylalanine. These three changes enhanced the turnover rate of the initially slower  $S_p$ -isomer by approximately one order of magnitude and reduced the rate of turnover of the initially faster  $R_p$ -isomer by the same amount. The location of the residues previously mentioned is shown in a diagram of the active site in Figure 2.12.

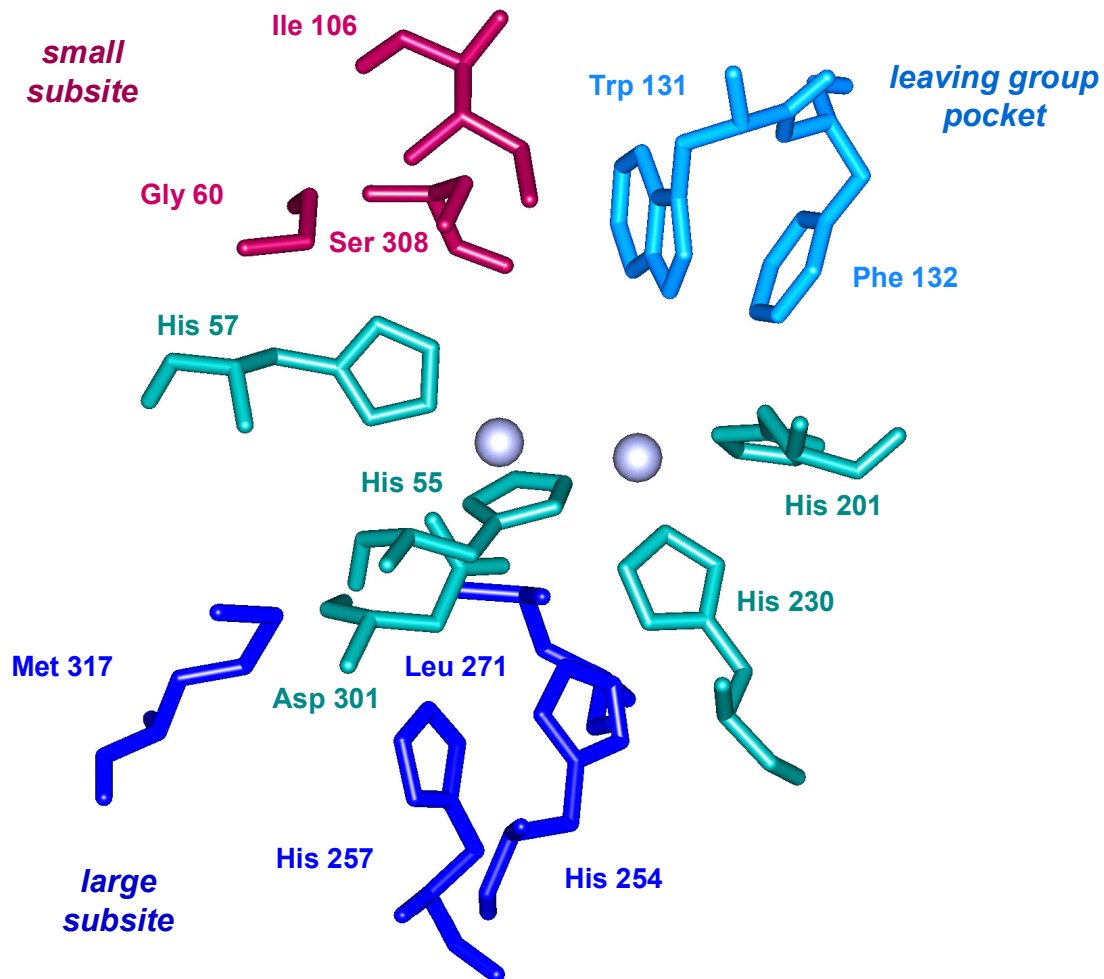


Figure 2.12. The active site residues and ligand binding residues of PTE. Both residues Gly 60 and Ile 106 are located within the *small subsite*, while the residue His 257 is located within the *large subsite*.

### *Enzymatic Hydrolysis of Soman Analogs*

All four analogs of the soman stereoisomers were substrates for the wild type PTE. However, there was a rather large variance in the rate of substrate turnover that was very much dependent on the specific stereochemical configuration around the phosphorus center and the chiral pinacolyl substituent. The extreme values of  $k_{\text{cat}}$  differed by a factor of approximately 1000 while  $k_{\text{cat}}/K_{\text{m}}$  for the  $R_pR_c$ -isomer of the soman analog was four orders of magnitude greater than it was for the corresponding  $S_pS_c$  isomer. The two diastereomers with the  $R_p$  configuration were better substrates than the two diastereomers with the  $S_p$  configuration. Moreover, the  $R_c$  isomer of the chiral pinacolyl substituent was preferred in both pairs of diastereomers by a factor of about 10 over the  $S_c$  configuration.

A comparison in the rates of overall turnover for the soman analog with the sarin analog clearly showed that the pinacolyl substituent was tolerated less well within the active site of the wild type enzyme than was the *i*-propyl group. For example, the  $R_p$  isomer of the sarin analog was hydrolyzed about two orders of magnitude faster than the  $R_pR_c$  isomer of the soman analog. A similar difference was found in the corresponding values of  $k_{\text{cat}}/K_{\text{m}}$ . The data collected in this investigation also demonstrated that the wild type PTE hydrolyzed the two stereoisomers of the most toxic analogs of soman significantly more slowly than the analogs of the two least toxic stereoisomers. If PTE is going to be an effective reagent for the catalytic destruction of soman then the rate of hydrolysis of the most toxic stereoisomers must be significantly enhanced through site-directed and combinatorial mutagenesis. For the  $S_pS_c$  enantiomer, an increase in  $k_{\text{cat}}$  and  $k_{\text{cat}}/K_{\text{m}}$  of nearly 4 orders of magnitude should be obtainable. The catalytic properties of the I106A-F132A-H257Y mutant with the analogs of the two  $S_p$  diastereomers of soman

showed that such gains in catalytic activity are likely to be achieved. This mutant had a 50-fold enhancement in the value of  $k_{\text{cat}}$  and a 75-fold increase in  $k_{\text{cat}}/K_m$  for the  $S_pS_c$  enantiomer of soman.

### *Enzymatic Hydrolysis of the Nerve Agents, Sarin and Soman*

In preliminary experiments conducted in collaboration with Drs. Steven Harvey and Joseph DeFrank of the Edgewood Chemical and Biological Center, the wild type PTE, in addition to the I106A-F132A-H257Y and G60A mutant enzymes, has been shown to catalyze the hydrolysis of racemic mixtures of sarin and soman. The time courses have also been shown to be bi-phasic and thus consistent with differential turnover rates for the individual enantiomers. Turnover rates exceeded  $1000 \text{ s}^{-1}$  for the I106A-F132A-H257Y mutant PTE with racemic sarin. This value is three times larger than is the value of the wild type enzyme but the catalytic constants for the individual enantiomers have not, as yet, been determined. For racemic soman, the G60A mutant has a turnover number that is greater than  $10 \text{ s}^{-1}$  and is approximately three times faster than the wild type enzyme. The turnover numbers for the sarin and soman analogs measured in the investigation reported here were very similar to the preliminary values obtained for sarin and soman themselves. Therefore, the utilization of the chiral enantiomers in the development of novel mutants of PTE with enhanced catalytic activities will be productive. Experiments designed to sample a larger fraction of amino acid sequence space within the vicinity of the two binding subsites of PTE will be described in the following chapters.

## CHAPTER III

### EVOLUTION OF PTE TOWARDS EFFICIENT SOMAN HYDROLYSIS

#### **Introduction**

##### *Directed Evolution*

There are several protein engineering techniques that can be used to "breed" a desired feature or characteristic into an existing protein. Traditionally, the methods that have been used extensively in the past involve rational site directed mutagenesis. By examining the position of an inhibitor complexed within the enzyme active site, obvious key residues were identified from crystal structure data. Those residues were then targeted for manipulation in structure-function studies. However, there are limitations for the success of this methodology because relatively few residues are seen as important, as initially determined by the 3-D structure. These limitations have led to the development of newer techniques. Semi-rational mutagenesis techniques incorporate the possibility that functionally and catalytically important residues may not be obvious from examining the 3-D crystal data alone.

One example of this applied methodology was seen with directed evolution studies of cytochrome P450 BM-3 from *Bacillus megaterium* (Glieder et al., 2002). The wild type P450 BM-3 acts as a monooxygenase for medium-chain (i.e. C12-C18) fatty acids in the presence of oxygen and NADPH. However, it has very low activity with octane, as determined by colorimetric assays with *p*-nitrophenoxy octane as the alkane substrate. After several generations of random mutagenesis, the mutant 139-3 was



isolated and identified as having the fastest alkane hydrolase activity of any known enzyme (Glieder et al., 2002). This particular mutant had a total of eleven amino acid substitutions, of which only one residue was in direct contact with the substrate as implied by the 3-D structural data (Glieder et al., 2002).

Screens and selections are necessary for detecting the desired characteristic of mutants in directed evolution experiments (Olsen et al., 2000). Both techniques require the use of a marker to indicate the presence or absence of a particular feature. The process of screening is more time consuming and less efficient than a selection. In a screen, all phenotypes must be sampled as seen in the “blue-white” screen, which screens for bacteria that have lost the ability to digest x-gal. This particular screen has been particularly useful to detect the interruption of a multiple cloning site (MCS) within a selectable marker region of a plasmid, so that the disruption (e.g. insertion of a portion of a gene) of the MCS would result in the formation of a white colony forming unit (CFU). The bacteria that are able to digest the sugar form a blue CFU. This is a useful technique if the sample number is relatively small. If a large number of samples were to be surveyed, the use of a selection would be more practical. In a selection, the desired phenotype is physically linked to survival, which results in the removal of all unwanted phenotypes. As an example, plating on an ampicillin plate will allow only bacteria that have ampicillin resistance to grow.

#### *Directed Evolution of PTE*

PTE is a good candidate for future use in decontamination applications for a number of reasons. The structure of the enzyme has been determined, and many

biophysical studies have been done, elucidating the structure-function relationship (Benning et al., 1995)(Chen-Goodspeed et al., 2001a,b). Other appealing aspects of this protein are its thermodynamic stability and its ability to be produced in quantity (Grimsley et al., 1997). Of the available nerve agent detoxifying proteins, it is the only one that is capable of cleaving phosphorus-oxygen, phosphorus-fluorine, phosphorus-sulfur, and phosphorus-cyanide bonds (Di Sioudi et al, 1999). In addition, PTE has already been shown to successfully act as a protective agent when injected into mice before nerve agent exposure (Tuovinen et al., 1994). However, the obstacle that remains to be solved is improving the rate of hydrolysis for which the enzyme catalyzes reactions. To date, the optimum PTE mutant hydrolyzes soman (GD) at the rate of  $40 \text{ s}^{-1}$  (Steven P. Harvey, personal communication). In order for PTE to become fully effective at detoxifying the nerve agents, the catalytic activity of the enzyme must be significantly enhanced. It is believed that the enzymatic properties of this protein may be greatly improved via directed mutagenesis experiments. In this chapter, efforts directed at enhancing the catalytic efficiency of hydrolysis for the toxic isomers of the soman (GD) analog will be described.

## **Materials and Methods**

### *Mutagenesis*

The plasmid, *pJWO1*, was derived from a pBS+ vector (Stratagene) and designed to contain the *opd* gene without the 29 amino acid leader sequence. This construct served as the template for all of the following genetic manipulations, and the map of the 4.1 kb plasmid is shown in Figure 3.1.

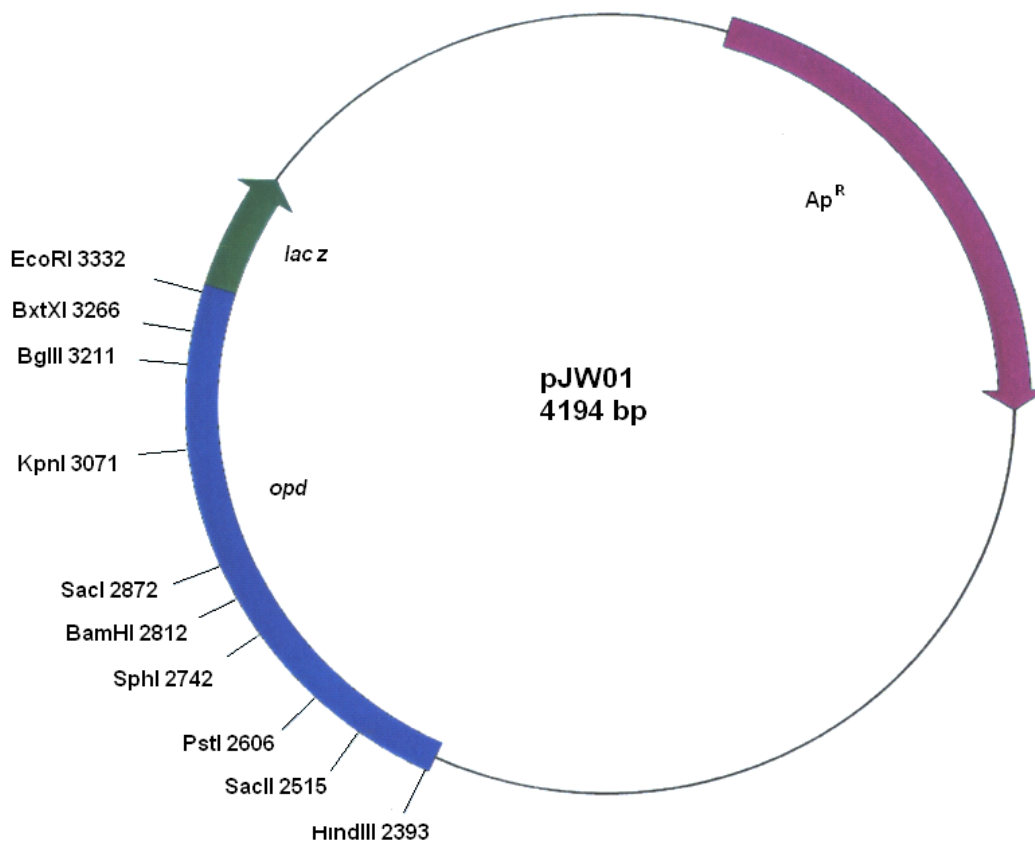


Figure 3.1. A map of the plasmid, *pJW01*, shows a multiple cloning site similar to that of pUC 18, as well as ampicillin resistance (Ap<sup>R</sup>), and the *lacZ* gene. This map was constructed using Savvy, a plasmid drawing program available by SeWeR at the following web address (<http://www.bioinformatics.org/savvy/cgi-bin/savvy.cgi>) (Basu, 2001).

Protein libraries were constructed by random mutagenesis methodology, involving the use of degenerate oligonucleotides targeting specific regions within the gene. Single and double substitution libraries were constructed by either cassette mutagenesis or Quikchange mutagenesis (Stratagene). For cassette mutagenesis, unique restriction sites on either side of the target region were identified and excised within the vector, *pJW01*. All restriction enzymes were obtained from New England Biolabs. Isolation of the restricted fragment was done by gel electrophoresis, and subsequent purification was performed by following the protocol for DNA purification (Promega Wizard DNA Purification Kit). The appropriate cassettes containing degenerate oligonucleotides for the codon corresponding to the targeted position(s) were obtained from the Gene Technologies Laboratory at Texas A&M University. In the case of Quikchange mutagenesis, a set of primers containing degenerate oligonucleotides was designed to amplify the desired linear product.

For the randomization at each position, two oligonucleotides were used and the randomization is coded as *N* or *S* within each primer, in which *N* is either A, T, C, or G and *S* is either G or C. The primers are listed in Table 3.1.

Table 3.1. The primers used for the single and double substitution libraries.

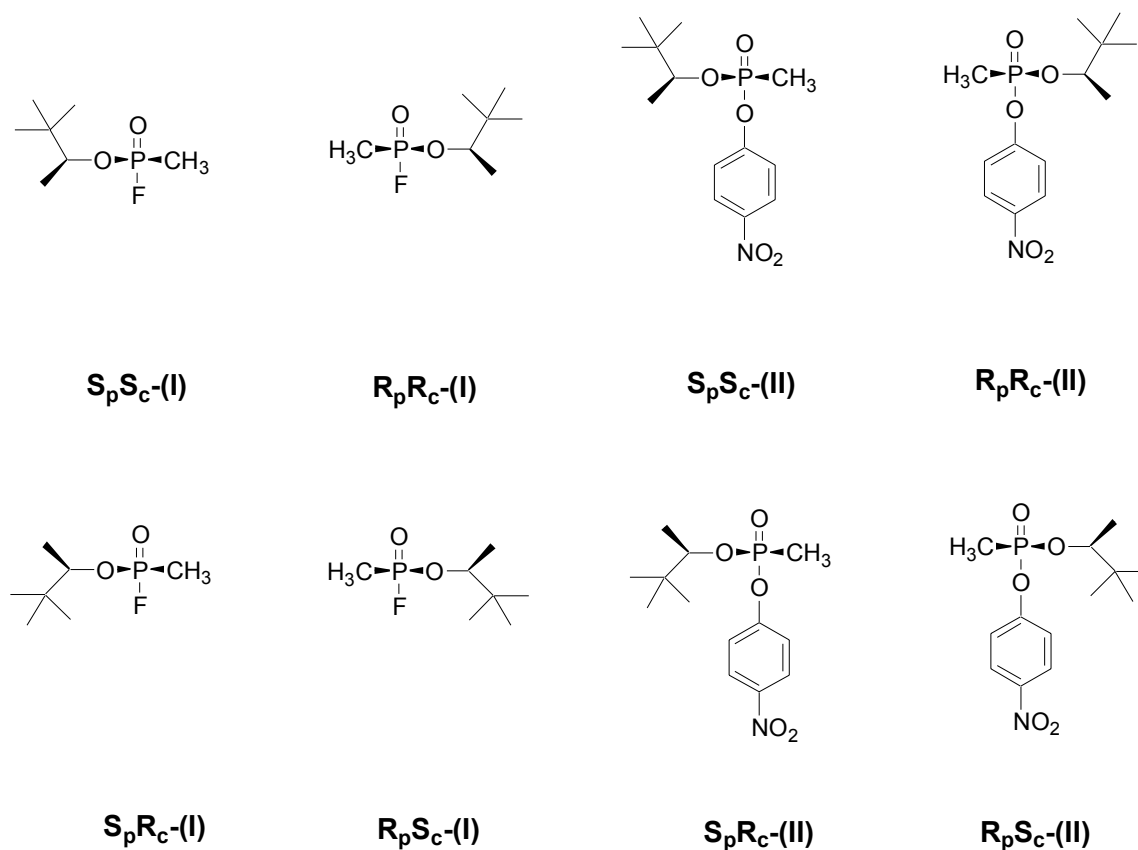
Target Residue	Primer Direction	Primer (5' to 3')
254	forward	CGGTCTGGACNNNATCCCCGACTCC
254	reverse	GGAGTGCGGGGATNNGTCCAGACCG
257	forward	GACCACATCCCGNNNTCCGCTATCG
257	reverse	GGATAGCGGANNNCGGGATGTGGTC
271	forward	CCGCTTCCGCTNNNCTGGGTATCCG
271	reverse	CGGATACCCAGNNNAGCGGAAGCGG
308	forward	GGCTGTTCCGGTTTCTCGNNNTACGTTACCAAC
308	reverse	GTTGGTAACGTANNNCGAGAAACCCGAACAG
309	forward	GGCTGTTCCGGTTTCTCGAGCANNNGTTACCAAC
309	reverse	GTTGGTAACNNNGCTCGAGAAACCCGAACAG
317	forward	CATGGACGTTNNGACCCGTGTTAACCC
317	reverse	GGGTTAACACGGTCNNNAACGTCCATG
60	forward	CCCACGAAACACATCTGCNNSTCCCTCCGGGGTTTCC
60	reverse	GGAAACCCGCGGAGGASNNGCAGATGTGTCGTGGG
106	forward	CGTTTCCACCTTCGACNNSGGCCGTGACGTTTCCC
106	reverse	GGGAAACGTCACGGCCSNNGTCGAAAGGTGGAAACG
254 and 257	forward	CTGATCGGTCTGGACNNNATCCCGNNNTCCGCTATCGGTCGTGGAAGACAATGCA
254 and 257	reverse	TTGTCTTCCAGACCGATAGCGGANNNCGGGATNNGTCCAGACCGATCAGGTAC

Ligation of the cassette with the restricted gene was performed at 16 °C overnight, using T4 DNA Ligase (New England Biolabs). Transformation was performed by electroporation, and the resulting variants were inserted in BL21 (DE3) *E. coli* cells and plated on Luria-Bertani Broth (LB) ampicillin plates. Following mutagenesis, PCR sequencing of the resulting transformants was performed to ensure randomness of sample.

#### *Culture Growth Conditions and Screening*

The resulting colony forming units (CFU) were inoculated into deep 96-well plates containing super broth (SB), 0.1 mM CoCl<sub>2</sub> and 100 µg/mL ampicillin, and incubated at 30 °C, shaking at 250 rpm for approximately 40 hours. The culture was diluted 10-fold and the cell density was measured spectrophotometrically at 600 nm. A small portion of the sample (i.e. 25 µL) of the diluted culture was used to test for paraoxonase activity, in which the resulting *p*-nitrophenol product was detected spectrophotometrically at 400 nm.

Each of the following substrates, GD analog racemate, the S<sub>p</sub> pair of isomers, and the individual S<sub>p</sub>S<sub>c</sub> isomer, was tested. Throughout each assay, the same buffer conditions were maintained: 50 mM CHES, pH 9.0, 1% (v/v) Bugbuster (Novagen), and 0.1 mM substrate. However, more of the cell culture was used for slower substrates. For example, 25 µL of culture was used for the S<sub>p</sub> pair of isomers and the S<sub>p</sub>S<sub>c</sub> isomer of the GD analog. The chemical structure of each individual isomer of GD, as well as the corresponding isomer for the GD analog, is shown in Scheme 1.



Scheme 1. The structures of the individual stereoisomers of soman (I) and the corresponding stereoisomers of the soman analog (II) used in this study.

### *Enzyme Purification*

Both the mutants and the wild-type were expressed in *Escherchia coli* BL21 cells and grown in LB, which was used to inoculate terrific broth (TB) supplemented with cobalt chloride. Expression of protein was induced by the addition of IPTG to a final concentration of 0.6 mM after 24 hours of incubation at 30 °C. The cells were harvested 40 hours post induction, and PTE was purified according to the published protocol

(Omburo et al., 1992). SDS-PAGE indicated that the purified mutants were the same size as the wild-type PTE and were at least 95% pure.

### *Kinetic Measurements and Data Analysis*

The enzymatic hydrolysis of the GD analog (*p*-nitrophenyl pinacolyl methyl phosphonate) was measured by monitoring the accumulation of *p*-nitrophenol at 400 nm ( $\epsilon = 17,000 \text{ M}^{-1} \text{ cm}^{-1}$ ) at pH 9.0, 25 °C using a Gilford Model 260 spectrophotometer. The enzyme activity was measured in 50 mM CHES, pH 9.0 containing 10 % methanol for the GD analog. One unit of activity is defined as the amount of enzyme required to catalyze the hydrolysis of one  $\mu\text{mol}$  of paraoxon per minute. The kinetic constants were obtained by fitting the data to Equation 3.1, where  $v$  is the initial velocity,  $k_{\text{cat}}$  is the turnover rate,  $A$  is the concentration of substrate, and  $K_m$  is the Michaelis constant.

$$v / E_t = k_{\text{cat}} A / (K_m + A) \quad (3.1)$$

Enzyme assays involving nerve agent were done at Edgewood Chemical Biological Center by Dr. Steven P. Harvey, and conducted with a fluoride electrode attached to a Fisher Accumet 925 meter. Reactions were conducted in a temperature-controlled vessel in a total volume of 5 mL. Buffering was provided by a 50 mM solution of bis-tris-propane, pH 7.2.

Kinetic parameters were determined from assays conducted at 25 °C. EZ-Fit™ version 5.03 software was used for determination of kinetic, and the accompanying



statistical analyses. EZ-Fit™ uses the Nelder-Mead simplex and Marquardt nonlinear regression algorithms sequentially to determine the kinetic parameters from the Michaelis-Menten plot of velocity versus substrate concentration. The program relies upon using two regression methods in tandem to fit the  $k_{cat}$ ,  $K_m$ , and inhibition data to a non-linear curve.

### *Time Course Ratios*

The ratios of rates of hydrolysis for each isomer within the racemic GD analog were determined for a group of 17 mutants and the wild type enzyme. A series of 7 serial dilutions were made for each enzyme. Each concentration was assayed with 60  $\mu$ M racemic GD analog buffered in a 50 mM CHES, pH 9.0 solution. Hydrolysis of the solution was spectrophotometrically determined by following the appearance of the *p*-nitrophenol leaving group at 400 nm. The data were fit to Equations 3.2 and 3.3 using SigmaPlot2000, and the amplitudes and rates were recorded. The rates were used in calculating the observed time course ratios.

$$y = y_0 + a(1 - e^{-bx}) \quad (3.2)$$

Equation 2. The equation describing a single exponential curve, in which  $y_0$  is the *y*-intercept,  $a$  is the amplitude of the curve,  $b$  is the rate constant, and  $x$  is a variable and the exponent.

$$y = y_0 + a(1 - e^{-bx}) + c(1 - e^{-dx}) \quad (3.3)$$

Equation 3.3. The equation describing a double exponential curve, in which  $y_0$  is the y-intercept,  $a$  and  $c$  are the amplitudes of the curve,  $b$  and  $d$  are the rate constants, and  $x$  is a variable and the exponent.

## Results

### *Construction of the Single Substitution Libraries*

A single substitution library was constructed for positions His254, His257, Leu271, Ser308, Tyr309, Met317, Gly60, and Ile106 by using the method of Quikchange with degenerate oligonucleotides targeting a specific residue. Sample randomness was confirmed by sequencing selected CFUs from each library, and is shown in Table 3.2. Transformants from each library were inoculated into two deep, 96-well growth plates containing SuperBroth.

In addition to the transformants, PTE mutants with established kinetic constants were inoculated into each culture plate as standards. The standards used in each library always included the wild type enzyme. Each library was screened with paraoxon, the racemic GD analog, the  $S_p$  pair of isomers of the GD analog, and the individual  $S_pS_c$  isomer. The results from the crude assay were determined in units of  $\text{mA}_{400} \text{ min}^{-1}$ , and were adjusted based on the cell density at 600 nm. In general, cell growth variation of 0.5 to 0.7 AU was observed after a 10  $\mu\text{L}$  of culture was diluted 25-fold. Vertical plots were constructed showing the normalized activity of the mutants with the library and the standards, and shown in the following figures for the  $S_p$  pair of isomers of the GD analog and the individual  $S_pS_c$  isomer. There was little variation in activity for the hydrolysis of paraoxon and the racemic GD analog, and the results are not shown.

Table 3.2. The identities of 5 colony forming units (CFU) isolated from each single substitution library.

<b>His 254</b>		<b>His 257</b>		<b>Leu 271</b>		<b>Ser 308</b>	
CAC	wild type	CAC	wild type	CTG	wild type	AGC	wild type
AGC	Ser	AGG	Arg	CAG	Gln	CTC	Leu
AAG	Lys	CGA	Arg	CCG	Pro	CCC	Pro
AGG	Arg	GGG	Gly	GTG	Val	AGG	Arg
GTG	Val	GCG	Ala	ATC	Ile	TCC	Ser
TGC	Cys	ATG	Met	GCG	Ala	TTC	Phe
<b>Tyr 309</b>		<b>Met 317</b>		<b>Gly 60</b>		<b>Ile 106</b>	
TAC	wild type	ATG	wild type	GGT	wild type	ATC	wild type
TTT	Phe	CTG	Leu	TGC	Cys	GAC	Asp
GAA	Glu	CTC	Leu	CCC	Pro	AGG	Arg
TGG	Trp	ACG	Thr	CTC	Leu	GAG	Glu
GTG	Val	ATC	Ile	GTC	Val	TGG	Trp
GCT	Ala	GCG	Ala	TCC	Ser	CCG	Pro

The H254X single substitution library was screened with paraoxon, the racemic GD analog, the  $S_p$  pair of GD analog isomers ( $S_pR_c/S_pS_c$ -(II)) and the individual  $S_pS_c$  isomer. However, there was very little variation for hydrolysis of paraoxon and the racemic GD analog (results not shown). The results for the hydrolysis of the  $S_p$  isomers and the  $S_pS_c$  isomer are shown in Figure 3.2, in which the standards used were wild type, G60A, I106A-F132A-H257Y, and H254G-H257W. The activity of the wild type was much higher than expected for the hydrolysis of the  $S_p$  pair of isomer. In the other libraries described, the relative order of activities is such that H254G-H257W is greater than I106A-F132A-H257Y, which is greater than wild type, which is greater than G60A. The screen results indicated the activity of all library members within H254X was equal to or lower than the activity of the known standards. Several of the most active samples were identified as having a His, Ala, or Arg at position 254.

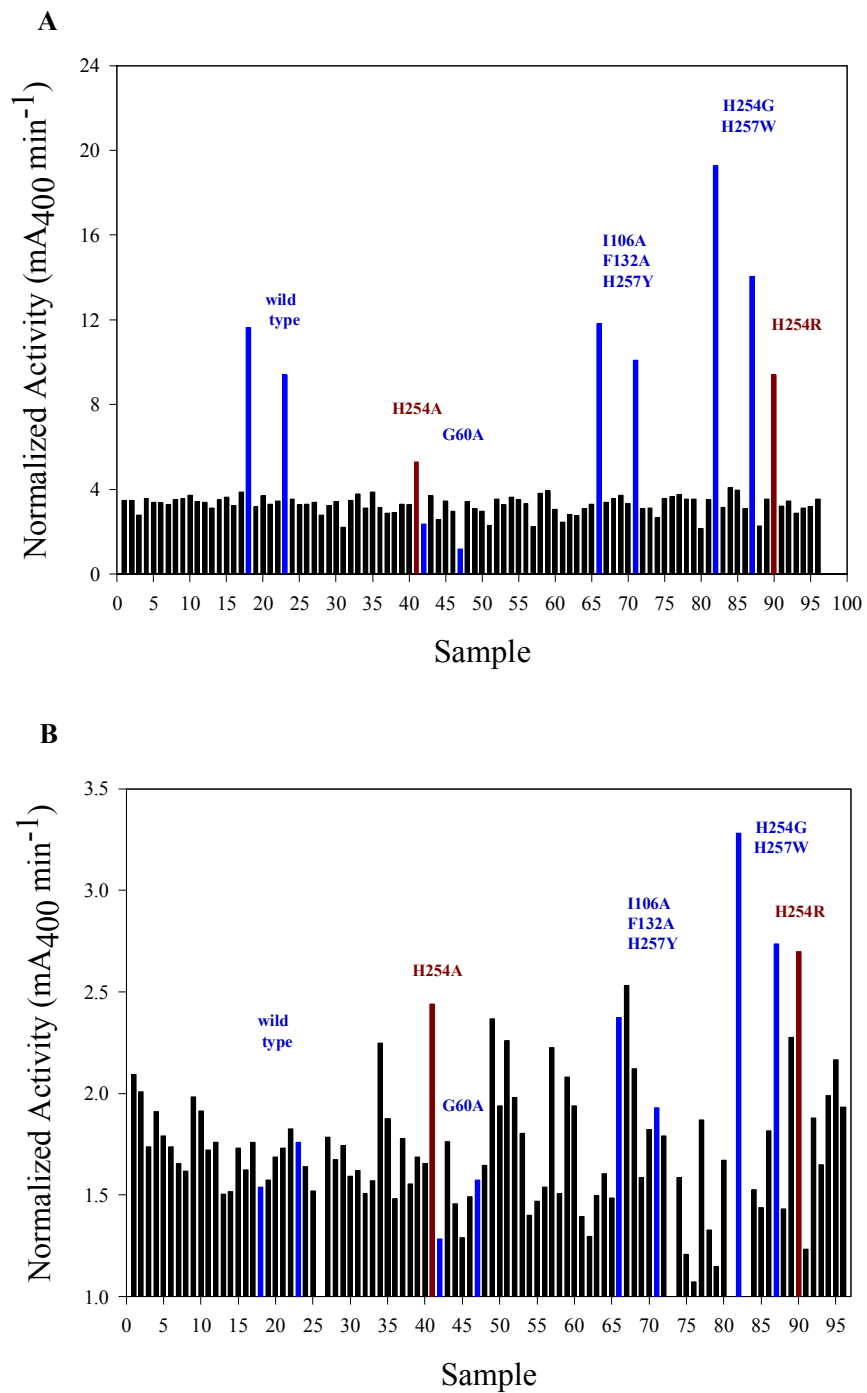


Figure 3.2. The results from the GD analog hydrolysis assays for the H254X single substitution library. The library was screened with  $S_pR_e/S_pS_e$ -(II) (A) and with  $S_pS_e$ -(II) (B).

The H257X library was screened with the  $S_p$  pair of GD analog isomers and the individual  $S_pS_c$  isomer. The standards used were wild type, H254A, H254Q-H257F, I106A-F132A-H257Y, and H254G-H257W, and they are shown in blue in Figure 3.3. In comparison to other libraries, there is variation between the levels of activity of the standards and little differentiation among them in this library. In most cases, the activity of wild type shows up among the background when assayed with the two slow substrates, the  $S_p$  pair and the  $S_pS_c$  isomer, and the relative order of activity is such that H254G-H257W-L303T is greater than H254Q-H257F, which is greater than I106A-F132A-H257Y, which is equal to H254A, but greater than wild type. However, results from this assay indicate that H2545Q-H257F has the highest activity of the standards for the hydrolysis of the  $S_p$  pair of isomers, and there is little discrepancy among the remaining standards. Many of the samples screened had activity equal to that of the parent wild type, which was higher than expected in the assay. The two members that were isolated for having increased activity for GD analog hydrolysis were identified as H257Y and H257W.

The L271X library was screened with the  $S_p$  pair of GD analog isomers and the individual  $S_pS_c$  isomer. The standards used were wild type, G60A, I106A-F132A-H257Y, and H254G-H257W. Results from the assays imply that H254G-H257W has the highest activity among the standards, followed by I106A-F132A-H257Y, and then wild type and G60A. The activity of all members was approximately the same as wild type for both the  $S_p$  pair of isomers and the  $S_pS_c$  isomer. None were higher than the I106A-F132A-H257Y or H254G-H257W standards. Two CFUs previously identified by sequencing were L271Q and L271A, as shown in Figure 3.4.

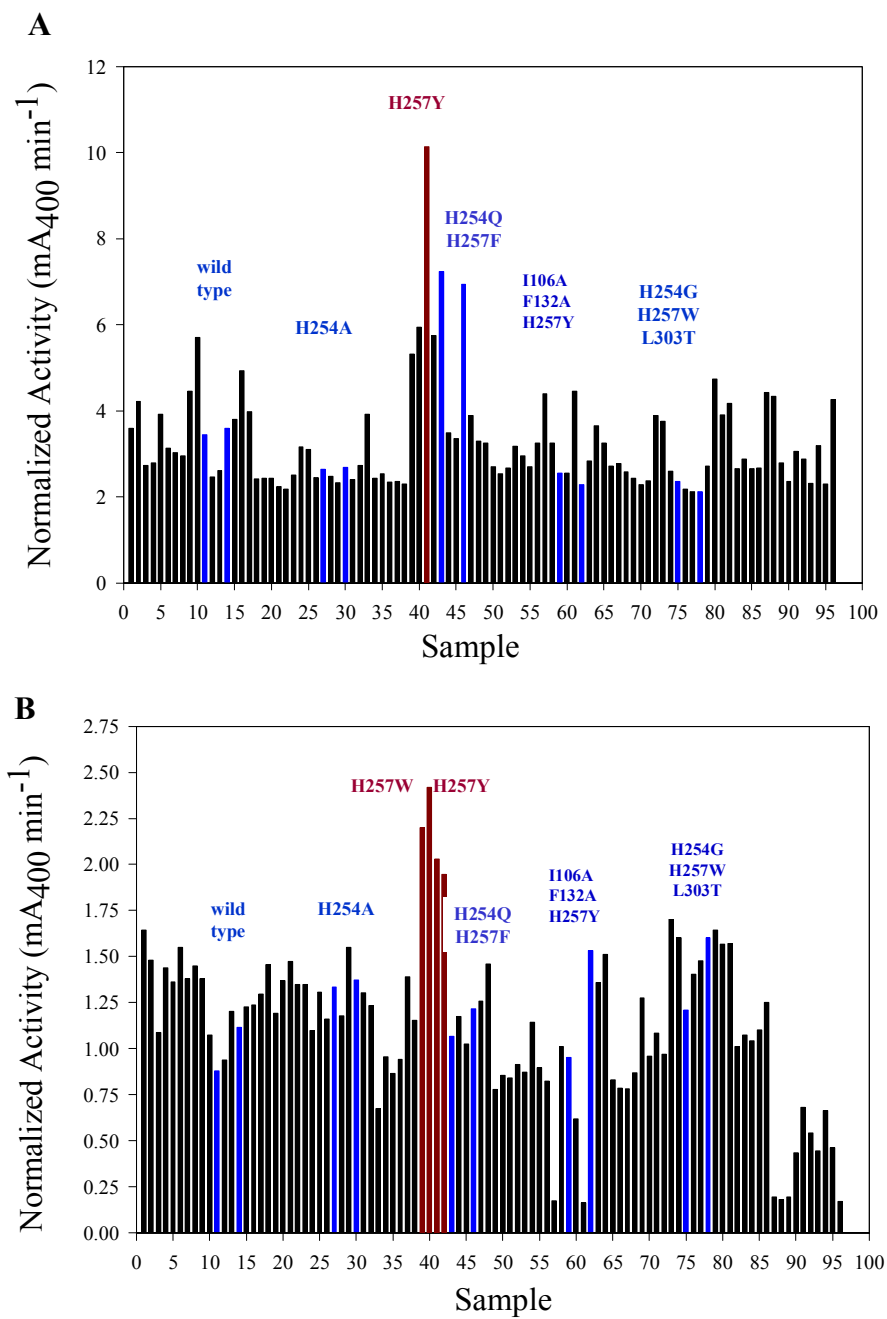


Figure 3.3. The results from the crude culture screen for the H257X single substitution library. The library was screened with  $S_pR_c/S_pS_c$ -(II) (A) and with  $S_pS_c$ -(II) (B).

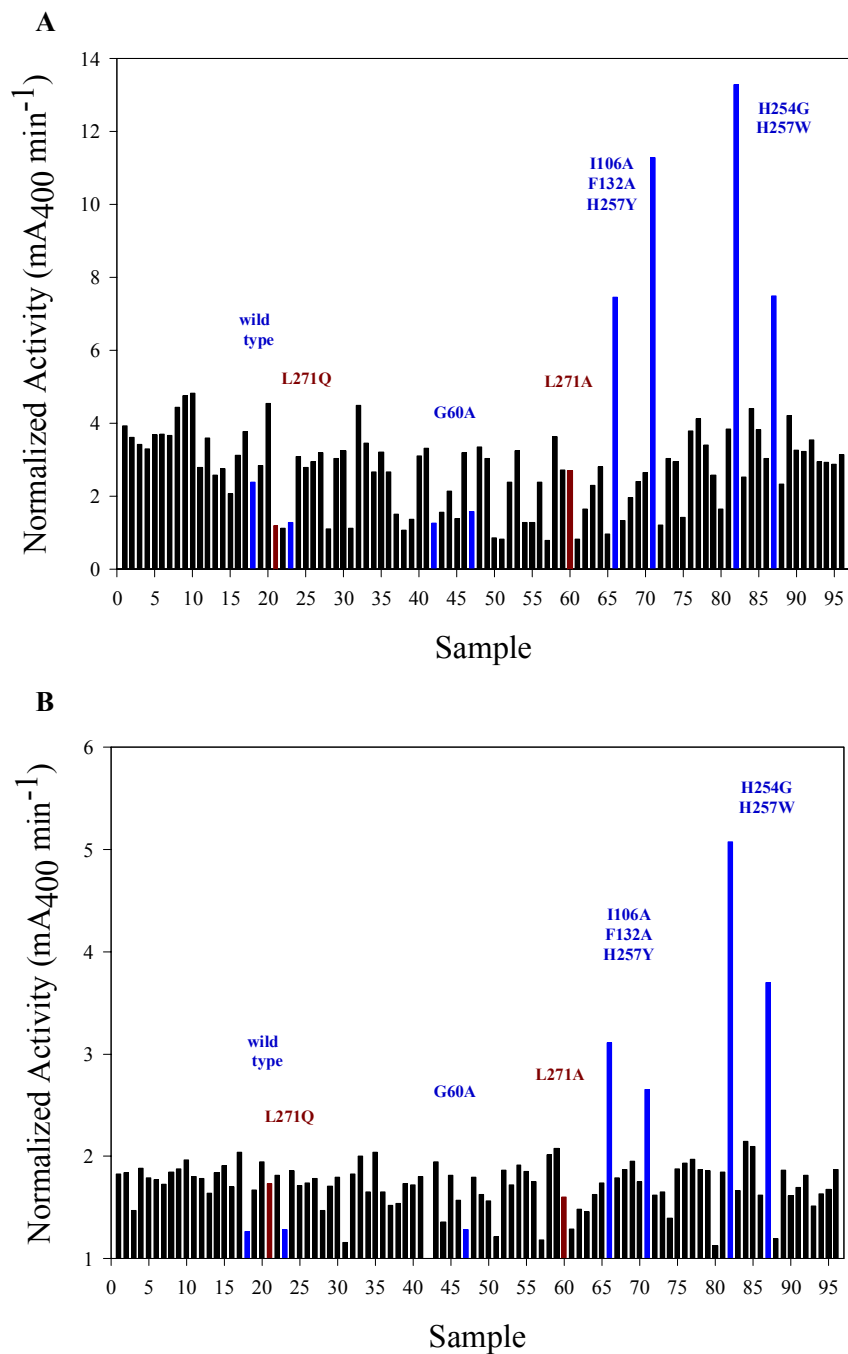


Figure 3.4. The results from the crude culture screen for the L271X single substitution library. The library was screened with  $S_pR_c/S_pS_c$ -(II) (A) and with  $S_pS_c$ -(II) (B).



The S308X library was screened with the  $S_p$  pair of GD analog isomers ( $S_pR_c/S_pS_c$ -(II)) and the individual  $S_pS_c$  isomer. However, there was relatively poor growth with this library as compared to other libraries, in terms of cell density spectrophotometrically determined at 600nm. While growth in other libraries was consistently around 0.5 to 0.7 AU at 600nm, the growth in the S308X library was slightly lower at 0.3 to 0.6 AU. Repeated attempts also resulted in poor cell growth. Standards used in this library included wild type, G60A, I106A-F132A-H257Y, and H254G-H257W. The H254G-H257W standard had the highest activity, followed by I106A-F132A-H257Y. Though, the activities of both wild type and G60A were significantly lower than other samples and do not register for the assay with the  $S_p$  pair of isomers, they do appear in position numbers 18, 23, and 42, 47 of the assay plate for the hydrolysis of the  $S_pS_c$  isomer in Figure 3.5. Many members of this single substitution library had very low activity for the  $S_p$  pair of isomers, as well as for the individual  $S_pS_c$  isomer. S308A was identified as having enhanced activity with the  $S_p$  pair of isomers, and was identified at positions 53 and 78 of the assay plate.

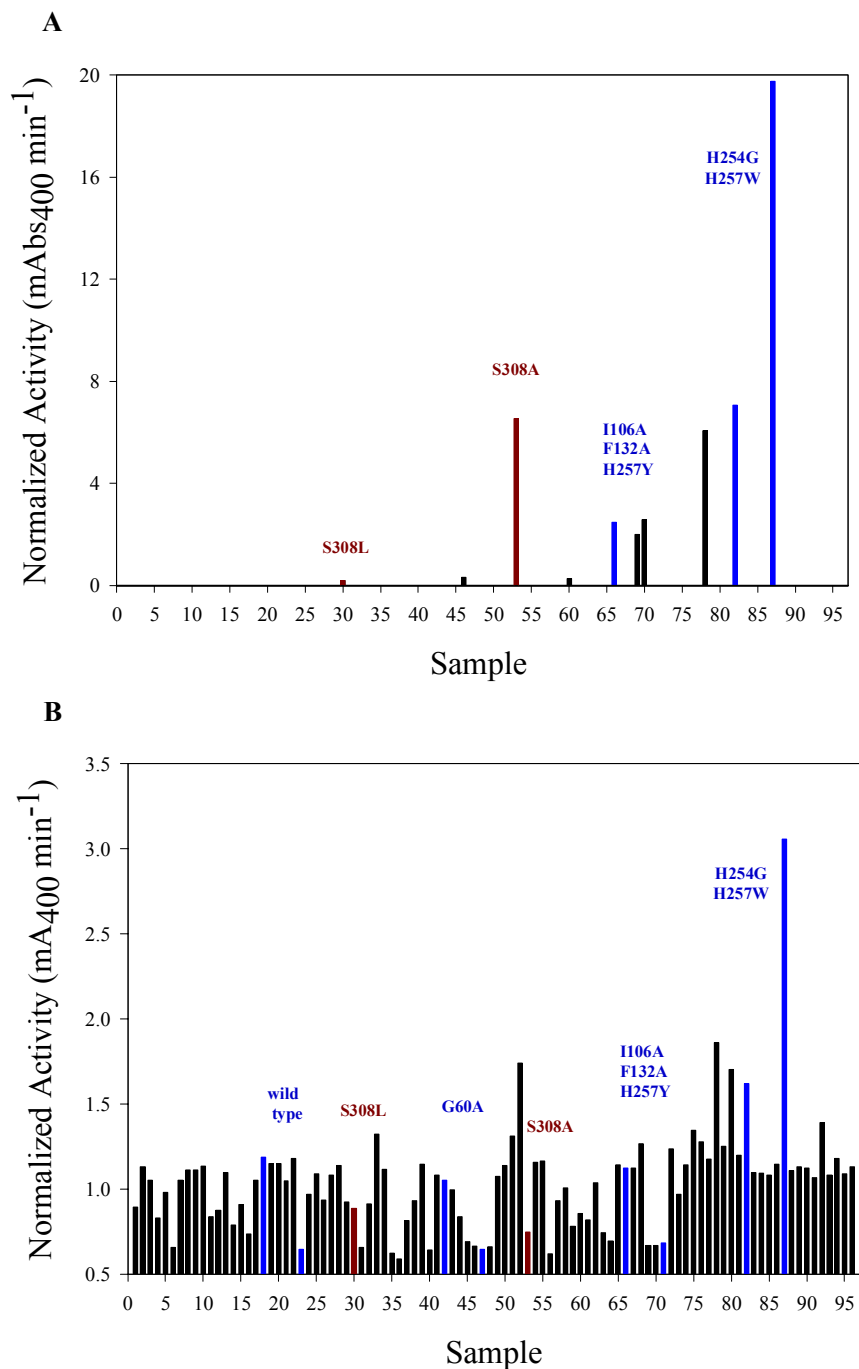


Figure 3.5. The results from the crude culture screen for the S308X single substitution library. The library was screened with  $S_pR_c/S_pS_c$ -(II) (A) and with  $S_pS_c$ -(II) (B).

The same standards were used for the Y309X single substitution library shown in Figure 3.6. The I106A-F132A-H257Y standard had the highest activity for the hydrolysis of the  $S_p$  pair of isomers, followed by I106A-F132A-H257Y, G60A, and wild type. However, the order of relative activities was different for the hydrolysis of the  $S_pS_c$  isomer, for which H254G-H257W had the highest activity, followed by I106A-F132A-H257Y, wild type, and then G60A. Members of this library had activity equal or lower than the wild type parent, with the exception of Y309F and Y309W. Y309F had the highest activity for hydrolysis of the  $S_p$  pair of isomers, but did not appear as having enhanced activity for individual  $S_pS_c$  isomer. In contrast, the mutant Y309W had enhanced activity for the individual  $S_pS_c$  isomer, but no activity for the  $S_pR_c/S_pS_c$  pair of isomers.

The M317X single substitution library was screened with the  $S_p$  pair of GD analog isomers, as well as the individual  $S_pS_c$  isomer. The standards used were wild type, G60A, I106A-F132A-H257Y, and H254G-H257W, and the results are shown in Figure 3.7. The relative order of activities for the hydrolysis of the  $S_p$  pair of isomers indicated that I106A-F132A-H257Y was greater than H254G-H257W, which was greater than wild type and G60A. Results from the hydrolysis of the individual  $S_pS_c$  isomer indicate the same order. No significant increase in activity was observed with any member of the library. Two samples identified as having activity similar to the wild type parent were M317L and M317 (i.e. wild type).

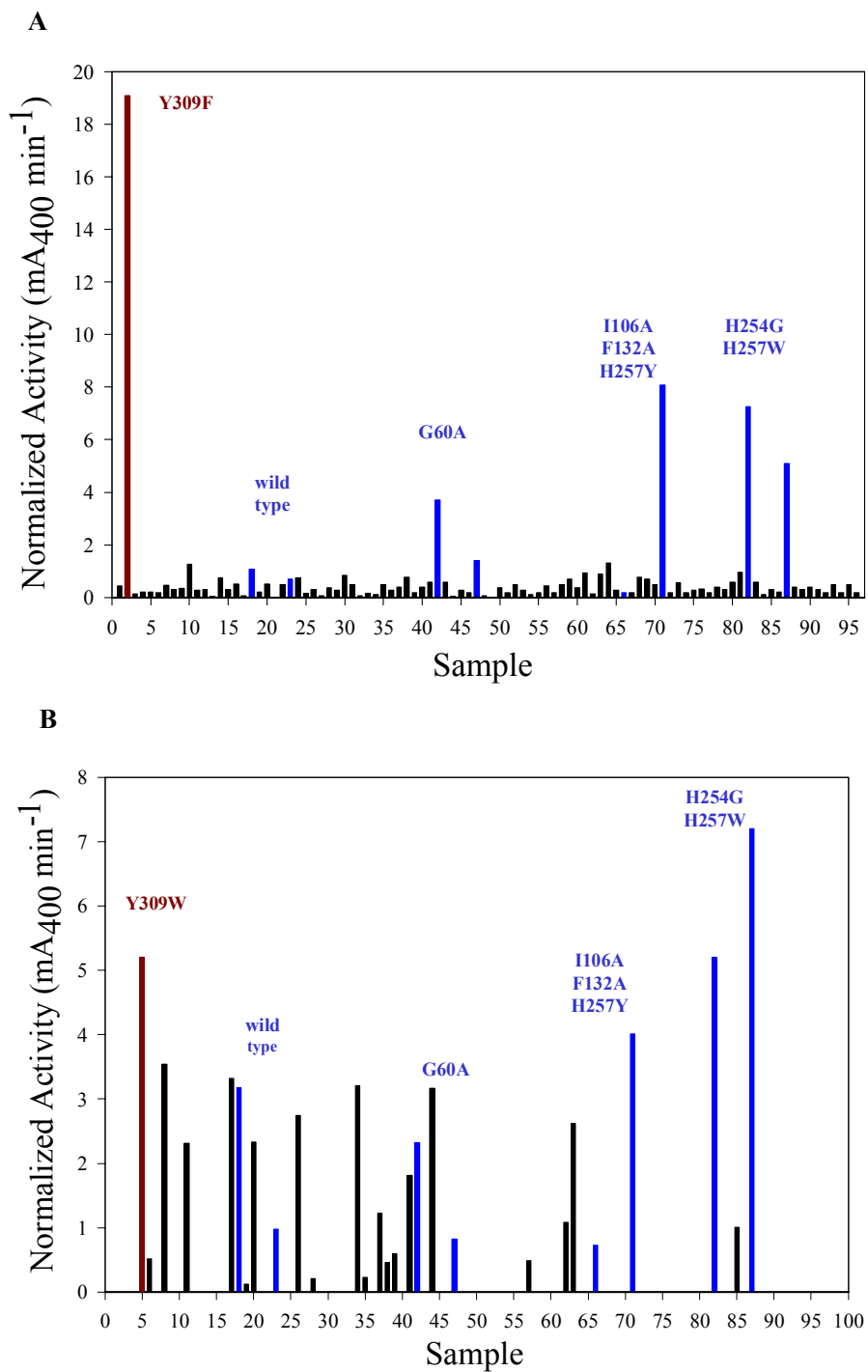


Figure 3.6. The results from the crude culture screen for the Y309X single substitution library. The library was screened with  $S_pR_c/S_pS_c$ -(II) (A) and with  $S_pS_c$ -(II) (B).

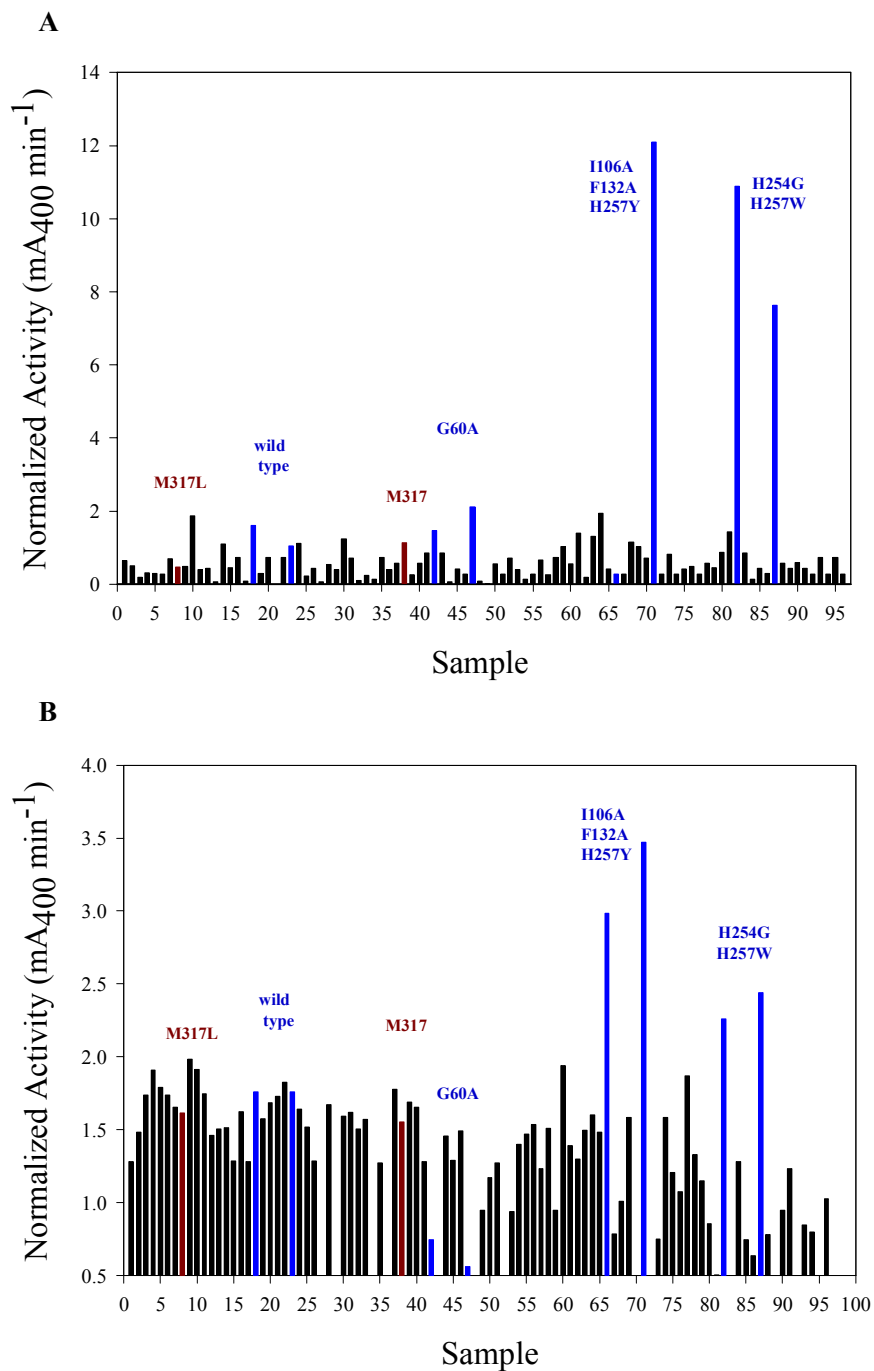


Figure 3.7. The results from the crude culture screen for the M317X single substitution library. The library was screened with  $S_pR_c/S_pS_c$ -(II) (A) and with  $S_pS_c$ -(II) (B).

The G60X and I106X single substitution libraries were screened together on one plate, as shown in Figure 3.8. The standards used in the assays were wild type, H254Q-H257F, and H254G-H257W-L303T. Results from the assay with the S<sub>p</sub> pair of isomers indicated that H254Q-H257F had the highest activity, followed by H254G-H257W-L303T, and then wild type. The order was different for the hydrolysis of the S<sub>p</sub>S<sub>c</sub> isomer. The triple mutant H254G-H257W-L303T had the highest activity, which was greater than H254Q-H257F, which was in turn greater than wild type. The G60T, I106A, and I106S mutants were identified as having increased activity for the hydrolysis of both the S<sub>p</sub> pair of isomer and the individual S<sub>p</sub>S<sub>c</sub> isomer. The mutant I106G, located in position 55, was also identified as having enhanced activity for the hydrolysis of the S<sub>p</sub>S<sub>c</sub> isomer, and the G60V mutant had activity similar to wild type.

*The Double Substitution Library, [H254X-H257X]*

Results from previous experiments described by Chen-Goodspeed et al. indicated that certain residues within the active site were critical for determining stereoselectivity of the enzyme (Chen-Goodspeed et al., 2001a, b).

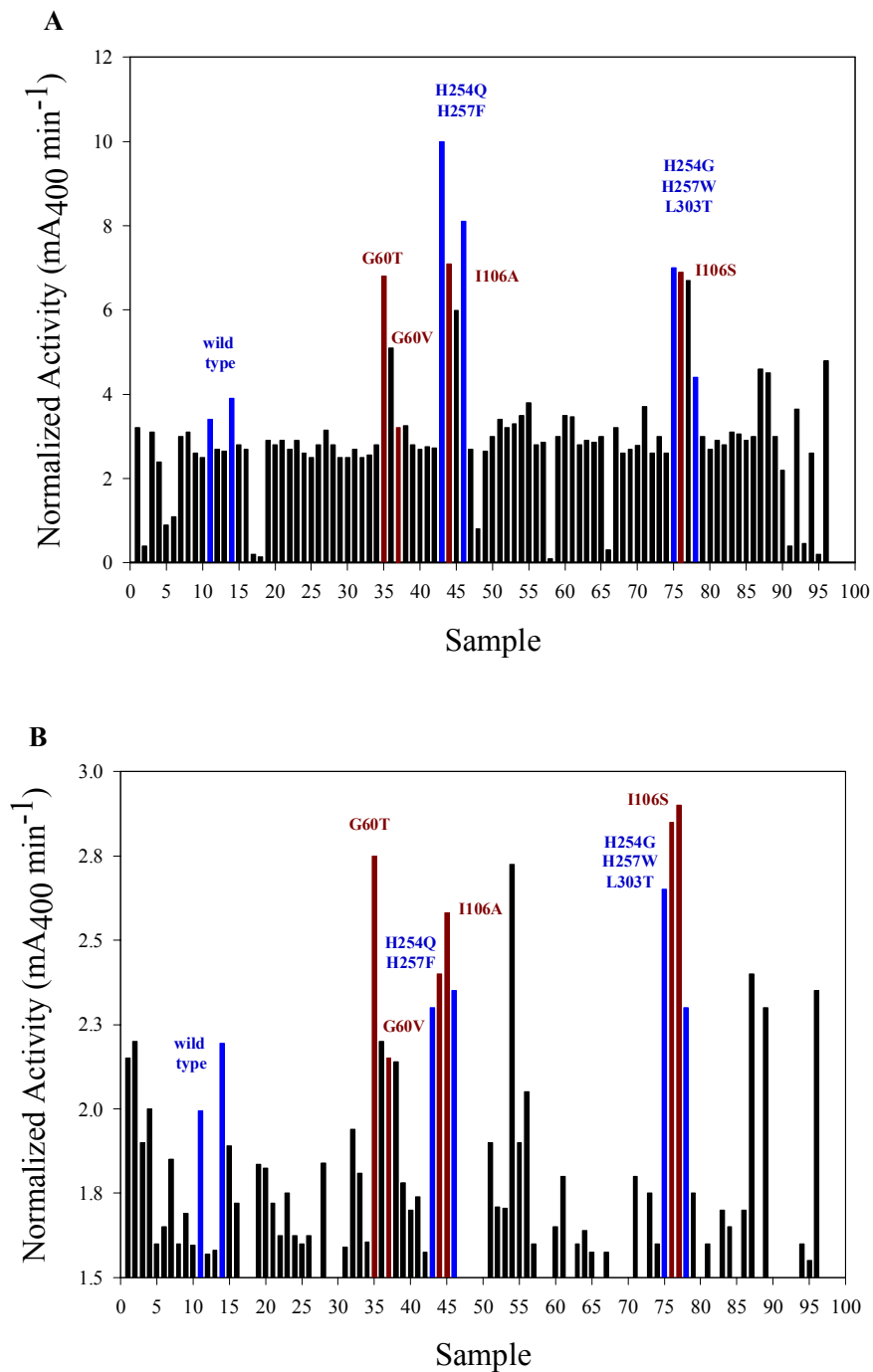


Figure 3.8. The results from the crude culture screen for the G60X and I106X single substitution libraries. Both libraries were screened with  $S_pR_c/S_pS_c$ -(II) (A) and with  $S_pS_c$ -(II) (B).

An example of this was seen with the triple mutant, I106A-F132A-H257Y described in that investigation. By decreasing the space available within the *large subsite*, while increasing the space available in the *small subsite*, the stereoselectivity of the enzyme was reversed in relation to wild type PTE. In particular, positions His254 and His257 were among the critical residues in the *large subsite*, and Gly60 was one of the residues in the *small subsite*.

Randomizations at positions His254 and His257 were made in three different parent constructs; wild type, G60A, and L303T. The PCR sequencing results for each double substitution library are shown in Table 3.3. Twelve plates were screened for the double substitution libraries made in wild type and L303T, and two plates were screened for the double substitution library made in G60A. Similar results were obtained for the libraries made from the wild type and L303T parents. In both, several mutants containing either an Arg or Gly at position 254 were found to have an increase in catalytic activity for the S<sub>p</sub> GD isomers, as seen with the following figures. No samples within the [H254X-H257]-G60A exhibited improvements with the substrates tested.



Table 3.3. The identities of 5 colony forming units (CFU) isolated from each double substitution library.

<b>H254X-H257X</b>			
CAC	wild type	CAC	wild type
CAT	His	CTT	Leu
AAA	Lys	CTA	Leu
AGT	Ser	AGA	Arg
TGT	Cys	CCA	Pro
TTT	Phe	TGG	Trp

<b>[H254X-H257X]-L303T</b>			
CAC	wild type	CAC	wild type
CCT	Pro	AGG	Arg
GGG	Gly	AGC	Ser
AAG	Lys	GTT	Val
TGT	Cys	GGG	Gly
ATC	Ile	CAC	His

<b>G60A-[H254X-H257X]</b>			
CAC	wild type	CAC	wild type
GCT	Ala	GAC	Asp
TTG	Leu	TCG	Ser
GGG	Gly	CAG	Gln
GTG	Val	AGT	Ser
TAA	Term	ACT	Thr

The H254X-H257X library was first created using the wild type as the parent. The standards within each assay plate were wild type and H254R. Although wild type does not appear in Figures 3.9 and 3.10, it is present at positions 19 and 22 for both figures. Figure 3.9 represents plate 3, and Figure 3.10 represents plate 6 of the twelve plates screened. In Figure 3.9, the mutants H254Q-H257F and H254G-H257W have enhanced activity for hydrolysis of the  $S_pR_c/S_pS_c$  isomers. The H254G-H257W was also identified as having increased activity for the individual  $S_pS_c$  isomer, as well as the similar H254G-H257R double mutant. Results from Figure 3.10 indicate that H257Y had the highest activity for hydrolysis of the  $S_p$  pair of isomer, followed by the double mutant H254R-H257A. H254R was also identified in the assay, in addition to the two other H254R standards within the plate. The results were similar with the assay of the individual  $S_pS_c$  isomer, in which H257Y had the highest activity, followed by H254R-H257A. The only difference is that the double mutant H254R-H257L appeared to have high activity for this substrate, as it appears twice on the same plate at positions 4 and 55, but does not appear in the assay with the  $S_p$  pair of isomers. The H254R-H257L mutant has also been determined as having enhanced activity for GD analog hydrolysis in studies conducted by the Wild Laboratory (Lai, 1994).

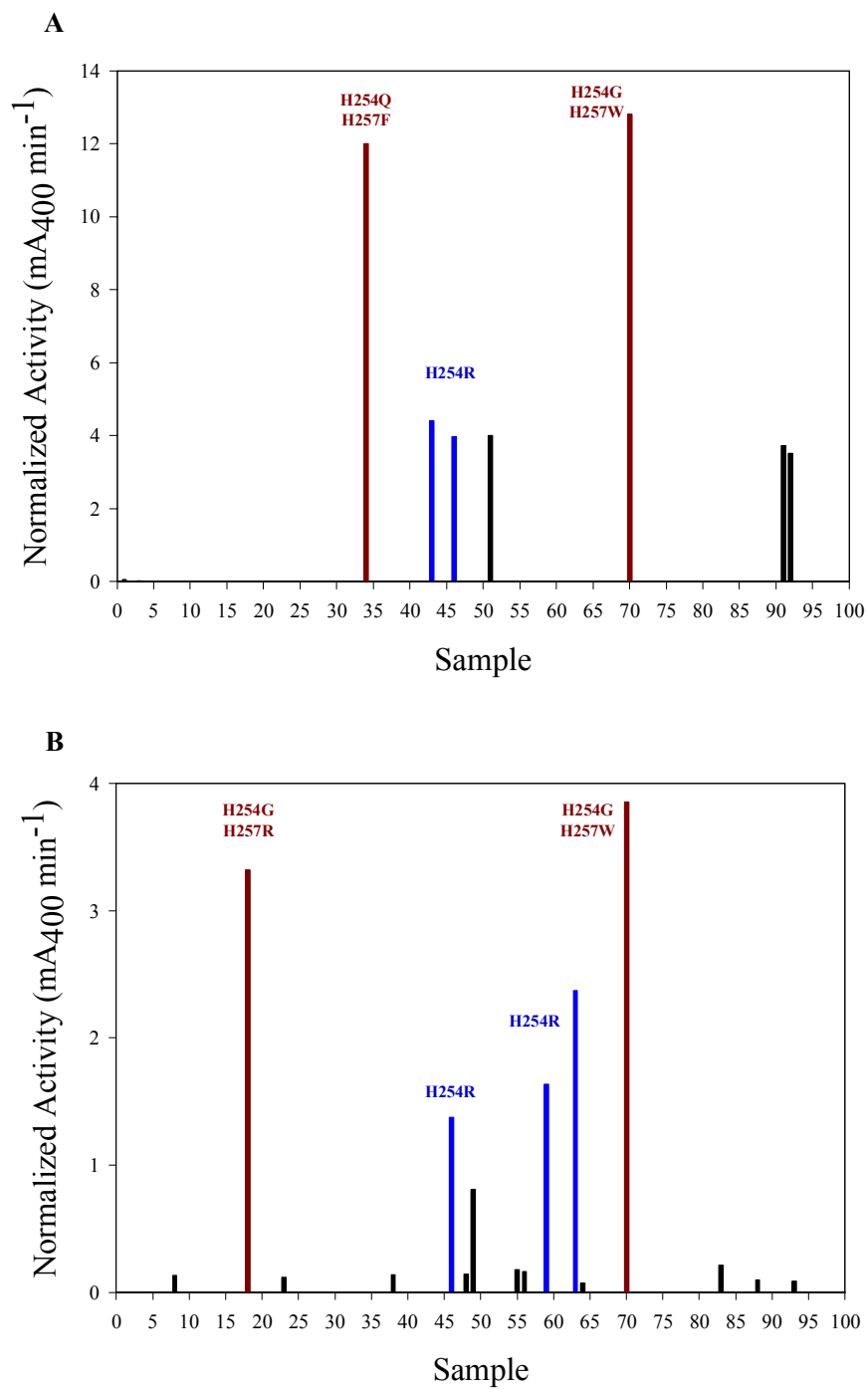


Figure 3.9. The results from the GD analog hydrolysis assays for plate 3 of the H254X-H257X double substitution library. The library was screened with  $S_pR_e/S_pS_e$ -(II) (A) and with  $S_pS_e$ -(II) (B).

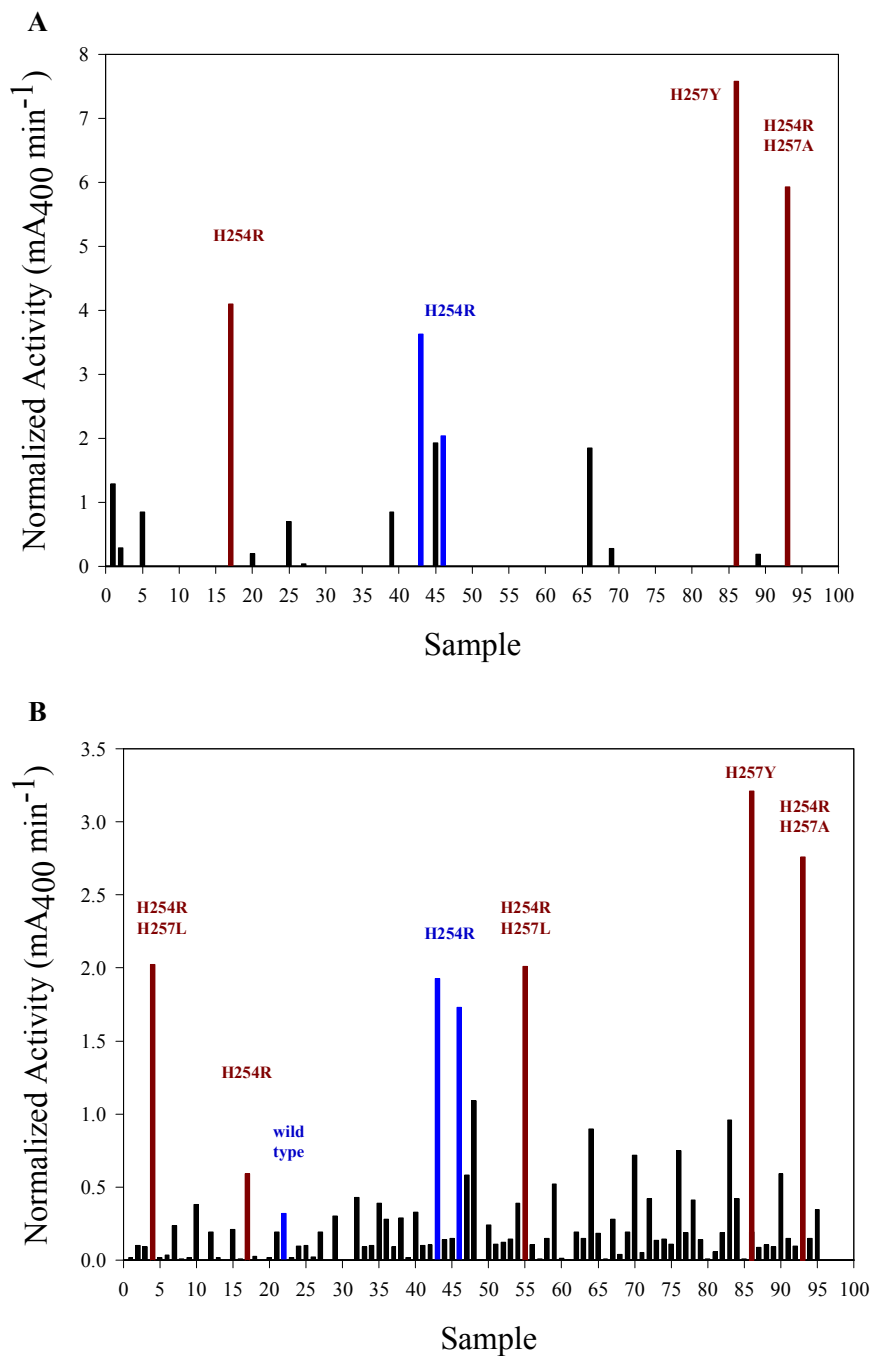


Figure 3.10. The results from the GD analog hydrolysis assays for plate 6 of the H254X-H257X double substitution library. The library was screened with  $S_pR_e/S_pS_e$ -(II) (A) and with  $S_pS_e$ -(II) (B).

In the H254X-H257X library, many of the mutations found to have improved activity for S<sub>p</sub> GD hydrolysis had either an Arg or Gly at position 254. The following double mutations were of this description: H254R, H254R-H257A, H254R-H257L, H254G-H257W, and H254G-H257R as shown in Figures 3.9 and 3.10. Of these mutations, both H254G-H257W and H254R-H257A were isolated more than once on the basis of observed improvement in the crude assays.

In the same manner, the double substitution library was constructed in G60A. However, only two 96-well plates were assayed because initial testing with the library indicated that all samples within the library were far less active than the standards, as shown in Figure 3.11. The standards used in the library were G60A, I106A-F132A-H257Y, and H254G-H257W. Wild type PTE was not used as a standard because G60A was the parent construct used in this library. The highest activity was seen with H254G-H257W, followed by I106A-F132A-H257Y, which was followed by G60A. There was a substantial difference between the activities of H254G-H257W and G60A. The samples that exhibited the highest activity among the library members were identified as having the parent genotype, G60A. Two mutants that were identified as having activity similar to the parent G60A were found to have a H254L-H257S double mutation, and a H254Y mutation (Figure 3.11). Almost all of the remaining samples were below that of the parent for the assays with the S<sub>p</sub> pair of isomers and the individual S<sub>p</sub>S<sub>c</sub> isomer.

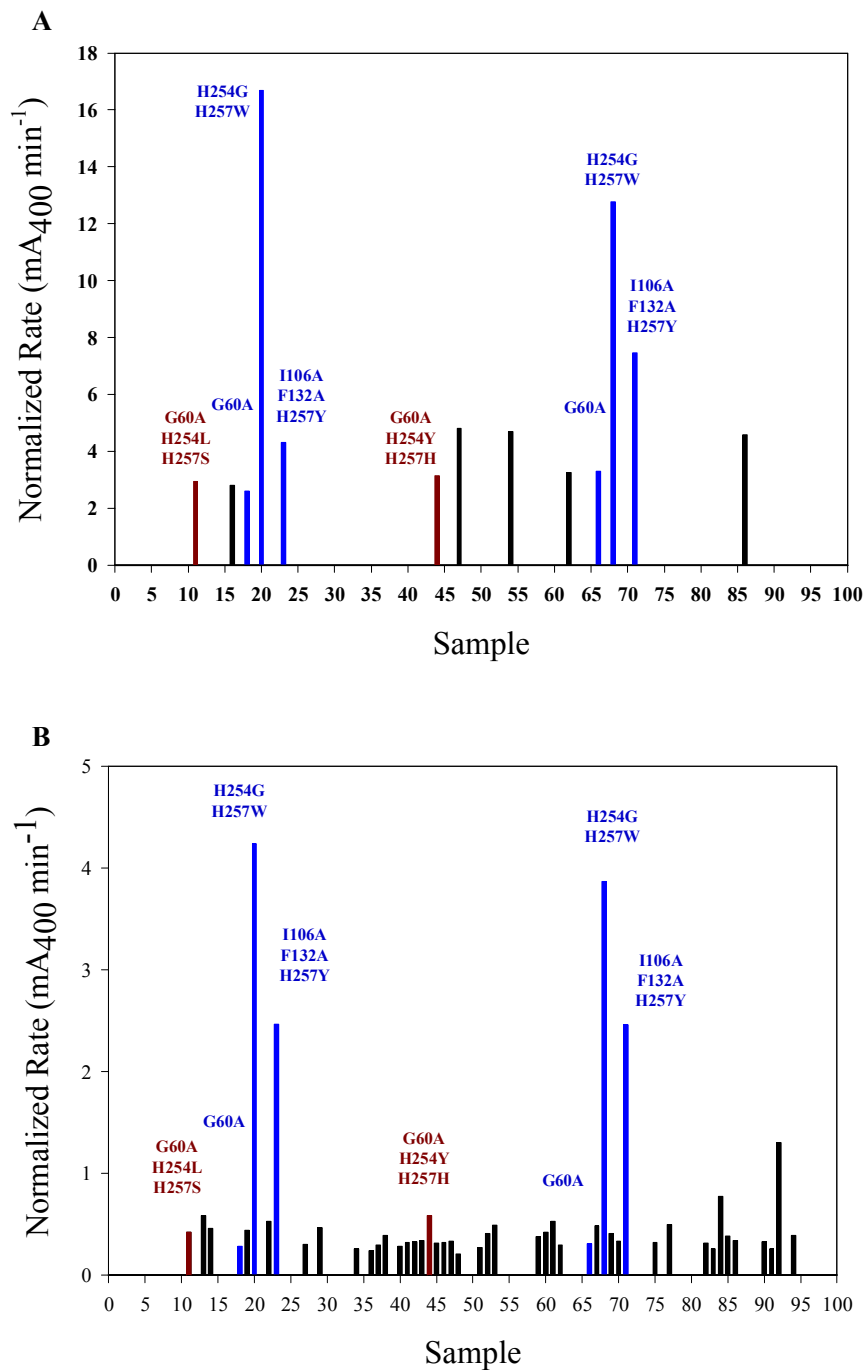


Figure 3.11. The results from the GD analog hydrolysis assays for the G60A-[H254X-H257X] double substitution library. The library was screened with  $S_pR_e/S_pS_e$ -(II) (A) and with  $S_pS_e$ -(II) (B). Wild type is not used as a standard in this library because G60A is the parent construct.

From the H254X-H257X library constructed in wild type, the double mutant H254G-H257W was identified as having significantly higher activity for the hydrolysis of the  $S_p$  isomers of the GD analog. In previous studies by Dr. Craig Hill, this particular double mutant was used as the parent for a single substitution library at position Leu303. In this manner, the triple mutant H254G-H257W-L303T, was identified as having the highest activity for GD analog hydrolysis from the single substitution L303X library. In addition, the triple mutant had the highest kinetic constants for  $S_p$  GD analog hydrolysis of any PTE mutant. To confirm the finding of the H254G-H257W-L303T mutant, the double substitution library was constructed using L303T as the parent.

The H254X-H257X library was constructed in L303T, and the standards used throughout the assays were wild type, G60A, I106A-F132A-H257Y, H254G-H257W, and H254G-H257W-L303T. Twelve plates were screened for this library. In the  $S_pR_c/S_pS_c$  hydrolysis assay plot shown in Figure 3.12, the H254G-H257W-L303T standard and the H254R-L303T appeared to be the most active. The triple mutant standard also appeared to have the highest activity for hydrolysis of the individual  $S_pS_c$  isomer. Both H257Y-L303T and H254R-H257A-L303T appeared to be higher than H254G-H257W, but not H254G-H257W-L303T.

Many mutants obtained from the crude screen assays with enhanced activity for  $S_pR_c/S_pS_c$  isomers hydrolysis had an Arg at position 254, such as H254R-L303T, H254R-H257S-L303T, and H254R-H257A-L303T. The H257Y-L303T mutant and the three previously mentioned mutants were purified and the kinetic constants were determined for the individual GD analog isomers as reported in Table 3.4.

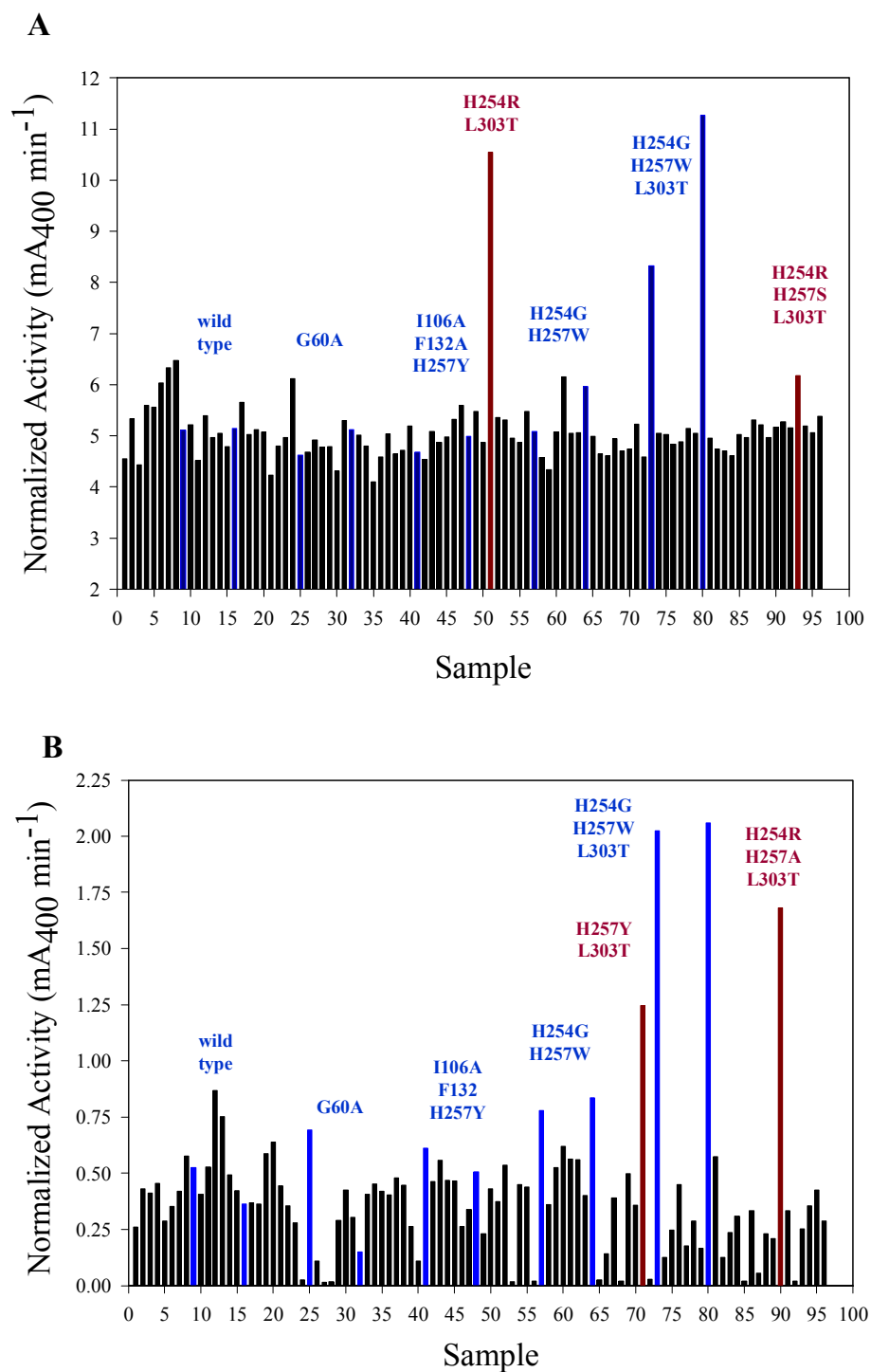


Figure 3.12. The results from the GD analog hydrolysis assays for the [H254X-H257X]-L303T double substitution library. The library was screened with  $S_pR_e/S_pS_e$ -(II) (A) and with  $S_pS_e$ -(II) (B).



Table 3.4. The kinetic constants for the individual GD analog isomers.

Protein	RpRc		RpSc		SpRc		SpSc	
	s <sup>-1</sup>	M <sup>-1</sup> s <sup>-1</sup>	s <sup>-1</sup>	M <sup>-1</sup> s <sup>-1</sup>	s <sup>-1</sup>	M <sup>-1</sup> s <sup>-1</sup>	s <sup>-1</sup>	M <sup>-1</sup> s <sup>-1</sup>
wt-PTE	48	1.6E+05	4.8	1.2E+04	0.3	3.8E+02	0.04	1.6E+01
G60A	120	1.5E+05	33	5.6E+04	0.07	7.0E+00	0.02	7.1E+00
I106A-F132A-H257Y	0.3	2.8E+02	0.3	5.6E+01	11	9.2E+03	2.1	1.2E+03
I106A-S308A-H257Y	5.3	6.7E+02	2.6	2.0E+03	17	1.1E+04	2.7	9.0E+02
H254R	22	7.3E+04	8.6	6.2E+03	1.7	1.5E+04	4.2	5.9E+03
H257L	80	3.1E+05	57	5.2E+04	6.4	3.8E+04	0.07	3.0E+02
H254G-H257W	14	1.4E+02	2.5	4.9E+02	4.8	7.9E+03	0.64	4.5E+02
H254G-H257R	62	1.6E+04	10	1.1E+04	3.5	2.4E+03	1.7	1.7E+03
S308A	114	4.2E+04	14	7.5E+03	11	3.2E+03	11	4.8E+03
I106A-H257Y	1.9	7.3E+02	1.2	5.7E+02	11	4.0E+03	1.3	5.0E+02
H257Y-L303T	8.3	2.3E+03	18	3.6E+03	294	3.3E+04	37	7.4E+03
H254R-H257A-L303T	1.3	4.5E+02	1.7	1.0E+03	N/A	1.3E+04	7	2.4E+03
H254R-H257S-L303T	17	1.3E+04	18	8.1E+03	13	3.4E+04	3.5	3.1E+03
H254R-L303T	3.1	1.2E+04	2.8	5.1E+04	1	2.8E+04	0.6	5.1E+03
H254A	47	2.5E+04	0.52	8.1E+02	3.2	6.0E+03	7.5	4.2E+03
H257Y	5.6	3.6E+03	11	7.0E+03	9.7	3.5E+03	1.5	1.0E+03
I106A-F132A-H257W	4.9	5.5E+02	0.22	4.6E+02	11	3.4E+04	3.1	1.0E+03
H254Q-H257F	3.1	1.3E+04	2.4	7.4E+03	1.3	2.5E+04	0.8	1.6E+03

### *Comparison of Ratios Obtained from Both Kinetic Data and Time Course Data*

A group of 17 PTE mutants, along with the wild type, was selected for purification. Throughout four separate kinetic assays, the turnover rate and catalytic efficiency for each of the isomers were determined for each protein (Table 3.4). For many of the mutants tested, there were considerable decreases for the catalytic efficiency for the hydrolysis of the  $R_pR_c$  and  $R_pS_c$  isomers in comparison to the wild type. However, significant increases were made for the  $S_pR_c$  and  $S_pS_c$  isomers.

From the catalytic efficiency, the ratio of rates for hydrolysis of each isomer was calculated. For comparison, the ratio of rates for the hydrolysis of each of the isomers was determined from time course assays (Table 3.5). In the time course assays, rates of hydrolysis for the individual isomers within the racemic mixture were measured. For example, the wild type protein exhibited a ratio of rates of 13:1, 32:1, and 24:1 corresponding to the ratios of  $R_pR_c$ :  $R_pS_c$ ,  $R_pS_c$ :  $S_pR_c$ , and  $S_pR_c$ :  $S_pS_c$  isomers, as determined from the catalytic efficiency for each of the isomers (Table 3.4). In comparison, wild type exhibited ratios of 13:1, 24:1, and 18:1 for the isomers within a racemic mixture (Table 3.5), as determined from the rates calculated in several single and double exponential plots of hydrolysis. An example of the time course derived rates can be seen with the wild type in Figures 3.13, 3.14, and 3.15.

Table 3.5. The comparison of ratios obtained from kinetic and time course data.

Protein	Ratios from Kinetic Parameters				Ratios from Timecourse			
	$R_pR_c$	$R_pS_c$	$S_pR_c$	$S_pS_c$	$R_pR_c$	$R_pS_c$	$S_pR_c$	$S_pS_c$
wt-PTE	10000	750	24	1	5616	432	18	1
G60A	21428	8000	1	1	n/a	n/a	2	1
I106A-F132A-H257Y	0.23	0.05	8	1	0.34	0.06	19	1
I106A-S308A-H257Y	0.74	2	12	1	0.07	2	5	1
H254R	12	1	3	1	20	2	18	1
H257L	1033	173	126	1	714	238	119	1
H254G-H257W	0.31	1	18	1	0.04	1	2	1
H254G-H257R	9	6	1	1	12	3	3	1
S308A	9	2	0.67	1	5	5	0.33	1
I106A-H257Y	1	1	8	1	8	4	19	1
H257Y-L303T	0.31	0.48	4	1	0.08	0.83	2	1
H254R-H257A-L303T	0.19	0.42	5	1	0.05	0.32	1	1
H254R-H257S-L303T	4	3	11	1	4	2	14	1
H254R-L303T	2	10	5	1	2	5	5	1
H254A	6	0.19	1	1	19	0.33	2	1
H257Y	4	7	4	1	2	2	1	1
I106A-F132A-H257W	0.55	0.46	34	1	0.13	0.13	11	1
H254Q-H257F	8	5	16	1	8	1	11	1

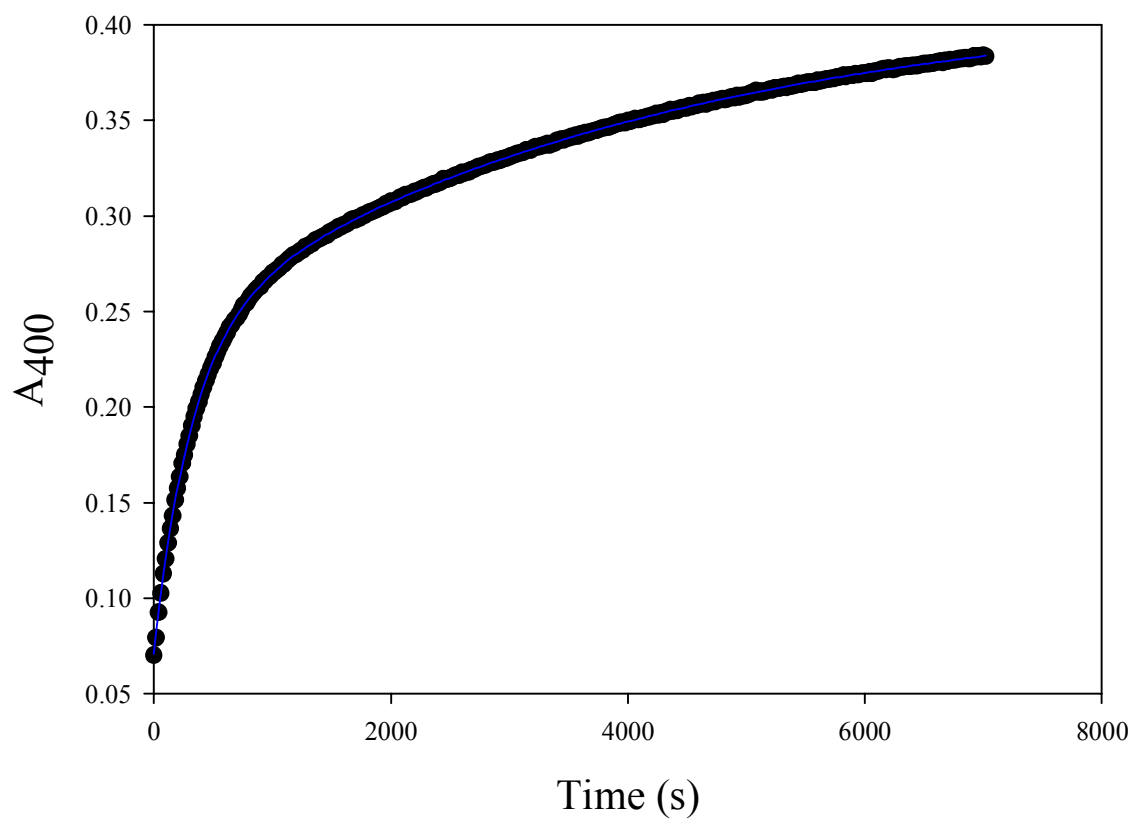


Figure 3.13. Wild type-catalyzed hydrolysis of the first two isomers within the racemic GD analog. The amount of protein used was 0.217  $\mu\text{g}$ , and the rates were calculated as  $3.11 \times 10^{-3} \text{ s}^{-1}$  and  $2.44 \times 10^{-4} \text{ s}^{-1}$ , resulting in a 13-fold difference.

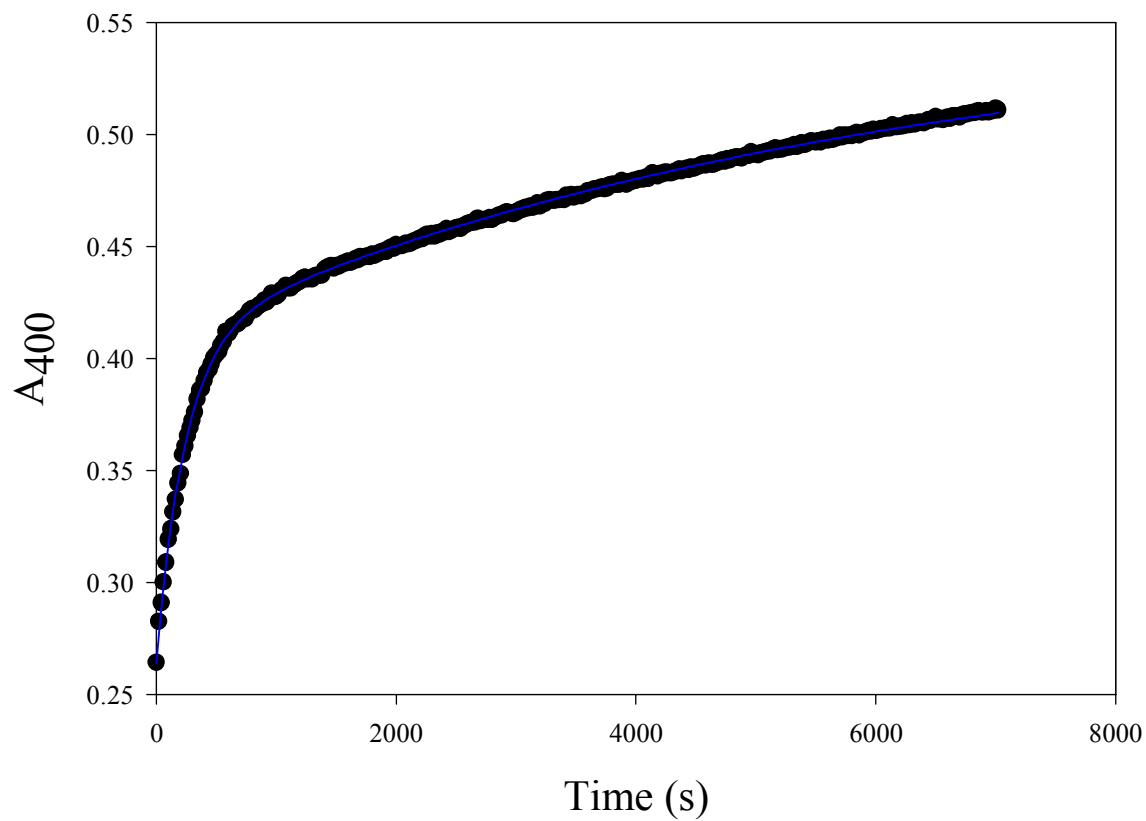


Figure 3.14. Wild type-catalyzed hydrolysis of the second and the third isomers within the racemic GD analog. The amount of protein used was 3.475  $\mu\text{g}$ , and the rates were calculated as  $4.17 \times 10^{-3} \text{ s}^{-1}$  and  $1.72 \times 10^{-4} \text{ s}^{-1}$ , resulting in a 24-fold difference.

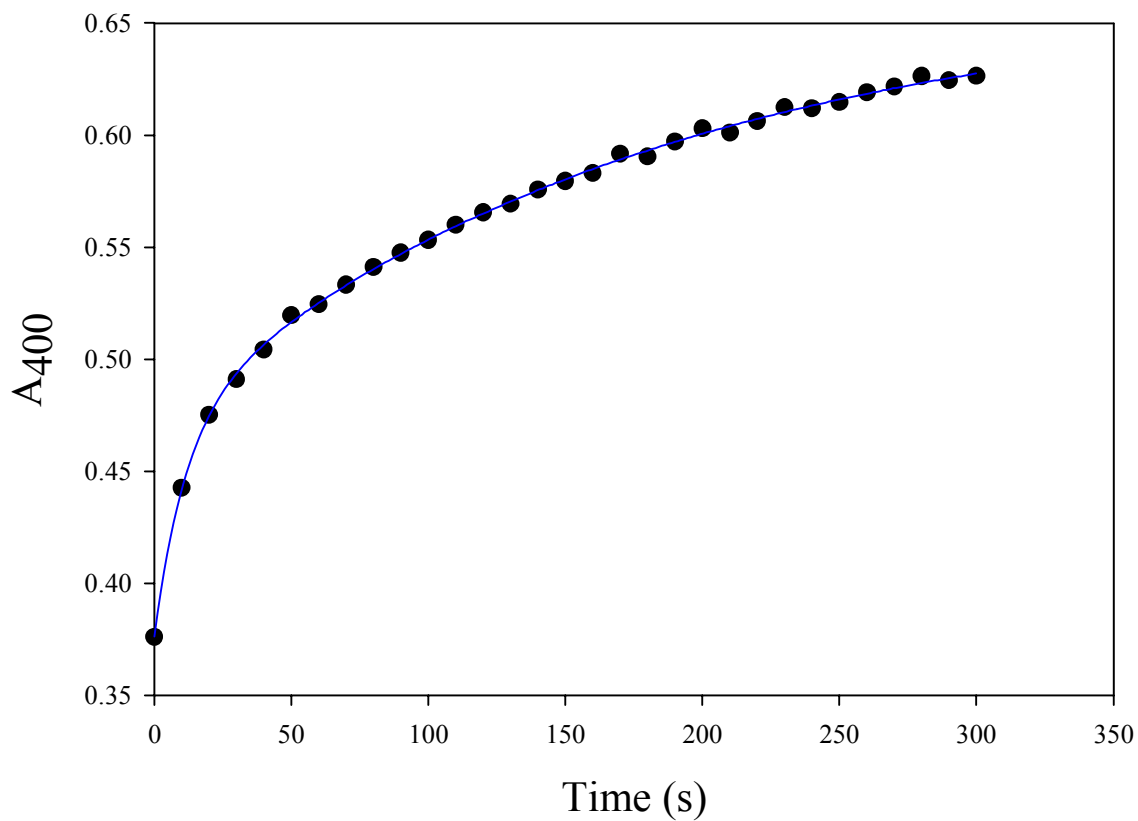


Figure 3.15. Wild type-catalyzed hydrolysis of the third and fourth isomers within the racemic GD analog. The amount of protein used was 6.95  $\mu\text{g}$ , and the rates were calculated as  $8.75 \times 10^{-2} \text{ s}^{-1}$  and  $4.97 \times 10^{-3} \text{ s}^{-1}$ , resulting in a 18-fold difference.

Many of the mutants from the H254X-H257X libraries had different stereoselectivities with respect to wild type. For example, the double mutant H257Y-L303T preferred the stereoisomers of the GD analog in the following order;  $S_pR_c$ ,  $S_pS_c$ ,  $R_pS_c$ , and  $R_pR_c$ , but the ratio between the first and the fourth isomer was significantly smaller than the ratio reported for wild type.

#### *Kinetic Constants with Soman*

The six mutants, H254R, H257L, H254G-H257W, H254G-H257R, H254Q-H257F, and H257Y, were purified and the kinetic constants were determined for the individual isomers of the GD analog, which are shown in Table 3.4. In addition, several other mutants were purified and sent to Steven P. Harvey at Edgewood Chemical Biological Center for testing with soman (Table 3.6). Of these, the three double mutants containing Gly254 showed the most improvement with H254G-H257L having the highest  $V_{max}$  of the group, reported as  $28 \mu\text{molmin}^{-1}\text{mg}$ . However, the double mutants H254A-H257W and H254R-H257F, appeared to be less active than the wild type.

Table 3.6. Maximal velocity for PTE catalyzed hydrolysis of the nerve agent GD (S.P. Harvey, personal communication).

<b>Protein</b>	<b>V<sub>max</sub> (μmol min<sup>-1</sup> mg)</b>	<b>Activity Relative to wild type</b>
wild type	6	1.00
I106A-H257Y	3	0.47
H254A	13	2.20
H257Y	6	1.06
I106A-H257Y-S308A	7	1.16
I106A-F132A-H257Y	6	1.03
S308A	7	1.10
G60A	19	3.22
H254R	6	1.08
H254R-H257F	2	0.41
H254G-H257W	16	2.71
H254A-H257W	4	0.71
H254G-H257L	28	4.74
H254G-H257Y	8	1.28



## Discussion

### *Targeting the S<sub>p</sub> Isomers of the GD Analog within the Single Substitution Libraries*

In considering the toxicity elicited by the nerve agent GD, there are only two isomers that are biologically relevant - the S<sub>p</sub>R<sub>c</sub> and S<sub>p</sub>S<sub>c</sub> isomers. The remaining two R<sub>p</sub> diastereomers are rarely detected long after exposure, and are believed to be readily taken up by carboxylesterases present in blood (Langenberg et al., 1998). Therefore, directed evolution studies on PTE have focused on improvements for hydrolysis and detoxification of the S<sub>p</sub> pair of isomers.

Based upon previous studies, it is believed that modifications in the *large subsite* of the active site would be beneficial to substrates with large substituents such as GD and VX. The residues His254, His257, and Met317 are found in the *large subsite*. Gly60 and Ile106 are located in the *small subsite*. Tyr309 is in the *leaving group pocket*, and Ser308 is found between the *small subsite* and the *leaving group pocket*.

There were only a couple of mutants identified from the H254X library as having enhanced activity for the S<sub>p</sub>R<sub>c</sub> and S<sub>p</sub>S<sub>c</sub> isomers. The best mutant obtained was H254R, followed by H254A. Other samples isolated had a His at position 254.

The beneficial modifications identified from the H257X library were very conservative in comparison to wild type. The identification of H257Y and H257W indicated that an aromatic amino acid at position 257 is favored for enhanced catalytic efficiency of S<sub>p</sub>R<sub>c</sub>/S<sub>p</sub>S<sub>c</sub> isomer hydrolysis. In comparison to wild type, the catalytic efficiency for S<sub>p</sub>R<sub>c</sub> and S<sub>p</sub>S<sub>c</sub> hydrolysis was increased 57- and 88-fold, and 14- and 15-fold greater for H257Y and H257W, respectively. Although both mutants appeared to be faster than the H254Q-H257F standard in the crude assay shown in Figure 3.3, the

catalytic efficiency for the  $S_pS_c$  isomer was approximately the same and no improvement for the hydrolysis of the  $S_pR_c$  isomer was seen with the kinetic data shown in Table 3.4. The difference is attributed to either variation in expression levels for the different mutants, or inaccuracy associated with the intrinsic nature of a crude assay.

Screening of the L271X library resulted in no mutants with enhanced activity. Both assays were consistent in this finding. The standards of H254G-H257W and I106A-F132A-H257Y appeared distinct from the background, which again, confirms that no mutant in this library had enhanced activity for the  $S_p$  pair of isomers or the  $S_pS_c$  isomer.

Results from the S308X library indicated that substitution at this position is detrimental for hydrolysis of the  $S_p$  isomer of the GD analog. Almost all members were unable to hydrolyze the  $S_pR_c/S_pS_c$  isomers of the GD analog as indicated in Figure 3.5, with the exception of S308A. The kinetic parameters obtained from purified protein indicate that the catalytic efficiency for S308A is 8-fold higher for hydrolysis of the individual  $S_pR_c$  isomer, and 300-fold higher for hydrolysis of the individual  $S_pS_c$  isomer (Table 3.4). The activity for all other members was substantially lower than the wild type for the individual  $S_pS_c$  isomer.

Beneficial substitutions at the 309 position were quite conservative in relation to the tyrosine found in the wild type. Improvements were seen for the Y309F and Y309W mutants, as shown in Figure 3.6. In comparing the mutants to the wild type, both Y309F and Y309W had greater catalytic efficiencies for the  $S_p$  pair of isomers, and the individual  $S_pS_c$  isomer. The purified Y309F mutant exhibited a 7- and 53-fold improvement for hydrolysis of the  $S_p$  pair of isomers and the  $S_pS_c$  isomer the relative to the wild type. The enhancement was slightly higher in Y309W. There was a 22- and 88-

fold improvement. In comparing the mutants to the standard H254G-H257W, Y309F and Y309W had 2- and 3-fold better rates for hydrolysis of the toxic  $S_pS_c$  isomer.

There were no improvements for  $S_p$  GD analog hydrolysis from the M317X library. As shown in Figure 3.7, no mutants were identified as having higher activity than the standards. One mutant with activity similar to the parent was identified as having a Leu at the position, while M317 (wild type) was also identified among the library members through the screening as having activity similar to the wild type standard.

The G60X and I106X single substitution libraries were screened, and a few mutants were identified as having enhanced activity. The mutants G60T and I106S were identified as having enhanced activity for hydrolysis of the  $S_p$  pair of isomers. However, the background within the assay for hydrolysis of the  $S_pS_c$  isomer was very high and the identification of enhanced mutants was seen as a false positive. In addition, both residues are in the *small subsite* unlike the other previous single substitution libraries.

#### *Targeting the $S_p$ Isomers of the GD Analog within the H254X-H257X Libraries*

In the double substitution library H254X-H257X made in both the wild type and L303T construct, significant enhancements in catalytic activity were seen with manipulation of the large subsite residues, 254 and 257. The three mutants, H254G-H257W, H254G-H257R and H257Y, appeared to have the highest activity against the  $S_p$  pair of isomers and the individual  $S_pS_c$  isomer of the GD analog in the H254X-H257X library. They were purified, and the kinetic constants for each substrate were obtained to confirm results from the assays. The H254G-H257W mutant had a catalytic efficiency of

$4.7 \times 10^3 \text{ M}^{-1} \text{ s}^{-1}$  and  $4.5 \times 10^2 \text{ M}^{-1} \text{ s}^{-1}$  for the  $S_p$  pair and  $S_pS_c$  isomer, which was equal to a 12- and 28-fold enhancement over the wild type, respectively. Similar enhancement was seen with H254G-H257R. The catalytic efficiency for H254G-H257R was 12- and 43-fold higher than wild type for the  $S_p$  pair and  $S_pS_c$  isomer, respectively. The best improvement was seen with H257Y, which had a catalytic efficiency of  $5.4 \times 10^3 \text{ M}^{-1} \text{ s}^{-1}$  and  $1.4 \times 10^3 \text{ M}^{-1} \text{ s}^{-1}$ , which was equivalent to a 14- and 88-fold enhancement with the  $S_p$  pair and  $S_pS_c$  isomer, respectively. Because several of these mutants had enhanced activity against the analog, several were sent to Steven P. Harvey at Edgewood Chemical and Biological Center for testing with the actual nerve agent (Table 3.6). Enhancements of almost 5- and 3-fold over the wild type were seen with H254G-H257L and H254G-H257W, respectively (Table 3.6). However, the mutants H257Y and H254G-H257Y, both of which were identified as having increased activity from the crude assays, appeared to be just as efficient as the wild type.

In determining what modifications were beneficial, it was clear that the vast majority of the samples with enhanced activity in the assays contained either an Arg or Gly at the 254 position. It was noted that a Gly at position 254 was often accompanied by a residue approximately the same size as histidine or larger, as was seen with the appearance of H254G-H257W. Within the double mutations containing Arg at position 254, there was often a residue that was smaller than histidine, such as H254R-H257A or H254R-H257S. It appears that creating less available space within the *large subsite*, by replacing either His at 254 or 257 with a larger residue, is substantially beneficial for hydrolysis of the  $S_p$  GD isomers.

Several of the same double mutations isolated from the H254X-H257X library, were also found in the [H254X-H257X]-L303T library. Of these were H254R-H257A and H254R-H257S, both of which were isolated more than once on the basis of observed improvement in the crude assays for both libraries. In addition, both modifications proved to be beneficial for  $S_pR_c$  and  $S_pS_c$  hydrolysis. As seen in Table 3.4, the purified H254R-H257A-L303T exhibited a 34- and 150-fold enhancement in comparison to the wild type. The H254R-H257S-L303T had a 89- and 194-fold enhancement for the individual  $S_pR_c$  and  $S_pS_c$  isomers, respectively. Other beneficial modifications were the single mutations H254R and H257Y in L303T. Although in Figure 3.7 it appeared that the H257Y-L303T was less active than both the H254G-H257W and H254G-H257W-L303T standard, the kinetic data with the purified protein indicated that H257Y-L303T was more active. In fact, there was a 462-fold enhancement for catalytic efficiency reported for the  $S_pS_c$  isomer, and a 86-fold enhancement for the  $S_pR_c$  isomer in comparison to the wild type. The enhancement for  $S_pS_c$  hydrolysis was 16 times higher than the H254G-H257W standard, and slightly higher than the H254G-H257W-L303T, which has a reported value of  $7.2 \times 10^3 \text{ M}^{-1} \text{ s}^{-1}$  as a  $k_{\text{cat}}/K_m$  (Craig Hill, personal communication). The H257Y-L303T had a 3-fold enhancement for hydrolysis of the  $S_pR_c$  isomer in comparison to the standard H254G-H257W-L303T. The discrepancy is believed to be attributed to the inaccuracy associated with the intrinsic nature of a crude culture assay. Aspects such as effectiveness of the detergent used, and volume of media in the growth box might have contributed to variation.

It was apparent that there was a preference for the placement of an Arg at position 254 and a Tyr at position 257 among the mutants with improved activity in the [H254X-

H257X]-L303T library. In comparing these results to the sequence of the *opdA* gene from *Agrobacterium*, which shares a 90% identity in terms of amino acid sequence with *opd* from *Pseudomonas diminuta*, there is an Arg at position 254 and Tyr at 257 in the wild type (Yang et al., 2003). In particular, the emergence of Arg at position 254 was also noted in error prone PCR experiments using the *opd* gene, which were described in the same study. However, the evolution of the gene was directed towards hydrolysis of coumaphos and methyl parathion (Yang et al., 2003).

Results from the double substitution library constructed in G60A had clearly shown that almost all modifications in the 254 and 257 region were detrimental to activity against the  $S_p$  isomers of the GD analog. As discussed in the previous chapter, G60A shares the same order of preferential hydrolysis for the GD isomers with the wild type protein. The stereoselectivity exhibited by the parent may have been passed on to the members of this library even though modifications in the large pocket are beneficial to the rates of hydrolysis for the  $S_p$  isomers in the wild type.

### *Stereoselectivity of Hydrolysis*

As seen in Table 3.5, the wild type preferentially hydrolyzes the  $R_pR_c$  isomer, and it does so 10,000 times faster than the toxic  $S_pS_c$  isomer. The stereoselectivity of the wild type is in the direction of  $R_pR_c$ ,  $R_pS_c$ ,  $S_pR_c$ , and  $S_pS_c$ . However, this order of preference has been changed by several of the mutants obtained from the double substitution libraries. In general, the rates for  $R_pR_c$  and  $R_pS_c$  hydrolysis are fairly broad with most of the mutants exhibiting a catalytic efficiency within the range of  $10^2$  and  $10^4$   $M^{-1} s^{-1}$  for both of the isomers. Most of the mutations have detrimentally affected the ability to

hydrolyze the  $R_p$  diastereomers in comparison to wild type. The ability to hydrolyze the  $R_pR_c$  isomer decreased from 2- to 1142-fold with some of the mutants, as seen with H254R and H254G-H257W. Similarly, the ability to hydrolyze the  $R_pS_c$  was decreased from 4- to 245-fold, with the greatest decrease seen with the double mutant, H254G-H257R. In contrast, there were significant enhancements seen with the rates for the hydrolysis of the individual  $S_p$  diastereomers. As mentioned previously, protein engineering experiments were directed towards the hydrolysis of the  $S_p$  isomers. This was achieved with the double substitution libraries. The catalytic efficiency for  $S_pR_c$  hydrolysis was in the range of  $10^3$  and  $10^4 \text{ M}^{-1} \text{ s}^{-1}$ , and  $10^3 \text{ M}^{-1} \text{ s}^{-1}$  for the  $S_pS_c$  isomer. The enhancements were between 34- to 100-fold higher than wild type for the  $S_pR_c$  isomer, with the largest improvements demonstrated by H257Y-L303T and H257L. More substantial improvements were made for  $S_pS_c$  hydrolysis. The optimum enzyme was H257Y-L303T, with a 462-fold increase in rate. Both the H254R-H257A-L303T and H254R-H257S-L303T mutants had improvements of 150- to 194-fold relative to wild type. In addition, the order of stereoselectivity for many of these mutants was changed drastically. For both triple mutants,  $S_pR_c$  hydrolysis occurred the fastest. The same was true for H254G-H257W, H254G-H257R, and H254Q-H257F. In addition, the double mutant H257Y-L303T preferred both toxic isomers,  $S_pR_c$  and  $S_pS_c$ , over the less toxic isomers of  $R_pS_c$  and  $R_pR_c$ .

Stereoselectivity for hydrolysis was expressed as a ratio of 10,000:750:237:1 for the purified wild type protein, in terms of the preference of the  $R_pR_c$ :  $R_pS_c$ :  $S_pR_c$ :  $S_pS_c$  isomers within the racemic GD analog. The ratios for preference of the isomers in terms of pairs of isomer was determined to be 13:1, 32:1, and 24:1 corresponding to  $R_pR_c$ :  $R_pS_c$ ,

$R_pS_c$ :  $S_pR_c$ , and  $S_pR_c$ :  $S_pS_c$  as determined from the kinetic data. The time course ratios obtained were 13:1, 24:1, and 18:1, shown in Figures 3.13, 3.14, and 3.15. As seen from both ratios, the degree of stereoselectivity was readily observed for the wild type.

However, mutants obtained from the directed evolution studies had substantially smaller ratios of rates. As seen with H257Y-L303T, the rate of hydrolysis of the fastest isomer is only 14-fold greater than the rate of hydrolysis of the slowest isomer, as shown in Table 3.4. From the  $k_{cat}/K_m$  values, the ratio of hydrolysis for  $R_pR_c$ :  $R_pS_c$  was 1:2; for  $R_pS_c$ :  $S_pR_c$  the ratio was 1:8; and for  $S_pR_c$ :  $S_pS_c$  the ratio was 4:1. From the time course experiments, the ratio of hydrolysis for  $R_pR_c$ :  $R_pS_c$  was 1:11; for  $R_pS_c$ :  $S_pR_c$  the ratio was 1:2; and for  $S_pR_c$ :  $S_pS_c$  the ratio was 2:1. It was apparent from Tables 3.4 and 3.5 that improvements for the hydrolysis of the  $S_p$  isomers were made at the cost of the ability to hydrolyze the  $R_p$  isomers.

In general, the results from the crude culture assays are not accurate. The reasons include poor growth within the incubation plates, and perhaps variation in protein expression. The method of extracting protein may have also attributed to the variation in the assays. However, the crude assays were successful in the isolation and identification of enhanced mutants.

The intrinsic nature of a screen implies that all samples must be surveyed. Many samples were assayed, and some were positively identified as having enhanced activity for the substrates tested, and some were not but the directed evolution experiments are aimed at discovering a substantial enhancement of activity for hydrolysis of the toxic  $S_p$  isomers of GD. In this manner, any mutant with a substantial enhancement of activity would positively be identified through this crude assay system.



**CHAPTER IV**  
**DIRECTED EVOLUTION STUDIES AND STEREOSPECIFICITY**  
**INVESTIGATIONS ON SARIN HYDROLYSIS**

**Introduction**

Among the six most commonly found chemical warfare agents within the U.S. Chemical Munitions Stockpile, sarin (GB) (methyl phosphonofluoridate isopropyl ester) has been studied most extensively. It was first synthesized in 1938 by Gerhard Schrader at IG Farben (U.S. Department of Defense, 1998), and is the second of the *G agents* developed. The discovery of GB followed that of tabun (GA) and preceded soman (GD). As a class of nerve agents, the *G agents* share the characteristics of volatility and extreme toxicity. For instance, the projected model for aerosol dispersion of sarin depicts extreme vulnerability due to the compound's high volatility of 22,000 mg m<sup>3</sup> at 20° C, as well as projected rapid dispersion (Stewart et al., 2003). This particular characteristic of the compound dictates its ability to rapidly cause toxicity primarily via acute inhalation. As an indication of toxicity, a low observable adverse effect such as miosis is estimated to occur at a concentration as low as 3 mg min<sup>-1</sup> m<sup>3</sup> for 50% of the human population (USAMRICD, 1995).

Although GB is not a concern in terms of stagnancy as in the case of VX, the potential use of this agent is of grave concern due to several previous documented uses. It is believed that GB is the most easily obtained agent, and that there is a greater likelihood for its use in a situation of unplanned release (U.S. Congress, 1993). For these

reasons, the ability of the agent to cause mass casualties and to incite hysteria continues to pose a formidable threat to humanity.

In one such case during the 1980's, Iranian sources claimed that 50,000 casualties and 5000 deaths were caused by the use of nerve agents by Iraq in the Iran-Iraq war (Eisenstadt, 1990). Most of the Iraqi munitions were believed to contain a mixture of sarin (GB) and cyclosarin (GF) for greater persistence and toxicity. Another incident that occurred within the past 10 years was the use of GB gas by terrorists from the Aum Shinrikyo cult in Tokyo. The release of GB gas in a subway train led to over 3700 injuries and 12 deaths (Evison et al., 2002). Both cases further illustrate the immediate need for development of effective detoxification options.

To date, phosphotriesterase (PTE) is the fastest enzyme for sarin hydrolysis and the only one capable of detoxifying the deadly VX nerve agent (Di Sioudi et al., 1999). Variants of PTE have been shown to hydrolyze sarin at the rate of  $1700 \text{ s}^{-1}$ , with a  $k_{\text{cat}}/K_m$  of  $1.5 \times 10^6 \text{ M}^{-1} \text{ s}^{-1}$  (Steven P. Harvey, personal communication). Other enzymes such as butyrylcholinesterase, paraoxonase, and organophosphorus acid anhydrolase (OPAA) hydrolyze GB at a much slower rate. For example, human paraoxonase (PON1) hydrolyzes GB at a rate on the order of  $10^2 \text{ M}^{-1} \text{ s}^{-1}$ , which is almost 3 orders of magnitude slower than that of PTE (Josse et al., 2001). Catalysis by OPAA is also significantly slower for the GB analog (methyl isopropyl *p*-nitrophenyl phosphonate) hydrolysis when compared to PTE. Rates for both the  $R_p$  and  $S_p$  isomers of the GB analog are on the order of  $10^4$  greater with PTE (Hill et al., 2001).

In comparison with other organophosphate hydrolyzing enzymes, PTE is a superior candidate for use as a *sarinase*. However, stereoselectivity exhibited by the wild

type protein is still an issue because of preferential hydrolysis of the relatively non-toxic  $R_p$  isomer within a racemic mixture. The difference between the effects of the  $R_p$  versus the  $S_p$  isomers of GB is estimated to be quite substantial, as indicated by both toxicity and kinetic data. The  $LD_{50}$  value for the  $S_p$  isomer was 50 times smaller than the  $LD_{50}$  value for the  $R_p$  isomer when tested with mice (Spruit et al., 2000). Studies from Benschop et al. also indicate a difference of at least 4500-fold between the rate constants for inhibition of AChE by the two different GB isomers (Benschop and De Jong, 1988).

If used unmodified, wild type PTE would in fact potentiate the toxicity of GB by hydrolyzing the  $R_p$  isomer, thereby increasing the available concentration of the toxic  $S_p$  isomer. The issues of differential hydrolysis and toxicities are addressed in this chapter, as well as efforts directed at obtaining PTE mutants with an increased ability to hydrolyze the  $S_p$  isomer of the GB analog. In addition, the stereospecificity of catalysis within the racemic GB analog was investigated for several mutants of PTE as well as the wild type protein.

## **Materials and Methods**

### *Mutagenesis*

Mutants were obtained by cassette mutagenesis from both site directed mutagenesis studies and the creation of libraries. The *pJWO1* plasmid containing the *opd* gene without the leader sequence was used as the template for all genetic manipulations. Libraries of mutants were constructed by random mutagenesis methodology, involving the use of degenerate oligonucleotides targeting specific regions within a gene. Double substitution libraries were constructed by cassette mutagenesis. In cassette mutagenesis,

unique restriction sites on either side of the target region were identified and excised within the vector, *pJW01*. The KpnI and NsiI restriction enzymes were obtained from New England Biolabs and Promega. The restricted fragment was isolated by gel electrophoresis, and purification was performed according to the protocol for DNA Purification (Promega Wizard DNA Purification Kit). Cassettes containing degenerate oligonucleotides for the codon corresponding to the targeted positions of His254 and His257 were designed, and then obtained from the Gene Technologies Laboratory at Texas A&M University. The primer for the forward direction was 5' CTGATCGGTCTGGACNNNATCCCGNNNTCCGCTATCGGTCTGG AAGACAATGCA3', and in the reverse direction was 5' TTGTCTTCCAGACCGATAGCGGANNNCGGGATNNNGTCCAGACCGATCAGGTAC3'.

Ligation of the cassette with the restricted gene was performed at 16° C overnight, using T4 DNA Ligase (New England Biolabs). The recombinant vector was then transformed by electroporation into BL21 (DE3) *E. coli* cells, and subsequently plated on Luria-Bertani Broth (LB) ampicillin plates. Following mutagenesis, PCR sequencing of the resulting transformants was performed to ensure randomness of sample.

#### *Culture Growth Conditions and Screening*

The resulting transformants were inoculated into deep 96-well plates that contained super broth (SB), 0.1 mM CoCl<sub>2</sub> and 100 µg/mL ampicillin. The growth plates were incubated at 30 °C, shaking at 250 rpm. After 40 hours, the culture was diluted 10-fold and the cell density was measured spectrophotometrically at 600 nm. A small

portion of the sample (i.e. 25  $\mu$ L) of the diluted culture was assayed for paraoxon hydrolysis, in which the resulting *p*-nitrophenol product was detected spectrophotometrically at 400 nm. The following substrates were tested in a similar manner; GB analog racemate, the R<sub>p</sub> isomer, and the S<sub>p</sub> isomer. Throughout each assay, the same buffer conditions were maintained: 50 mM CHES, pH 9.0, 1% (v/v) Bugbuster (Novagen), and 0.1 mM substrate. Twelve growth plates, containing library members and known standards, were assayed in this manner.

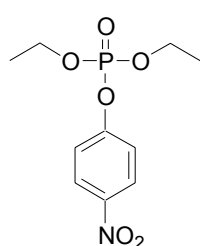
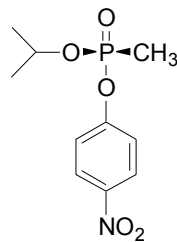
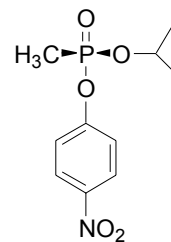
### *Enzyme Purification*

Both mutants and the wild-type were expressed in *Escherchia coli* BL21 cells and grown in LB overnight. The resulting culture was used to inoculate terrific broth (TB) supplemented with 100  $\mu$ M CoCl<sub>2</sub>. After a 24 hour period of incubation at 30 °C, the addition of IPTG to a final concentration of 0.6 mM induced expression of protein. The cells were harvested 40 hours post induction, and PTE was purified by following the protocol described in Omburo et al. (Omburo et al., 1992). SDS-PAGE indicated that the purified mutants were the same size as the wild-type PTE and were at least 95% pure.

### *Kinetic Measurements and Data Analysis*

The enzymatic hydrolysis of the sarin analog, isopropyl *p*-nitrophenyl methyl phosphonate, was measured by monitoring the accumulation of *p*-nitrophenol at 400 nm ( $\epsilon=17,000 \text{ M}^{-1}\text{cm}^{-1}$ ) at pH 9.0, 25°C using a Gilford Model 260 spectrophotometer. The enzyme activity was measured in 50 mM CHES, pH 9.0 for the sarin analog. One unit of activity is defined as the amount of enzyme required to catalyze the hydrolysis of

one  $\mu\text{mol}$  paraoxon per minute. The structures of paraoxon (I) and the isomers of the GB (II) analog are shown in Scheme 1.

**I****S<sub>p</sub>-(II)****R<sub>p</sub>-(II)**

The kinetic constants were obtained by fitting the data to the Equation 4.1, in which  $v$  is the initial velocity,  $k_{\text{cat}}$  is the turnover rate,  $A$  is the concentration of substrate, and  $K_m$  is the Michaelis constant.

$$v / E_t = k_{\text{cat}} A / (K_m + A) \quad (4.1)$$

Enzyme assays involving nerve agent were done at Edgewood Chemical Biological Center by Steve P. Harvey, and conducted with a fluoride electrode attached to a Fisher Accumet 925 meter. Reactions were conducted in a temperature-controlled vessel in a total volume of 5 mL. Buffering was provided by a 50 mM solution of bis-tris-propate at pH 7.2.

#### *Time Course Ratios*

The ratios of rates of hydrolysis for each isomer within the racemic GB analog were determined for a group of 18 mutants and the wild type. Serial dilutions were made

for each enzyme, and each concentration was assayed with 60  $\mu\text{M}$  racemic GB analog buffered in a 50 mM CHES, pH 9.0. Hydrolysis of the solution was spectrophotometrically determined by the appearance of the *p*-nitrophenol leaving group at 400 nm. The data were fit to Equations 4.2 and 4.3 using SigmaPlot2000, and the amplitudes and rates were recorded. The rates were used in calculating the observed time course ratios.

$$y = y_0 + a(1 - e^{-bx}) \quad (4.2)$$

Equation 2. The equation describing a single exponential curve, in which  $y_0$  is the  $y$ -intercept,  $a$  is the amplitude of the curve,  $b$  is the rate constant, and  $x$  is a variable and the exponential.

$$y = y_0 + a(1 - e^{-bx}) + c(1 - e^{-dx}) \quad (4.3)$$

Equation 3. The equation describing a double exponential curve, in which  $y_0$  is the  $y$ -intercept,  $a$  and  $c$  are the amplitudes of the curve,  $b$  and  $d$  are the rate constants, and  $x$  is a variable and the exponential.

## Results

### *The Double Substitution Library, H254X-H257X*

The double substitution library, H254X-H257X, was constructed using the wild-type *opd* gene, and the L303T construct. Sample randomness was confirmed by sequencing. As an example, the identities of 5 CFUs from each of these libraries are shown in Table 4.1.

Table 4.1. The identities of the codons from 5 random colony forming units of the H254X-H257X library made in both wild type and L303T.

<b>H254X-H257X</b>			
CAC	wild type	CAC	wild type
CAT	His	CTT	Leu
AAA	Lys	CTA	Leu
AGT	Ser	AGA	Arg
TGT	Cys	CCA	Pro
TTT	Phe	TGG	Trp

<b>[H254X-H257X]-L303T</b>			
CAC	wild type	CAC	wild type
CCT	Pro	AGG	Arg
GGG	Gly	AGC	Ser
AAG	Lys	GTT	Val
TGT	Cys	GGG	Gly
ATC	Ile	CAC	His



Twelve growth plates were screened for GB analog hydrolysis activity. Six of the assay plates are shown in the following figures, with several mutants identified on the basis of observed enhancement for hydrolysis of the S<sub>p</sub> isomer and the R<sub>p</sub> isomer.

In plate B1 of the H254X-H257X library, the standards used were wild type and H254R (Figure 4.1). Results from the S<sub>p</sub> isomer hydrolysis assay indicate that H254R has greater activity than wild type, but the reverse is true for the R<sub>p</sub> isomer hydrolysis assay. In this particular plate, the wild type standard located at position 11 is unusually high as compared to the other assay plates within the library. The mutants obtained from this plate were H257Y, H254G-H257D, and H254R-H257L. The single mutation, H257Y, had the highest activity on the plate, followed by H254G-H257D, which was similar to activity observed for the H254R standard. H254R-H257L appeared to have activity for the R<sub>p</sub> isomer of the GB analog.

The same standards are used in plate B2, which is shown in Figure 4.2. H254R has the highest activity, followed by H254G, H254R-H257L, and H254R-H257Y. The activity of wild type is relatively low compared to the activity of the members within this library. The normalized activity for wild type is around  $100 \text{ mA}_{400} \text{ min}^{-1}$ , while the activity for both H254G and H254R are well above  $1000 \text{ mA}_{400} \text{ min}^{-1}$ .

The three mutations obtained from the S<sub>p</sub> isomer hydrolysis assay also appear in the screen with the R<sub>p</sub> isomer, in which H254G has the highest activity, followed by H254R-H257L, H254R-H257Y, H254R, and then wild type.

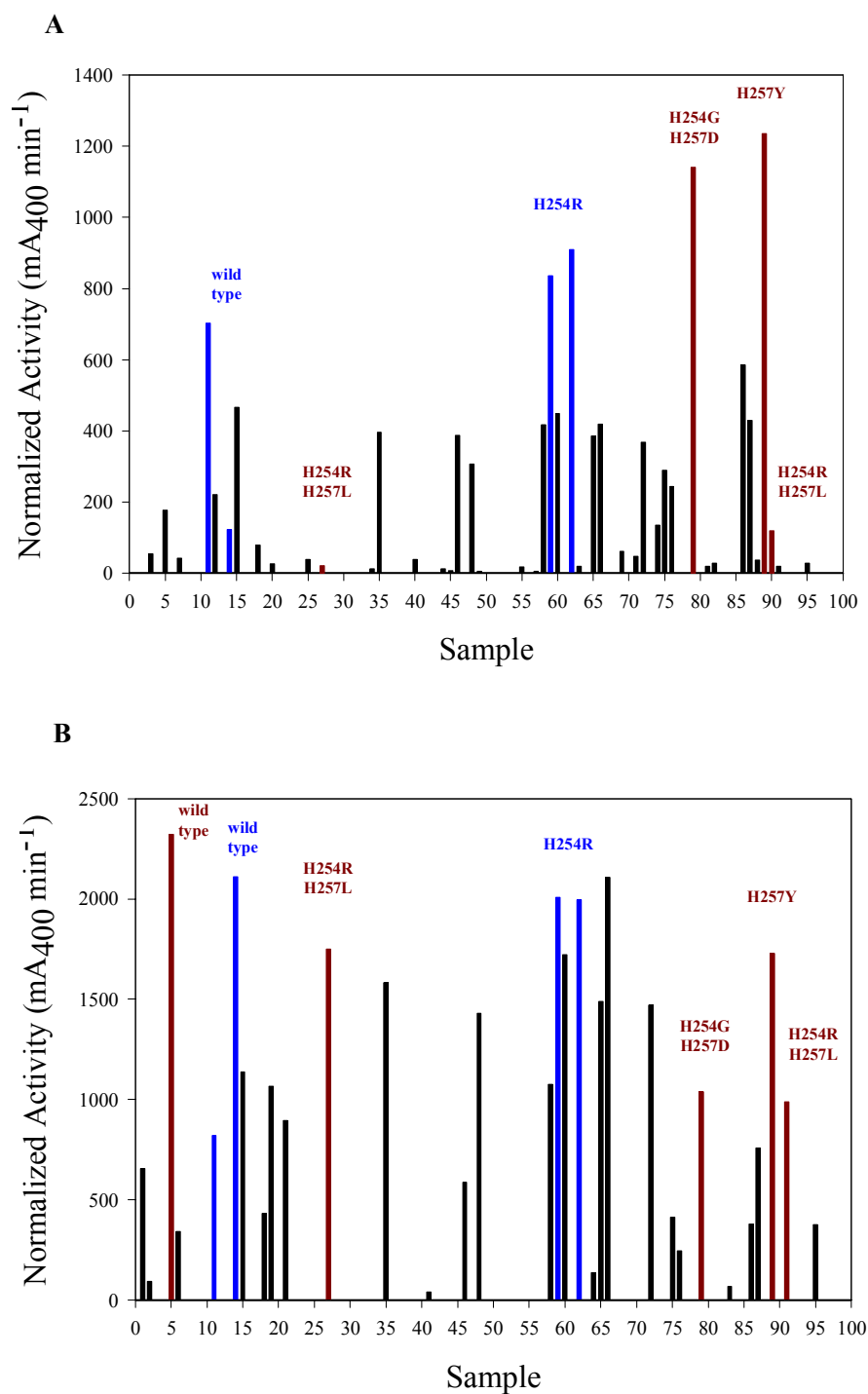


Figure 4.1. The results from the GB analog hydrolysis assays for plate B1 of the H254X-H257X library. The library was screened with  $S_p$ -(II) (A) and with the  $R_p$ -(II) (B).

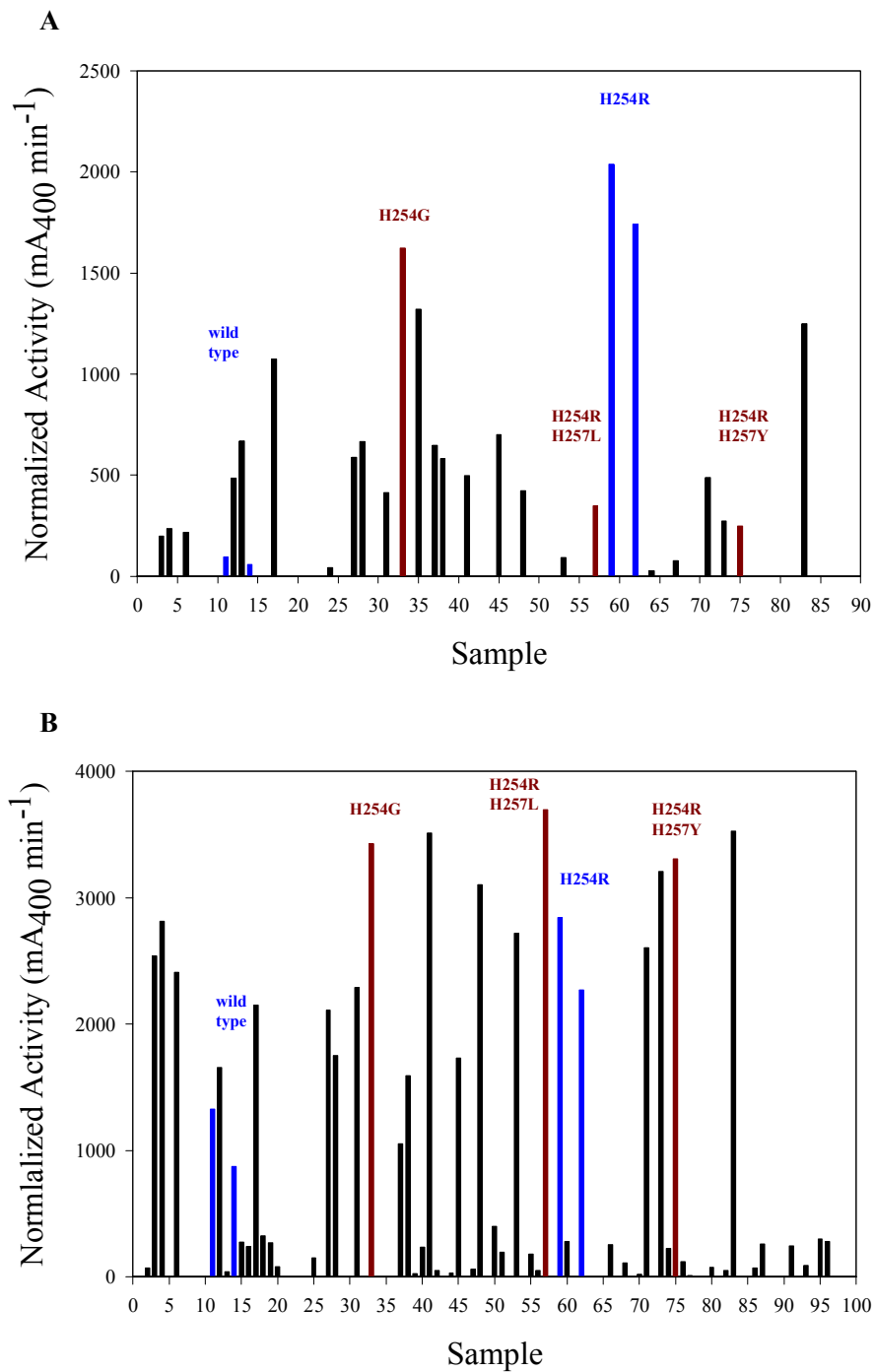


Figure 4.2. The results from the GB analog hydrolysis assays for plate B2 of the H254X-H257X library. The library was screened with  $S_p$ -(II) (A) and with the  $R_p$ -(II) (B).

Results from plate B3 are shown in Figure 4.3, in which the standards used are wild type and H254R. Two mutants were obtained from the  $S_p$  isomer assay. The H254R-H257M mutant had the highest activity on the plate, followed by the H254R standard. Another sample with enhanced activity was also identified as H254R-H257M, as well as a H254R single mutation. The variation in activity for identical mutants is revealed in this plate. The normalized activity for the H254R-H257M varied between 1000 to 1400  $\text{mA}_{400} \text{min}^{-1}$ , whereas the activity for H254R varied from 800 to 1200  $\text{mA}_{400} \text{min}^{-1}$ . However, both of the mutants had much higher activities than wild type, which was around 200  $\text{mA}_{400} \text{min}^{-1}$ .

The H254R standard had unusually high activity for hydrolysis of the  $R_p$  isomer. For this particular plate, the activity was around 4000  $\text{mA}_{400} \text{min}^{-1}$ , whereas in other plates it is generally half that value. Because of this, the activity of H254R was the highest, followed by H254R-H257M, and then wild type. In the other plates, wild type has activity higher than H254R.

Figure 4.4 shows the results from the  $S_p$  isomer assay with plate B4, in which H254G-H257Y has the highest activity, followed by the H254R standard. The H254G-H257R mutant has slightly less activity, followed by the H257Y mutant. There is a 5-fold difference between the activities of wild type and the H254R standard.

The H254R standard has very high activity for the hydrolysis of the  $R_p$  isomer assay. It is approximately 4500  $\text{mA}_{400} \text{min}^{-1}$ , where as the activity for wild type is around 3000  $\text{mA}_{400} \text{min}^{-1}$ . The mutants H254R-H257Y, H254G-H257R, H254G-H257Y, and H257Y have lower activity in comparison to wild type.

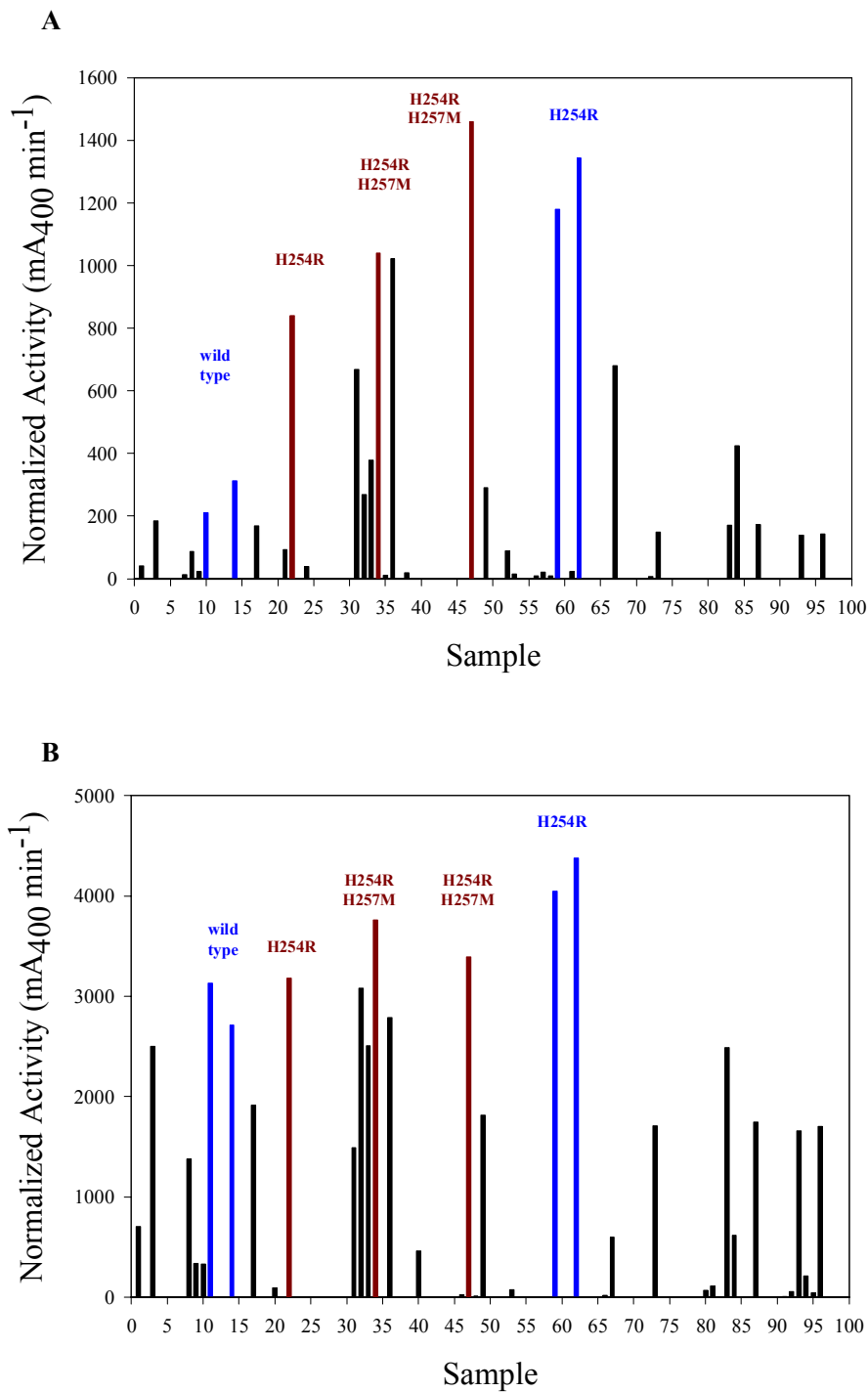


Figure 4.3. The results from the GB analog hydrolysis assays for plate B3 of the H254X-H257X library. The library was screened with  $S_p$ -(II) (A) and with the  $R_p$ -(II) (B).

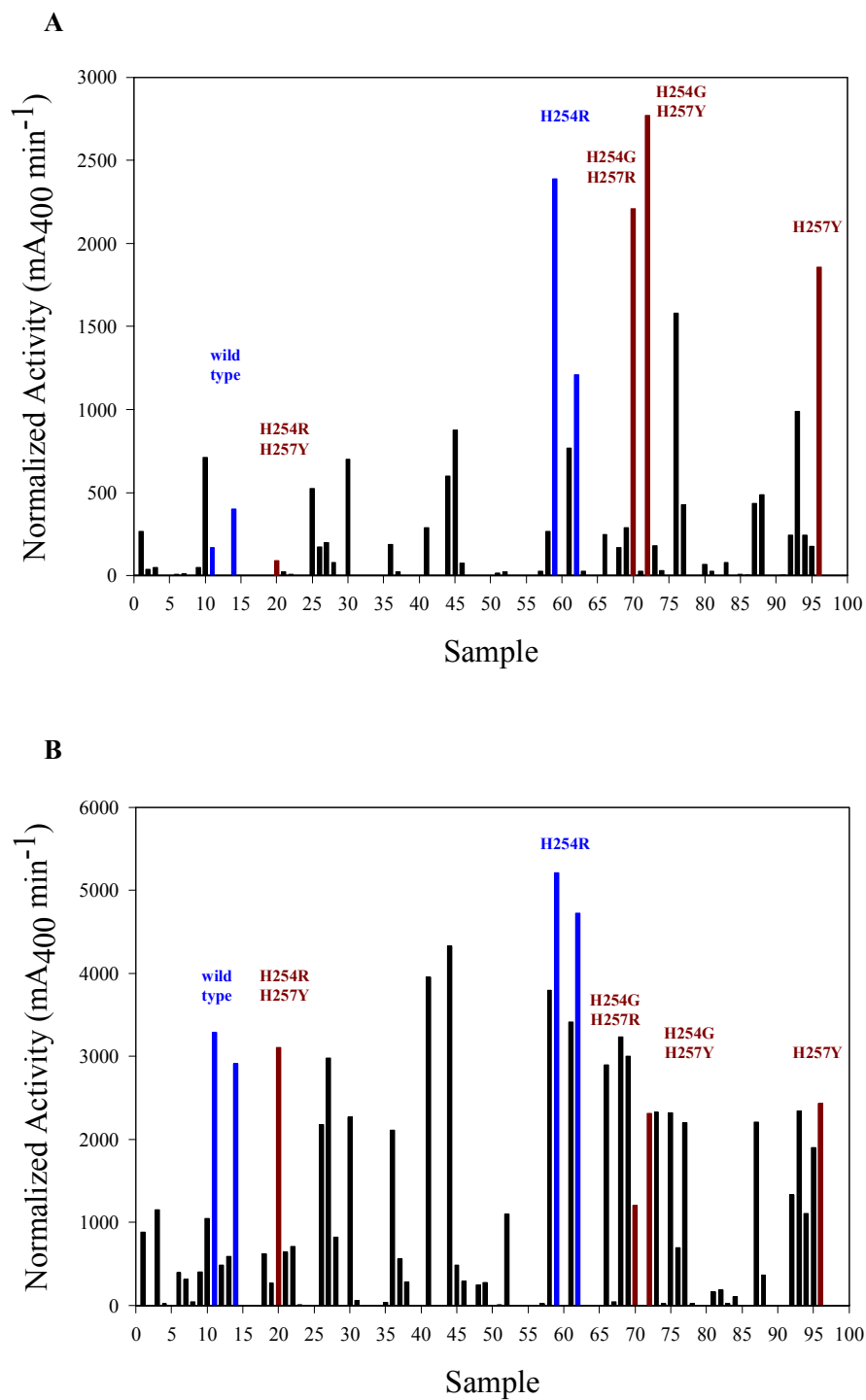


Figure 4.4. The results from the GB analog hydrolysis assays for plate B4 of the H254X-H257X library. The library was screened with  $S_p$ -(II) (A) and with the  $R_p$ -(II) (B).

In Figure 4.5, the results from plate 4 are shown. The activity of wild type is unusually high for the hydrolysis of the S<sub>p</sub> isomer. In most plates, wild type activity is typically under 500 mA<sub>400</sub> min<sup>-1</sup>. In this plate, it is approximately 800 mA<sub>400</sub> min<sup>-1</sup>. The mutant with the highest activity was H254R, followed by H254R-H257A. The H254R-H257V mutant had lower activity than wild type, but also appears in the R<sub>p</sub> hydrolysis assay.

The H254R-H257A mutant had the highest activity for the hydrolysis of the R<sub>p</sub> isomer. It was higher than wild type, followed by H254R, and then by H254R-H257V. Wild type was isolated and identified on the basis of enhanced activity. The activity of wild type was 2200 mA<sub>400</sub> min<sup>-1</sup>, whereas the wild type standard was lower than expected at 500 mA<sub>400</sub> min<sup>-1</sup>.

The results from plate 6 are shown in Figure 4.6. The H254R-H257A mutant had the highest activity for hydrolysis of the S<sub>p</sub> isomer. It was followed by H254S-H257Y, which had greater activity than H254A-H257W, and H254R. The normalized activity for H254R-H257A was around 200 mA<sub>400</sub> min<sup>-1</sup>. There was a relatively small difference between the H254R and wild type standards, of only about 200 or 300 mA<sub>400</sub> min<sup>-1</sup>.

The H254R-H257L mutant appeared three times in the assay with the R<sub>p</sub> isomer. The activity of this mutant was approximately 200 mA<sub>400</sub> min<sup>-1</sup>, and was significantly higher than the standards on the plate. No other mutant was identified as having enhanced activity for R<sub>p</sub> isomer hydrolysis.

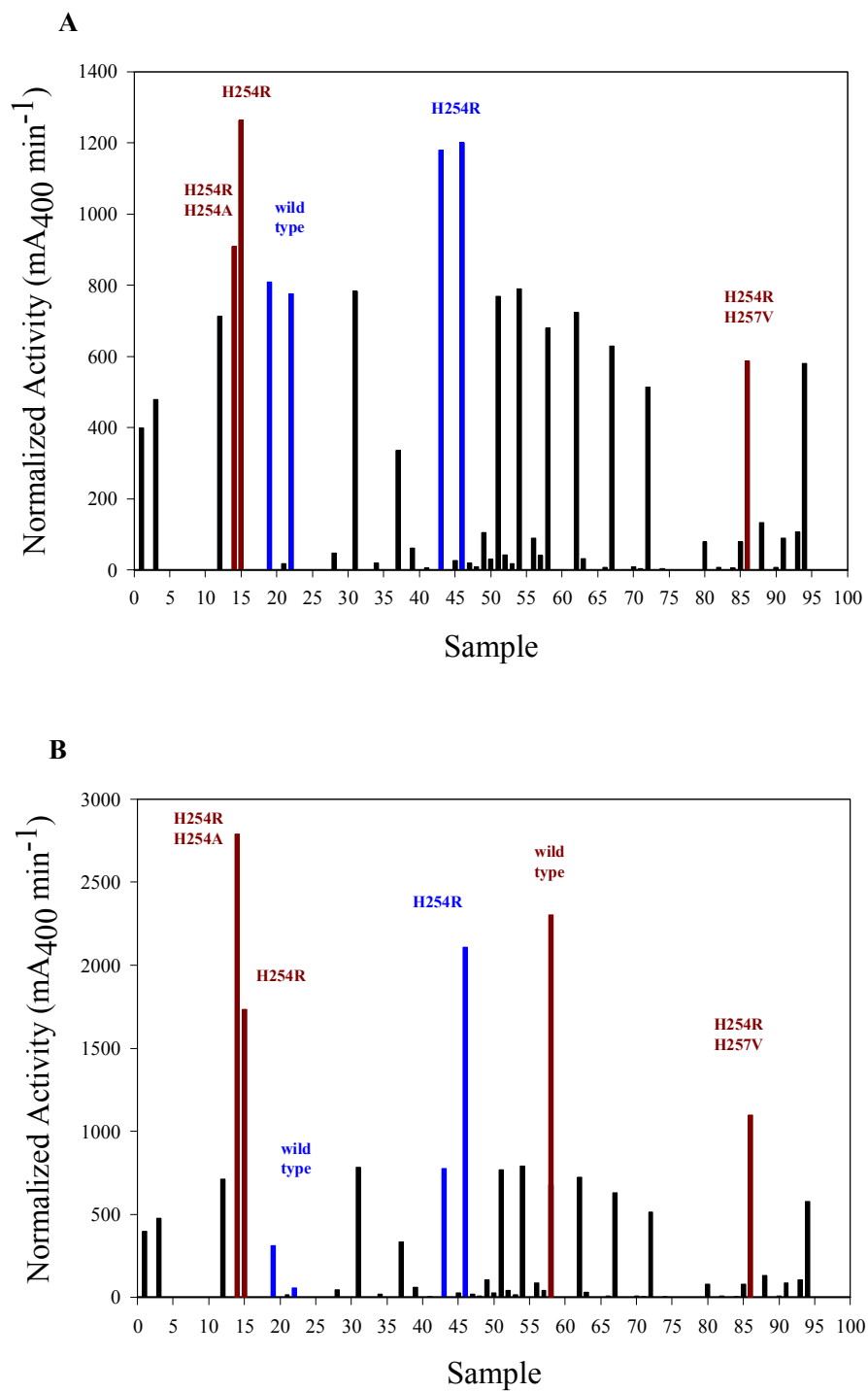


Figure 4.5. The results from the GB analog hydrolysis assays for plate 4 of the H254X-H257X library. The library was screened with  $S_p$ -(II) (A) and with the  $R_p$ -(II) (B).



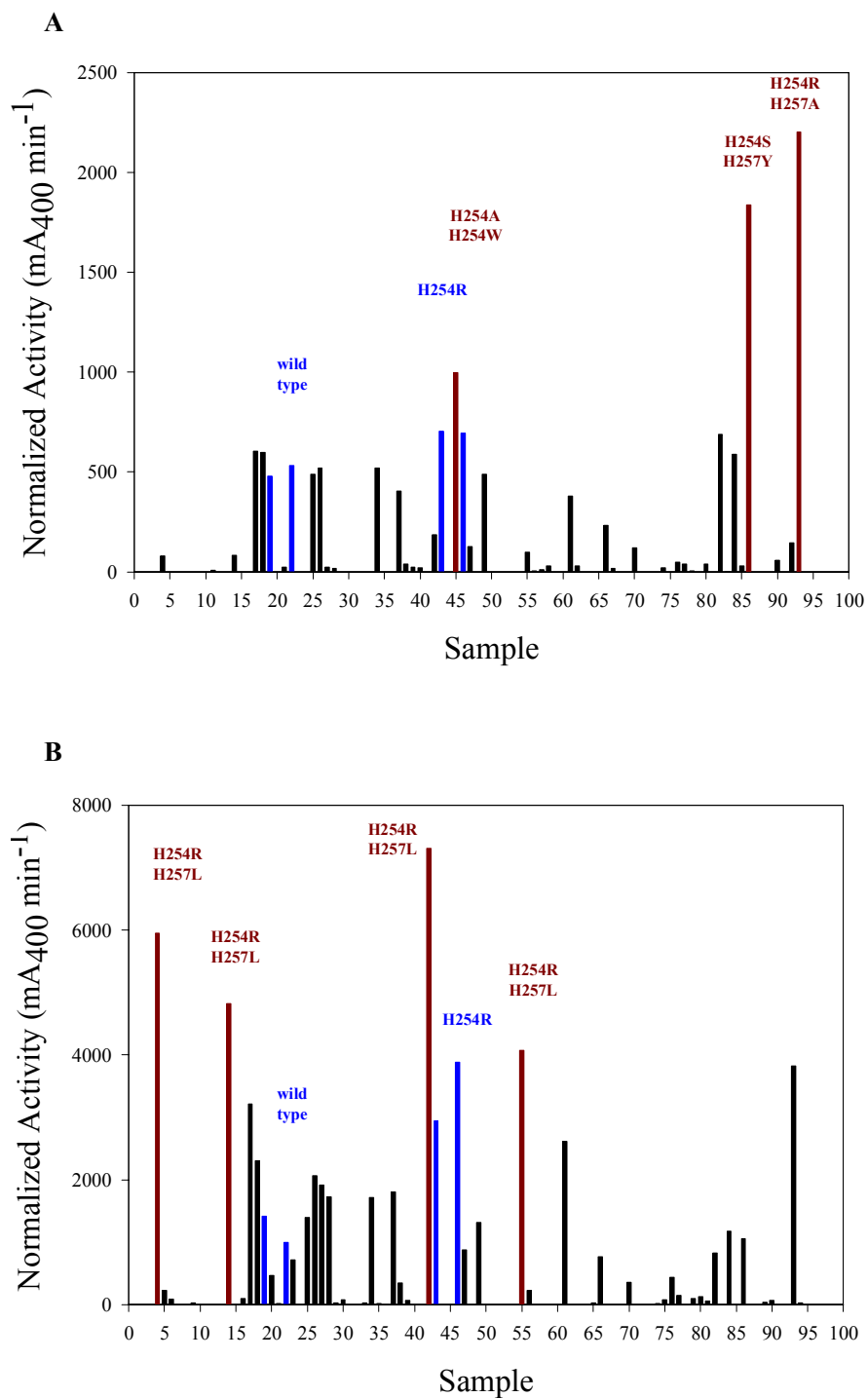


Figure 4.6. The results from the GB analog hydrolysis assays for plate 6 of the H254X-H257X library. The library was screened with  $S_p$ -(II) (A) and with the  $R_p$ -(II) (B).

The H254X-H257X library was constructed in the L303T construct. Fewer mutants were identified as having enhanced activity for isomers of the GB analog. In general, the background of library members was significantly lower than was seen in the H254X-H257X library created with the wild type. Figure 4.7 shows results from the S<sub>p</sub> and R<sub>p</sub> isomer hydrolysis assays. The standards used were wild type, G60A, I106A-F132A-H257Y, H254G-H257W, and H254G-H257W-L303T. The triple mutant I106A-F132A-H257Y had the highest activity for hydrolysis of the S<sub>p</sub> isomer, followed by H254G-H257W. H254G-H257W-L303T had lower activity, but was higher than wild type and G60A. The H254R-L303T and H254R-H257S-L303T mutants were identified as having activity higher than other library members within the plate.

Activity for hydrolysis of the R<sub>p</sub> isomer was higher for the library members. Wild type and G60A were among the samples with the highest activity. The remaining standards had very low levels of activity. Two mutants isolated after the assay were H254C-H257G-L303T and H254R-H257A-L303T.

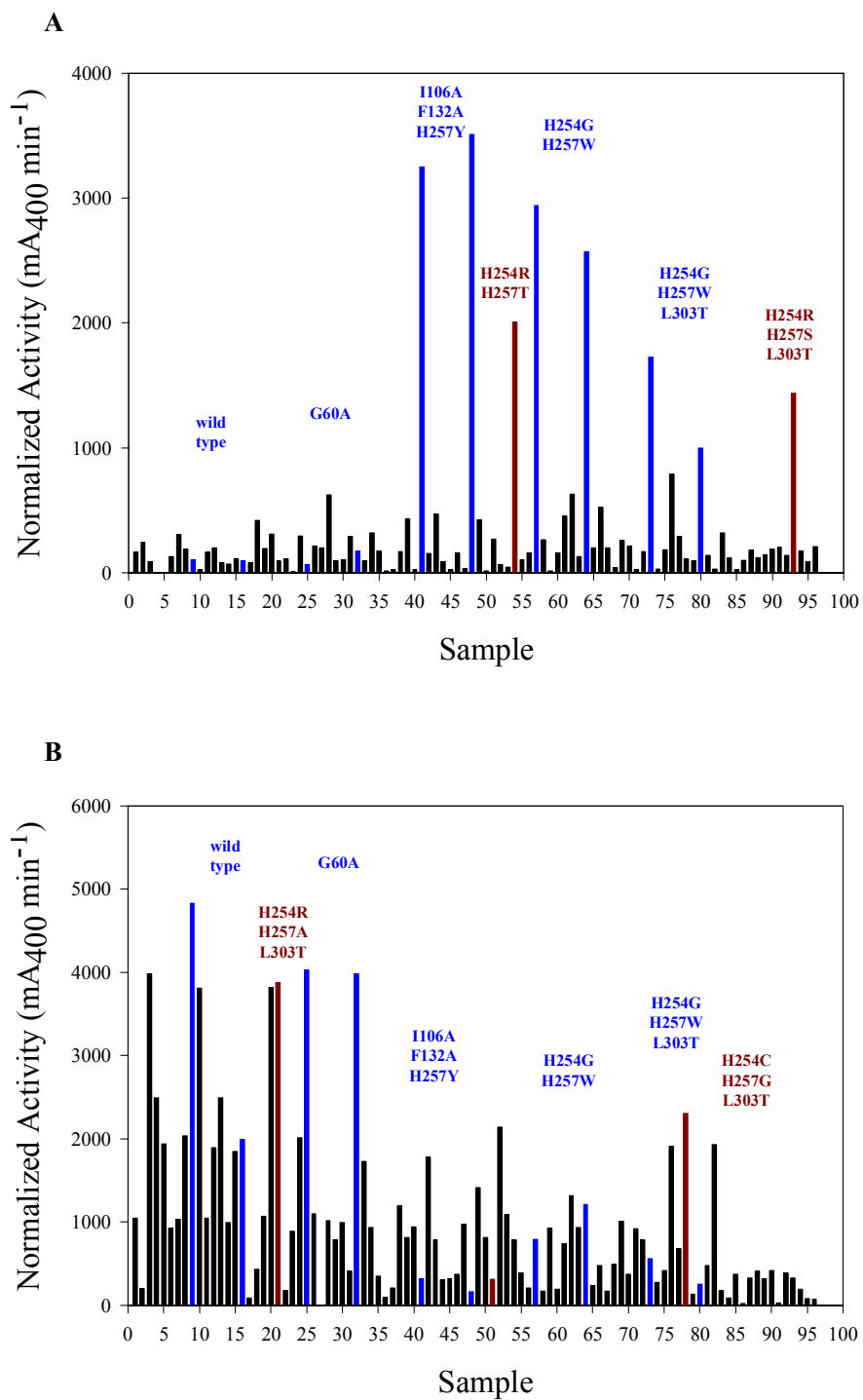


Figure 4.7. The results from the GB analog hydrolysis assays for the [H254-H257X]-L303T library. The library was screened with  $S_p$ -(II) (A) and with the  $R_p$ -(II) (B).

The relative activities of the mutants obtained from the assays were plotted in terms of increased activity with the hydrolysis of the  $S_p$  isomer of the GB analog, as determined from the crude culture assay. Many mutants with an increased rate in  $S_p$  GB analog hydrolysis had either an Arg or Gly at the 254 position. The identities of mutants that had an Arg at position 254, and had higher activity were H254R-H257M, H254R-H257A, H254R-H257L, H254R-H257V, and H254R-H257Y. Mutants with a Gly at position 254 were H254G-H257R, H254G-H257W, H254G-H257Y, and H254G-H257D. Other double mutations obtained were H254A-H257W and H254S-H257Y. In addition to the double mutations identified, several single substitution mutants displayed an increased rate of hydrolysis for the  $S_p$  isomer of the GB analog in comparison to wild type. These included H254G, H254R, and H257Y.

Several other mutants were chosen from the H254X-H257X double substitution library created in L303T. The mutants that were chosen had shown enhancements with the  $S_p$  isomers of soman analog screening, and were purified. The kinetic constants for the individual  $S_p$  and  $R_p$  isomers of the GB analog were determined for each protein, as shown in Table 4.2. The highest  $k_{cat}/K_m$  values for the  $S_p$  isomer were  $2.6 \times 10^6$  and  $1.9 \times 10^6 \text{ M}^{-1} \text{ s}^{-1}$  for H254R-L303T and H254R-H257S-L303T, respectively. The double mutant, H257Y-L303T, had a similar  $k_{cat}/K_m$  as the wild type. However, the turnover rate for this mutant was almost 10-times higher than that of the wild type. The lowest value for the  $S_p$  isomer was  $1.1 \times 10^4 \text{ M}^{-1} \text{ s}^{-1}$ , which was reported for H254R-H257A-L303T. All members from this library had higher  $k_{cat}/K_m$  values for the  $S_p$  isomer instead of the  $R_p$  isomer, with the exception of H254R-L303T. The  $k_{cat}/K_m$  for the  $R_p$  isomer was  $3.7 \times 10^6 \text{ M}^{-1} \text{ s}^{-1}$ .

Table 4.2. The kinetic constants for the individual  $R_p$  and  $S_p$  isomers of GB, along with the ratios determined from the catalytic efficiency and the ratios determined from the time course.

Protein	$R_p$	$S_p$	$R_p:S_p$ ( $k_{cat}/K_m$ )	Time Course Ratio		
wt-PTE	2600 ± 69	(8.3 ± 0.1) × 10 <sup>6</sup>	290 ± 2.2	(4.1 ± 0.1) × 10 <sup>5</sup>	20	10
G60A	2900 ± 200	(1.1 ± 0.1) × 10 <sup>7</sup>	58 ± 2	(7.2 ± 0.2) × 10 <sup>4</sup>	153	290
I106A-F132A-H257Y	410 ± 17	(9.0 ± 0.1) × 10 <sup>4</sup>	4200 ± 130	(2.7 ± 0.1) × 10 <sup>6</sup>	0.033	0.063
I106A-F132A-H257W	17 ± 0.9	(3.0 ± 0.1) × 10 <sup>4</sup>	2700 ± 118	(1.1 ± 0.1) × 10 <sup>7</sup>	0.003	0.002
I106A-S308A-H257Y	1800 ± 196	(5.7 ± 0.1) × 10 <sup>5</sup>	7200 ± 203	(2.8 ± 0.1) × 10 <sup>6</sup>	0.203	0.250
H254R	41 ± 1.2	(6.2 ± 0.1) × 10 <sup>5</sup>	30 ± 0.8	(3.3 ± 0.1) × 10 <sup>6</sup>	0.250	0.125
H257L	1849 ± 91	(2.7 ± 0.1) × 10 <sup>6</sup>	13 ± 0.1	(4.4 ± 0.1) × 10 <sup>4</sup>	61	44
H254G-H257W	56 ± 4.3	(2.2 ± 0.1) × 10 <sup>5</sup>	56 ± 2.1	(3.1 ± 0.1) × 10 <sup>6</sup>	0.071	0.167
H254G-H257R	484 ± 24	(2.7 ± 0.1) × 10 <sup>5</sup>	473 ± 55	(1.9 ± 0.1) × 10 <sup>6</sup>	0.143	0.333
S308A	8300 ± 115	(7.2 ± 0.1) × 10 <sup>6</sup>	220 ± 11	(1.2 ± 0.1) × 10 <sup>5</sup>	60	70
I106A-H257Y	2880 ± 231	(7.0 ± 0.1) × 10 <sup>5</sup>	6650 ± 189	(3.6 ± 0.1) × 10 <sup>6</sup>	0.250	0.333
H257Y-L303T	148 ± 35	(4.2 ± 0.1) × 10 <sup>4</sup>	2258 ± 62	(3.3 ± 0.1) × 10 <sup>5</sup>	0.100	0.333
H254R-H257A-L303T	36 ± 5.2	(1.1 ± 0.1) × 10 <sup>4</sup>	196 ± 27	(3.4 ± 0.1) × 10 <sup>4</sup>	0.333	0.500
H254R-H257S-L303T	177 ± 13	(3.1 ± 0.1) × 10 <sup>5</sup>	46 ± 2.6	(1.9 ± 0.1) × 10 <sup>6</sup>	0.167	0.167
H254R-L303T	368 ± 41	(3.7 ± 0.1) × 10 <sup>6</sup>	79 ± 5.8	(2.6 ± 0.1) × 10 <sup>6</sup>	1	1
H254A	460 ± 31	(2.9 ± 0.1) × 10 <sup>6</sup>	420 ± 19	(6.5 ± 0.1) × 10 <sup>6</sup>	0.500	0.333
H257Y	1900 ± 97	(2.2 ± 0.1) × 10 <sup>6</sup>	1700 ± 121	(3.6 ± 0.1) × 10 <sup>6</sup>	0.500	0.500
H254Q-H257F	42 ± 5.3	(1.1 ± 0.2) × 10 <sup>7</sup>	12 ± 0.8	(1.2 ± 0.1) × 10 <sup>5</sup>	83	133
H254R-H257A	6.7 ± 0.2	(1.2 ± 0.1) × 10 <sup>5</sup>	0.77 ± 0.05	(1.2 ± 0.1) × 10 <sup>5</sup>	1	4

Many of these mutants were purified to homogeneity, and the kinetic constants were determined for hydrolysis of the individual isomers of the GB analog. The mutants purified were H254R-H257A, H254Q-H257F, H254G-H257W, H254G-H257R, H254R-H257A-L303T, H254R, and H257Y. The mutants H254R-H257S-L303T and H257Y-L303T were previously obtained on the basis of enhancement observed with hydrolysis of the soman analog isomers.

In particular, three samples that displayed the highest activity were isolated and compared to wild type, G60A, and I106A-F132A-H257Y, for  $S_p$  GB analog hydrolysis as shown in Figure 4.8. All three were higher than wild type and G60A. The  $k_{cat}/K_m$  for  $S_p$  isomer hydrolysis was  $1.2 \times 10^6 \text{ M}^{-1}\text{s}^{-1}$ ,  $1.9 \times 10^6 \text{ M}^{-1}\text{s}^{-1}$ , and  $3.1 \times 10^6 \text{ M}^{-1}\text{s}^{-1}$  for the mutants H257R, H254G-H257R, and H254G-H257W, respectively. Only the mutant, H254G-H257W, was higher than the standard I106A-F132A-H257Y, which had a  $k_{cat}/K_m$  of  $2.7 \times 10^6 \text{ M}^{-1}\text{s}^{-1}$ .

A total of 18 mutants and the wild type were purified and assayed with both the  $R_p$  and  $S_p$  isomer of the GB analog. As seen in Table 4.2, there were three individual single mutants with  $k_{cat}/K_m$  values on the order of  $10^6 \text{ M}^{-1}\text{s}^{-1}$  for the  $S_p$  isomer. Among them, the highest was  $6.5 \times 10^6 \text{ M}^{-1}\text{s}^{-1}$  which was observed for H254A.

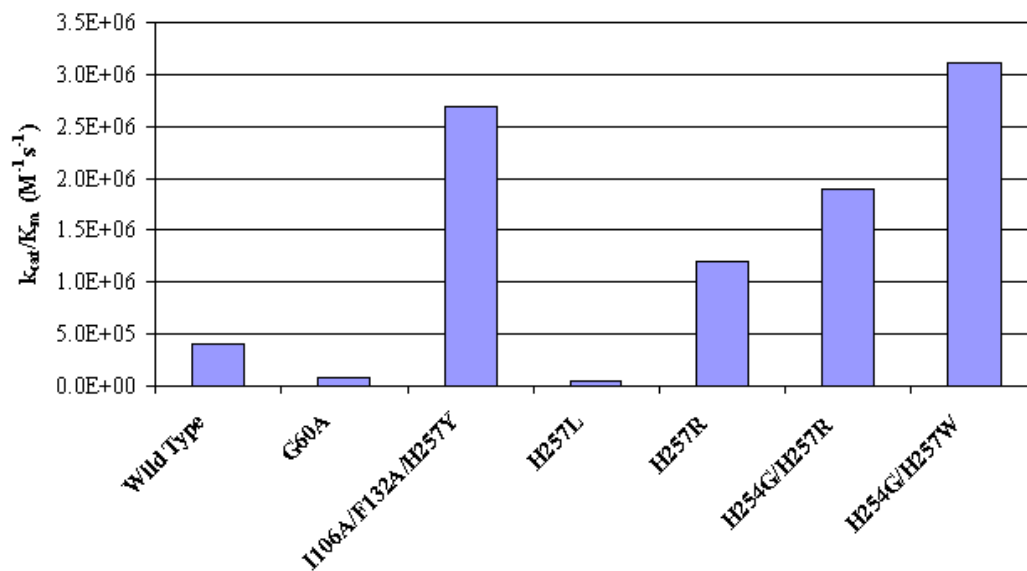


Figure 4.8. The catalytic efficiency of the purified mutants for the hydrolysis of the  $S_p$  isomer of the GB analog. These mutants were obtained from the screening of the H254X-H257X library.

### *Time Course Ratios*

As shown in Table 4.2, the kinetic constants for the individual isomers were determined for wild type and 18 mutant proteins. The turnover rate and catalytic efficiency were determined for each protein. Stereoselectivity was expressed as a ratio of preference for the R<sub>p</sub> isomer over the S<sub>p</sub> isomer, as calculated from the catalytic efficiency for hydrolysis of each isomer. A ratio of 1 would mean that there is equal preference for each isomer. This was obtained for both H254R-L303T and H254R-H257A. A ratio of 1:367 was reported for I106A-F132A-H257W, as the stereoselectivity for this protein has been reversed in comparison to wild type. The triple mutant greatly prefers the S<sub>p</sub> isomer over the R<sub>p</sub> isomer.

In comparison to the kinetic ratio, another ratio was determined from time courses with the racemic GB analog. Several serial dilutions of each protein were assayed with the racemic GB analog, and the rates of hydrolysis and amplitude(s) of curve were determined for each sample. By comparing each of the time courses, differential rates of hydrolysis of the substrate were determined. The ratios of rates were used in comparison to the kinetic ratios. The experimental ratios from both the individual isomers and the time course were similar.

As an example in Figure 4.9, there is a comparison of two different time courses constructed with wild type. One time course is done with 0.007 μg of wild type protein, and the other is done with 0.07 μg of wild type protein. The rate of hydrolysis as determined from the single exponential fit is different for each time course because of the different amount of enzymes added. The rate constants were  $9.45 \times 10^{-4}$  and  $9.38 \times 10^{-3}$ .



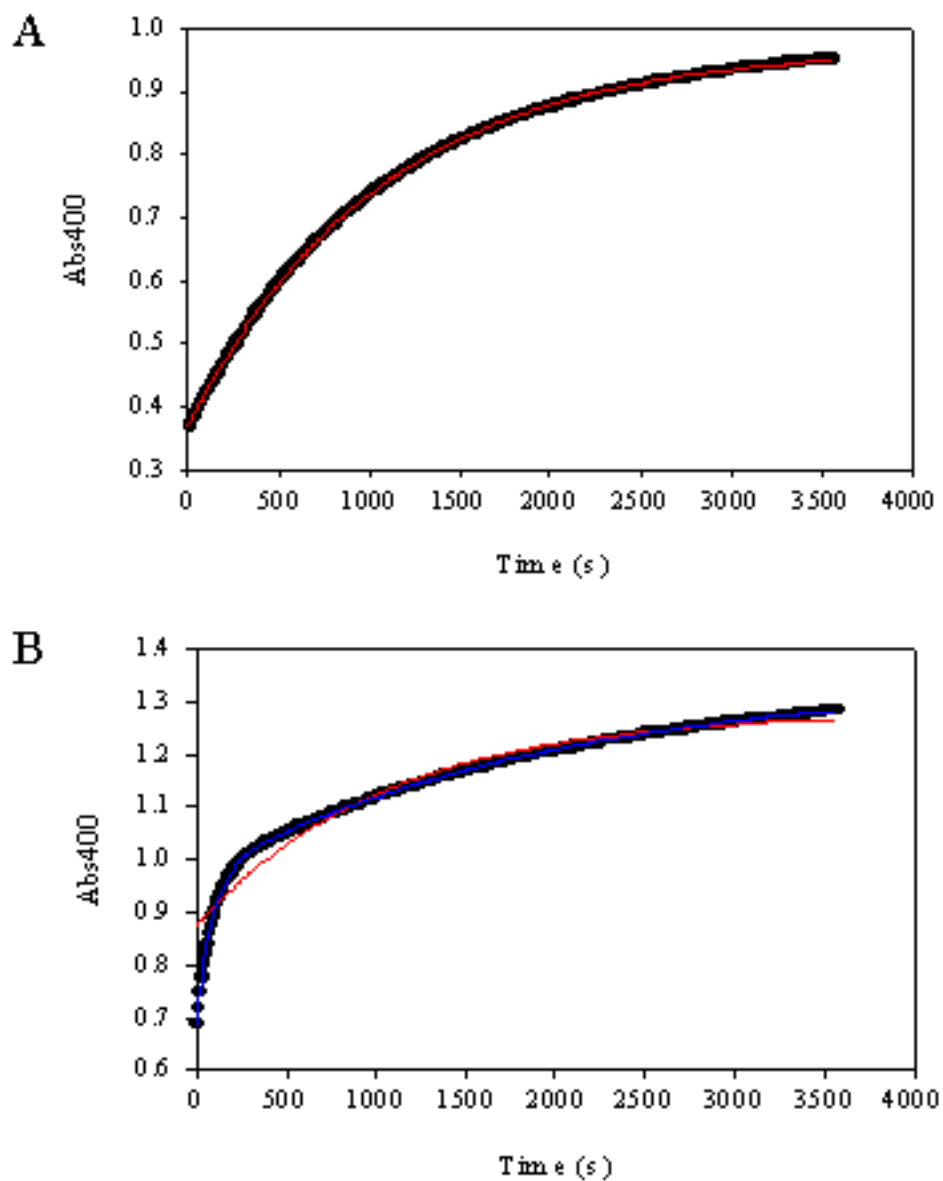


Figure 4.9. Two time courses from wild type catalyzed hydrolysis of the racemic GB analog. The first (A) is with 0.007  $\mu\text{g}$  of wild type, and the second (B) is 0.07  $\mu\text{g}$  of wild type diluted 100-times. By comparing the single exponential equations (red), there is a 10-fold difference between the two rates.

The rate for each is indicative of the rate for hydrolysis of one isomer. By comparing both plots, the difference in rates is obtained. In this example, the rate of hydrolysis was determined to be a 10. In comparison, the ratio from the kinetic data indicates there is difference of 20 between the catalytic efficiency of the R<sub>p</sub> and S<sub>p</sub> isomers of the GB analog, with the R<sub>p</sub> isomer preferred (Table 4.2).

In comparison, a greater difference can be seen with I106A-F132A-H257W as shown in Figure 4.10. The time courses were constructed with 0.005 μg and 0.45 μg of protein. The rate constants were  $4.8 \times 10^{-1}$  and  $9.6 \times 10^{-4}$ . The difference between the rates in the two plots was calculated as 505-fold. The ratio of catalytic efficiencies between the two isomers was 367, with the S<sub>p</sub> isomer preferred (Table 4.2).

The wild type and four mutant proteins were sent to Steven P. Harvey at the Edgewood Chemical Biological Center, to be assayed with racemic sarin. Time courses for wild type, G60A, I106A-F132A-H257Y, I106A-H257Y-S308A, and I106A-H257Y were constructed with 0.5 mM racemic GB. The concentration of fluorine released over time was recorded for each sample, in addition to non-enzymatic hydrolysis of the agent as shown in Figure 4.11. The hydrolysis of racemic GB by wild type, G60A, and I106A-H257Y were similar, and could be expressed as a single exponential function. The plots are shown in Figures 4.12, 4.13, and 4.14. However, hydrolysis catalyzed by both I106A-F132A-H257Y and I106A-H257Y-S308A appeared to be biphasic, and expressed as a double exponential function, as shown in Figures 4.15 and 4.16. The difference between rate constants was 22-fold for I106A-F132A-H257Y and 33-fold for I106A-H257Y-S308A. To confirm this observation, double enzyme plots were constructed using each enzyme.

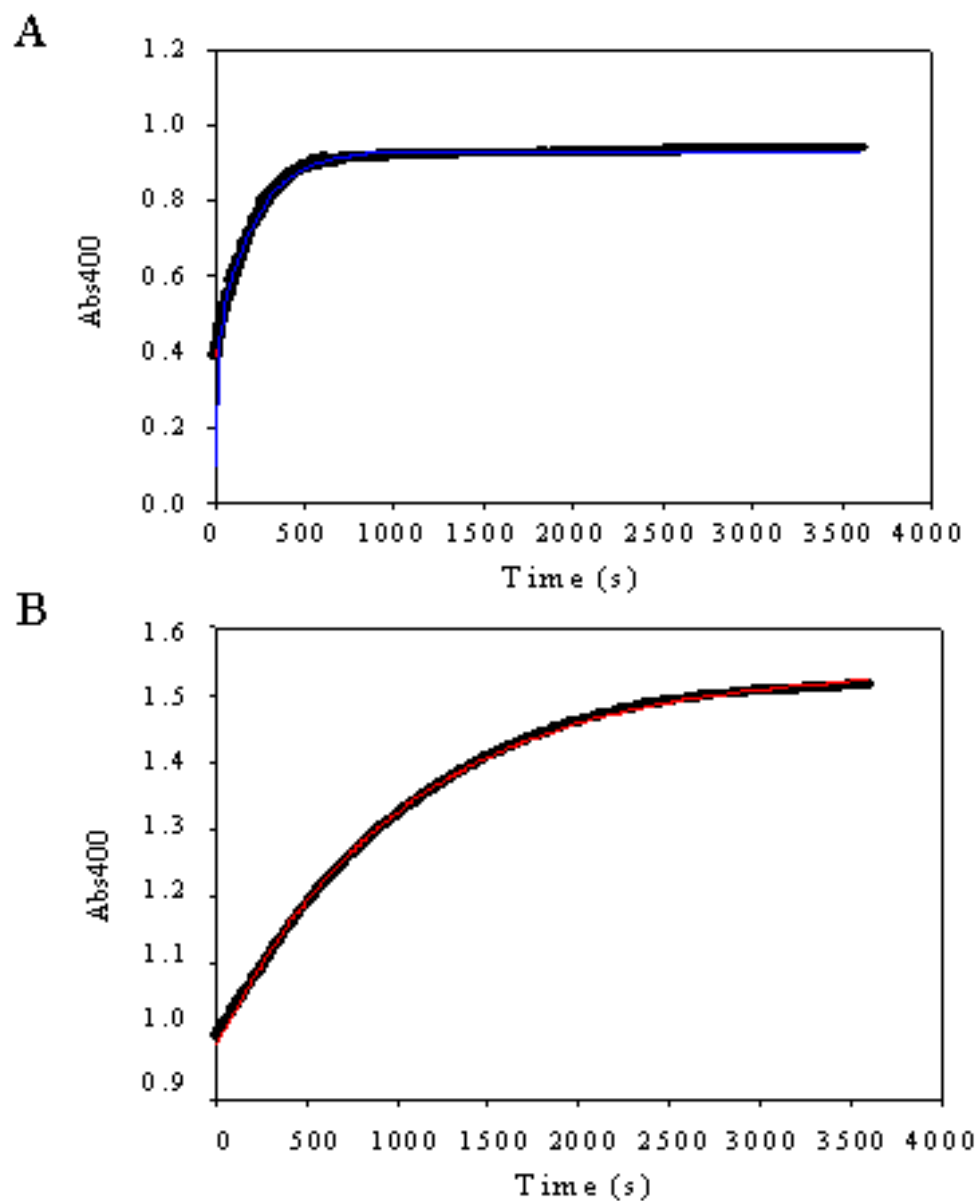


Figure 4.10. Two time courses from I106A-F132A-H257W-catalyzed hydrolysis of the racemic GB analog. The first (A) is with 0.0045  $\mu\text{g}$  of protein, and the second (B) is with 0.45  $\mu\text{g}$  of protein. By comparing the single exponential equations (red), the difference between the two phases is 505.

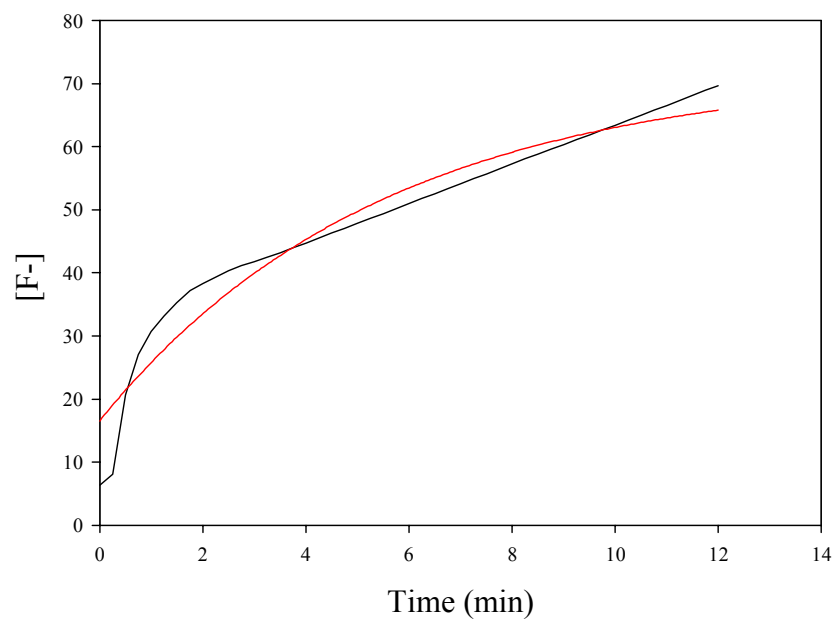


Figure 4.11. The non-enzymatic hydrolysis of 0.5 mM GB at pH 7.72 at 25 °C. The graph is expressed as concentration of fluorine in  $\mu\text{M}$  (y-axis) versus time in minutes (x-axis). The rate constant for hydrolysis was  $0.183 \text{ min}^{-1}$  and the amplitude was 55.4, as determined by the single exponential fit to the plot.

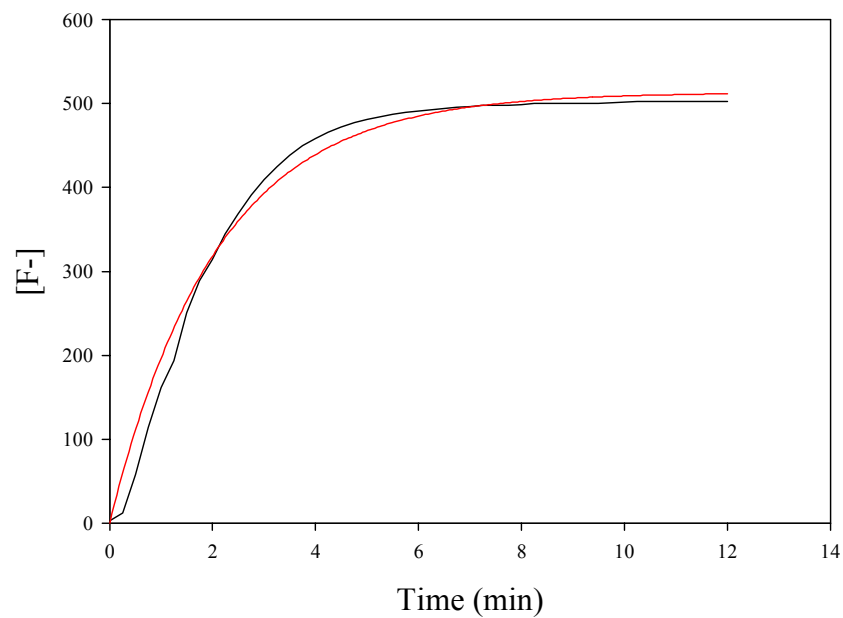


Figure 4.12. Wild type catalyzed hydrolysis of 0.5 mM GB at pH 7.72 at 25 °C. The graph is expressed as concentration of fluorine in  $\mu\text{M}$  (y-axis) versus time in minutes (x-axis). The rate constant for hydrolysis was  $0.484 \text{ min}^{-1}$  and the amplitude was 513, as determined by the single exponential fit to the plot.

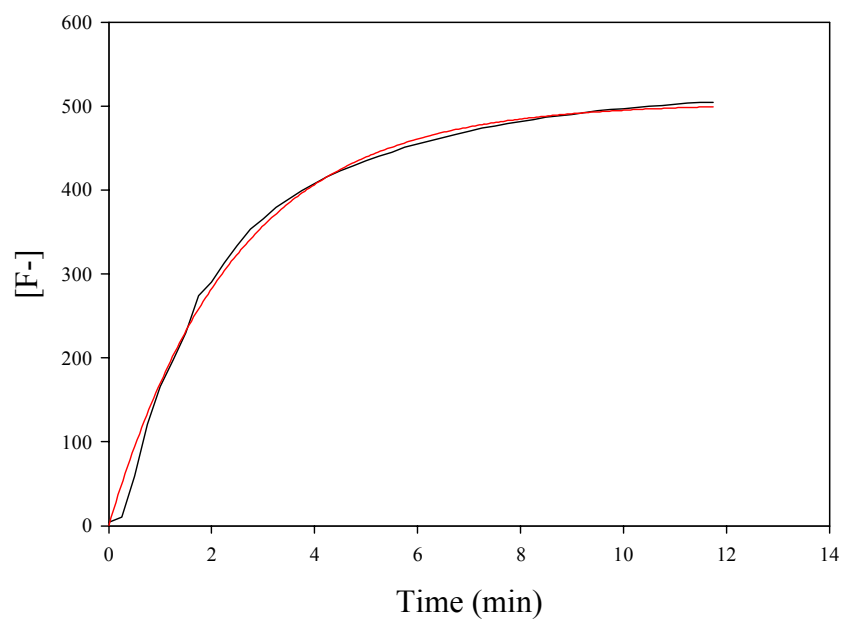


Figure 4.13. G60A catalyzed hydrolysis of 0.5 mM GB at pH 7.72 at 25 °C. The graph is expressed as concentration of fluorine in  $\mu\text{M}$  (y-axis) versus time in minutes (x-axis). The rate constant for hydrolysis was  $0.412 \text{ min}^{-1}$  and the amplitude was 503, as determined by the single exponential fit to the plot.

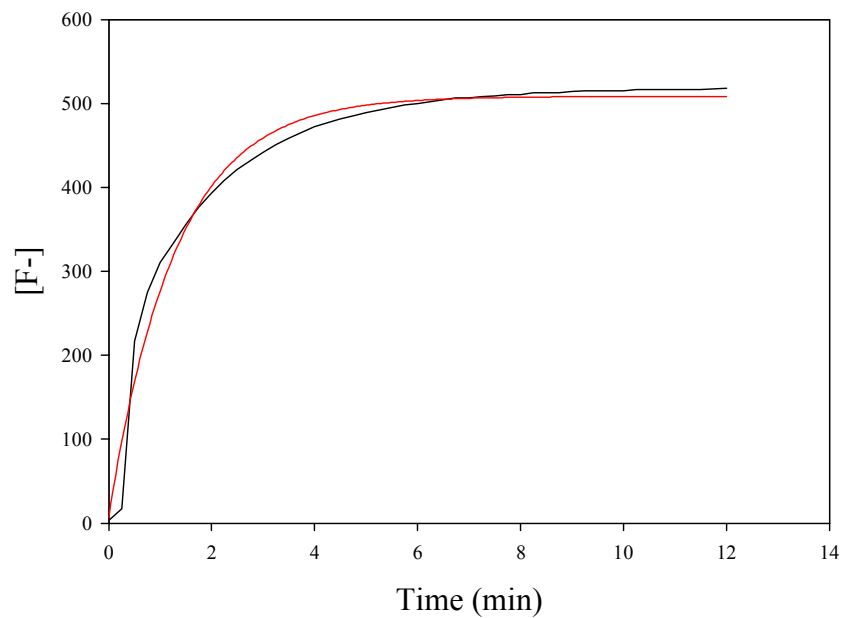


Figure 4.14. I106A-H257Y catalyzed hydrolysis of 0.5 mM GB at pH 7.72 at 25 °C. The graph is expressed as concentration of fluorine in  $\mu\text{M}$  (y-axis) versus time in minutes (x-axis). The rate constant for hydrolysis was  $0.772 \text{ min}^{-1}$  and the amplitude was 501, as determined by the single exponential fit to the plot.

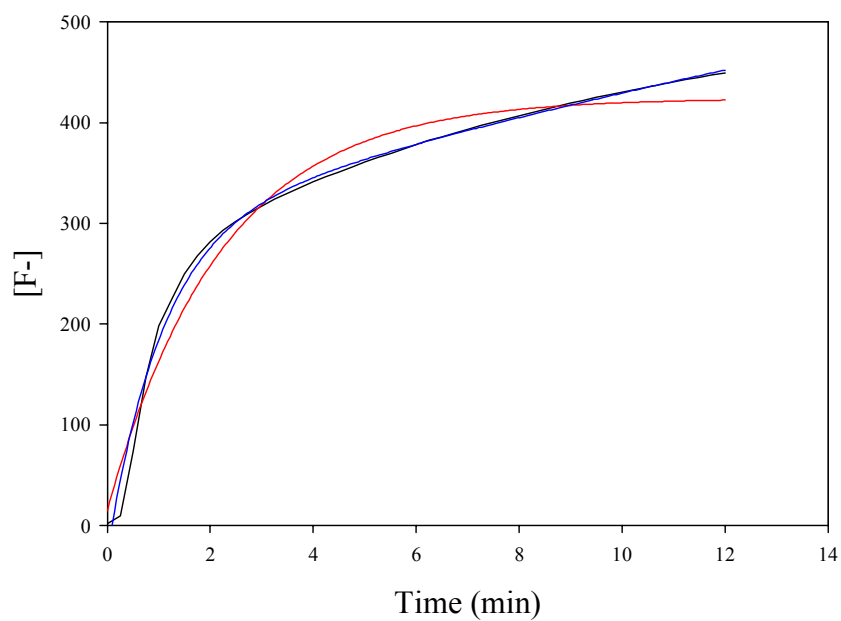


Figure 4.15. I106A-H257Y-S308A catalyzed hydrolysis of 0.5 mM GB at pH 7.72 at 25 °C. The graph is expressed as concentration of fluorine in  $\mu\text{M}$  (y-axis) versus time in minutes (x-axis). The rate constant for hydrolysis was  $0.451 \text{ min}^{-1}$  and the amplitude was 409, as determined by the single exponential fit to the plot. The rate constants for hydrolysis were calculated from a double exponential fit as  $0.954 \text{ min}^{-1}$  and  $0.029 \text{ min}^{-1}$ , and the amplitudes were 322 and 542.



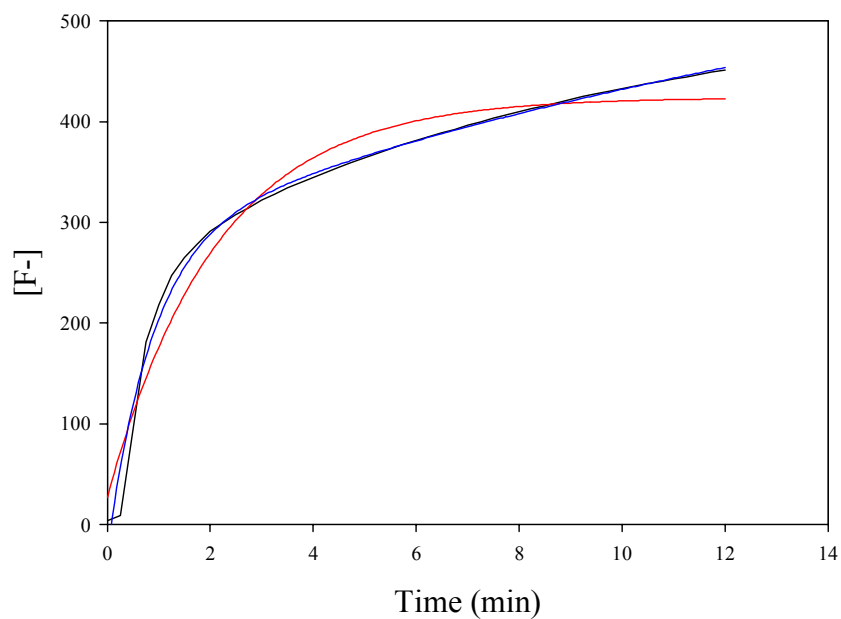


Figure 4.16. I106A-F132A-H257Y catalyzed hydrolysis of 0.5 mM GB at pH 7.72 at 25 °C. The graph is expressed as concentration of fluorine in  $\mu\text{M}$  (y-axis) versus time in minutes (x-axis). The rate constant for hydrolysis was  $0.0472 \text{ min}^{-1}$  and the amplitude was 398, as determined by the single exponential fit to the plot. The rate constants for hydrolysis were calculated from a double exponential fit as  $1.16 \text{ min}^{-1}$  and  $0.053 \text{ min}^{-1}$ , and the amplitudes were 309 and 366.

Double enzyme plots were constructed by adding enzymes pair wise into 0.5 mM racemic GB solution. In each case, the first enzyme was added at time zero. After one minute of hydrolysis, the second enzyme was added into the cuvette. The arrow in graphs A and B of Figure 4.17 denote the time of addition of the second enzyme. The detection of hydrolysis was measured by the release of fluorine over time.

In Figure 4.17A, I106A-F132A-H257Y was the first enzyme added. The addition of I106A-H257Y-S308A as the second enzyme is shown in with an orange line, and it appeared to behave in the same way as the addition of I106A-F132A-H257Y as the second enzyme, which is marked by the blue line. In contrast, there was a marked increase in fluorine when wild type protein was added as the second enzyme, which is illustrated by the red line in the graph. A similar situation is seen in Figure 4.17B, in which I106A-H257Y-S308A was used as the first enzyme. Both triple mutants behaved in the same manner, and a sharp increase in fluorine was seen with the addition of the wild type enzyme.

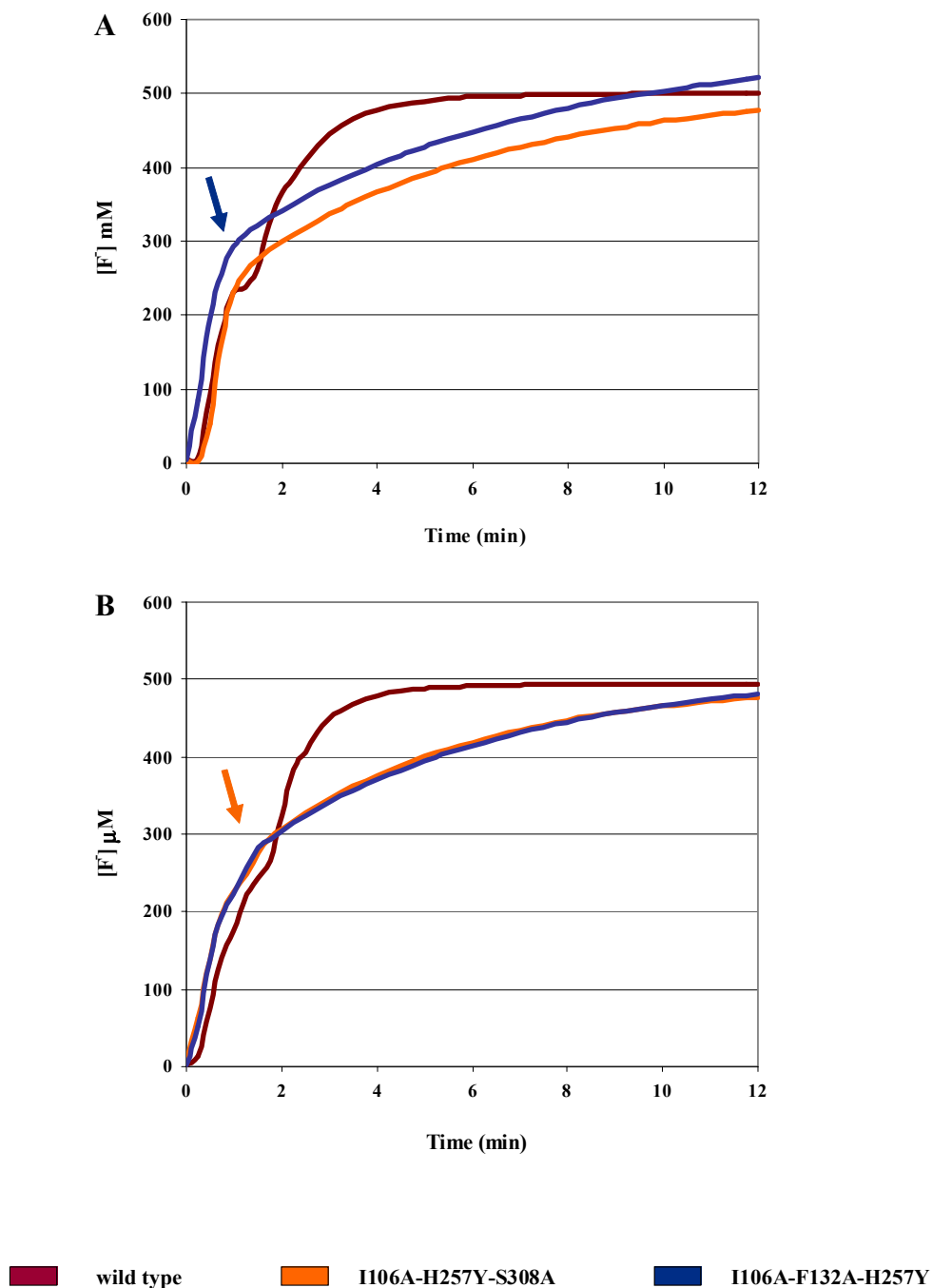


Figure 4.17. The double enzyme plot of GB hydrolysis. The triple mutant, I106A-F132A-H257Y is the first enzyme added in the first plot (A), and I106A-H257Y-S308A is the first enzyme added in the second plot (B).

## Discussion

### *Libraries of PTE Mutants*

Most of the improvements for GB analog hydrolysis were seen with the Arg and Gly containing mutants isolated from the H254X-H257X library. Almost all of the mutants identified as having increased activity for the S<sub>p</sub> GB analog hydrolysis were of that description, as seen in Figure 4.8. All of the mutants that appeared at least 2 times faster than the wild type from the crude culture screens did in fact have higher kinetic constants for the S<sub>p</sub> GB analog isomer. However, the ability to distinguish the level of enhancement was not accurately obtained from the screens. For example, the H257R mutant appeared to be over 5 times faster than the wild type as determined from the screening assays. Upon purification, the mutant was 3 faster for S<sub>p</sub> analog hydrolysis. Conversely, the H254G-H257W mutant appeared to be only 3.5 times faster than the wild type, but after purification, the mutant was 7.6 times faster than the wild type.

The mutants from the H254X-H257X library within L303T proved to be less efficient at GB analog hydrolysis. In fact, it appeared that fewer number of mutations within the His254-His257 region were beneficial. The highest catalytic efficiencies for S<sub>p</sub> isomer hydrolysis were reported for single mutants, or for mutants containing a single mutation within the *large subsite*. As observed with the triple mutant I106A-F132A-H257W, the catalytic efficiency for S<sub>p</sub> isomer hydrolysis was  $1.1 \times 10^7 \text{ M}^{-1} \text{ s}^{-1}$ , exceeding wild type and other mutants. Other single mutations such as H254A, H257Y, and H254R were also quite efficient, having catalytic efficiencies on the order of  $10^6 \text{ M}^{-1} \text{ s}^{-1}$ .

Although there was very little improvement for GB analog hydrolysis with mutants obtained from the double substitution library in L303T, the stereoselective preference was

successfully reversed in comparison to the preference elicited by wild type protein. Almost all of the mutants obtained from both H254X-H257X libraries were shown to preferentially hydrolyze the  $S_p$  isomer faster than the  $R_p$  isomer. These results indicate that reversal of stereoselectivity was successfully achieved through directed evolution experiments with PTE.

### *Kinetic Data Comparison*

Because the  $R_p$  isomer of the GB analog corresponds to the non-toxic isomer of GB, directed evolution experiments were only focused on improvements for  $S_p$  isomer hydrolysis. With the exception of the H254Q-H257F mutant, there were no improvements in  $R_p$  isomer hydrolysis within the H254X-H257X library. The catalytic efficiency of  $R_p$  isomer hydrolysis was 1.2 times faster for H254Q-H257F in comparison to the wild type.

Among the 17 samples tested, S308A had the highest turnover rate for  $R_p$  isomer hydrolysis, which was approximately 3 times faster than wild-type PTE. The mutant, G60A, had the highest catalytic efficiency for the hydrolysis of the  $R_p$  GB analog. It was 1000-times higher than the lowest catalytic efficiency, which was reported for H254R-H257A-L303T. Almost all of the mutants with one or more mutations in the *large subsite* were much slower than the wild type for  $R_p$  isomer hydrolysis.

Most of the improvements made for GB analog hydrolysis were seen with the improvement of rates for  $S_p$  isomer hydrolysis. Enhancement of  $S_p$  isomer hydrolysis is crucial for detoxification of GB because the  $S_p$  isomer corresponds to the toxic isomer.

Contrary to the results with the  $R_p$  isomer, many improvements were seen for  $S_p$  isomer hydrolysis with mutants containing only one mutation in the *large subsite*. Half of

the mutants listed in Table 4.2 had a turnover rate that was higher than the wild type. The mutant, I106A-S308A-H257Y, had the highest turnover rate for S<sub>p</sub> isomer hydrolysis, which was almost a 25-fold enhancement in comparison to the wild type. The highest catalytic efficiency for S<sub>p</sub> isomer hydrolysis was reported as  $1.1 \times 10^7 \text{ M}^{-1} \text{ s}^{-1}$ , and was equal to the highest catalytic efficiency for the complementary R<sub>p</sub> isomer, as seen in Figure 4.2. In fact, 75% of the mutants exhibited enhanced catalytic efficiency for the hydrolysis of the S<sub>p</sub> GB *p*-NP isomer.

#### *Stereoselectivity Expressed as a Ratio*

There was a good correlation between the ratio of stereoselectivity obtained from both the kinetic parameters and from the time course with the GB analog racemate. In general, the ratios differed from 1- to 2-times each other, and reflected comparable degrees of stereoselectivity. For example, both H254R-L303T and H254R-H257A exhibited a low ratio between the catalytic efficiencies for each isomer. Each protein had equal preference for the individual isomers as expressed in terms of  $k_{\text{cat}}/K_m$ , and a similar ratio of rates of hydrolysis within the racemic mixture. The difference in rates of hydrolysis within the racemic mixture was 1-fold for the H254R-L303T, and for H254R-H257A it was 4-fold different.

Even large ratios were distinguishable within the time course. As an example, I106A-F132A-H257W preferentially hydrolyzed the S<sub>p</sub> isomer in favor of the R<sub>p</sub> isomer 367 times faster, as determined by comparison of catalytic efficiencies. A high degree of stereoselectivity was also reflected from the time course. There was a 505-fold difference between rates of hydrolysis for the individual isomers within the racemic mixture.

Figures 4.12 to 4.16 were constructed from data with live nerve agent. The concentration of GB used was kept low at 0.5 mM, to eliminate the effects of racemization. The data suggested varying degrees of stereoselectivity for different mutants of PTE, which was assumed after observing similar results with the GB analog. Both triple mutants I106A-F132A-H257Y and I106A-H257Y-S308A displayed a greater degree of stereoselectivity for hydrolysis of the individual isomers, when compared to the wild type (Figures 4.15, 4.16, and 4.12). The differential rates of hydrolysis were visibly detected when compared to the wild type in Figure 4.12 and other mutant proteins in Figures 4.13 to 4.16. By fitting the data to double exponential curves, it was determined that each triple mutant preferentially hydrolyzed one isomer 24-times faster than the other. The ratio of 24, obtained from the rates of hydrolysis with live nerve agent, was similar to the ratio of 30, determined from the comparison of catalytic efficiencies between the individual pure isomers for I106A-F132A-H257Y.

In comparison, there was more variation between data with the live nerve agent and the analog for I106A-H257Y-S308A. The ratio obtained from the kinetic data for the individual isomers was almost 5-times smaller than what was observed with live nerve agent. The situation was reversed with the wild type protein in that the difference of 4-fold, observed with the live agent was smaller than the difference of 20-fold, calculated from kinetic data.

Pair wise additions of each of the triple mutants confirmed the stereoselectivity observed in Figure 4.17. It appeared that both I106A-F132A-H257Y and I106A-H257Y-S308A shared the same order of preference, as well as degree of stereoselectivity. In contrast, the wild type preference was complementary to that of the triple mutants. When

wild type was added, there was a sharp increase in fluorine detected. This would perhaps indicate that the order of preference has been reversed by the mutants, and would also correspond to similar results with the GB analog.



**CHAPTER V**  
**ORGANOPHOSPHATE NERVE AGENT ANALOG TOXICITY**  
**IN HYDRA ATTENUATA**

**Introduction**

Organophosphates have been utilized in various applications since their initial discovery in the early 19<sup>th</sup> century (Furtado and Chan, 2001). Their most noted employment is usage as agricultural insecticides and chemical warfare agents. Organophosphates were introduced as pesticides after World War II and subsequently incorporated into common agricultural practices ever since (Furtado and Chan, 2001). It is estimated that approximately 200 different organophosphate insecticides are currently used commercially worldwide (Klaassen, 1996). The accumulation of these pollutants has raised environmental concerns due to the inherent toxicity of these compounds (US EPA, 2001). In general, the mechanism of toxicity involves the inhibition of enzyme activities and the release of neurotransmitters (Klaassen, 1996). Acute toxicity results primarily from the inactivation of the enzyme acetylcholine esterase (AChE). However, other direct targets of organophosphate intoxication include the muscarinic and nicotinic acetylcholine receptors. Symptomatic manifestations of organophosphate intoxication leading to death include pinpoint pupils, breathing difficulties, coma, and convulsions. While the mechanism of toxicity is believed to be similar in all species, the chemical dosage directs the intensity of the response (Klaassen, 1996)(Ecobichon and Joy, 1994).

From studies on acute toxicity, LD<sub>50</sub> values of organophosphates for humans have been estimated based on studies using mammals with a variety of chemical warfare agents

(Committee on Toxicology, 1997). However, most of these studies were conducted between 1940 and 1980, and almost all of these measurements were focused on controlled, acute exposures (Reutter, 1999). The acquisition of new toxicity data is hampered by multiple regulations and government restrictions. Some of these limitations involve animal sample size and the enormous expense associated with such studies. In this investigation, the toxicities for chiral and achiral analogs of GB, GD, and VX were evaluated using *Hydra attenuata* as the model organism.

*Hydra attenuata* is a common freshwater Cnidarian found in slow-moving waters (Karntanut and Pascoe, 2000). Cnidarians are true metazoa with only two body layers; an outer epidermis and the inner gastrodermis. As diploblasts, all of the cells are in close proximity to the aqueous medium and the immediate environment. This particular feature enables *Hydra* to be very sensitive and susceptible to minute amounts of environmental toxicants. In addition to sensitivity, the *Hydra* bioassay is remarkably reproducible because of asexual reproduction, yielding clones of individual organisms. The cost and overall simplicity of this bioassay has contributed to an increase in the number of recent studies using *Hydra* in acute and chronic toxicity tests of water-soluble compounds (Ronco et al., 2002)(Diaz-Baez, 2002). Previous studies have exploited the use of the *Hydra* bioassay to assess the toxicity of various compounds including chlorinated phenols (Mayura, 1991), heavy metals (Karntanut and Pascoe, 2000), and estrogenic compounds (Pascoe et al., 2002). An investigation involving the invertebrate organism, *Daphnia magna*, has also shown a significant correlation with established rat oral LD<sub>50</sub> values (Guilhermino et al., 2000). Therefore, this system shows great potential as an alternative means to animal testing in pre-screening trials for the prediction of toxicity of specific organophosphate compounds.

Structure-activity relationships were established for the toxic properties using a series of chiral and achiral organophosphate analogs of the nerve agents GB, GD and VX. The toxicity of each organophosphate nerve agent was quantitatively assessed by determining the minimal effective concentration (MEC) in *Hydra* after 92 hours. The conclusions of this investigation correlate well with organophosphate toxicity studies previously described by Singh (Singh, 2001) and Makhaeva et al. (Makhaeva et al., 1998). Based on the data from this investigation, there is significant potential for the application of this bio-assay in the detection of organophosphate chemical warfare agents, in addition to the prediction of toxicity for structurally similar organophosphate compounds.

## **Materials and Methods**

### *Hydra attenuata*

*Hydra attenuata* were cultured from organisms that were received as a gift from E. Marshall Johnson, Jefferson Medical College (Philadelphia, PA). Cultures of *Hydra* were maintained in shallow bowls of culture solution, and stored at 18 °C. The culture solution contained 1.0 mM calcium chloride, 0.45 mM TES (N-tris[hydroxymethyl]methyl-2-aminoethane sulfonic acid) buffer, and 0.012 mM ethylenediamine tetracetic acid (EDTA), pH 7.0. Deionized water was used throughout all of the maintenance and assay solutions.

### *Artemia saliva*

*Axenic nauplii* of brine shrimp (*Artemia saliva*) were prepared on a daily basis, beginning three days before each bioassay was conducted. The procedure and conditions for incubation were adapted from Lenhoff (Lenhoff, 1983). After the *nauplii* were hatched in

1% (w/v) NaCl solution, they were treated with iodine (40 ppm) for 15 minutes and subsequently washed with deionized water. The *axenic nauplii* were fed to the *Hydra* once a day for a period of 30 minutes. After feeding, the debris from the feeding was removed by thorough rinsing of the *Hydra* with culture solution. Food was withheld beginning twenty-four hours before initiating the bioassay and throughout the testing period.

### *Assay Procedures*

Procedures for this study were modified from those described by Johnson *et al.* (Johnson *et al.*, 1982). Only adult *Hydra attenuata* were used in the bioassays and each test was run in triplicate. For each concentration of the tested compounds, 4 mL of culture media was placed in a small petri dish. The control dish consisted of culture media alone. All of the test dishes were incubated at 18 °C throughout the assay. Adult *Hydra* were observed for symptoms of toxic response at 0, 4, 20, 28, 44, 68, and 92 hours.

The minimal effective concentration (MEC) at 92 hours was determined for each compound tested through a series of assays, consisting of three phases. The first phase involved exposing adult *Hydra* to whole log concentrations of each compound, to determine the range of toxicity apparent within 92 hours. The “tulip” stage was defined as the toxic endpoint of each assay. The lowest concentration of the test compound resulting in the toxic endpoint (*e.g.* MEC) was carried forward to the second phase of testing. In phase II of testing, the highest and lowest concentrations of the compound were within one log unit of one another. The MEC from the second phase of testing was used as the highest concentration in the phase III testing. The results from the phase III test were used to confirm those of the previous assays.

### *Chemicals and Reagents*

All buffer reagents were purchased from Sigma Chemical Co. Aroclor 1254-induced male rat liver, post mitochondrial supernatant (S-9) was purchased from Molecular Toxicology (Boone, NC) and used as the microsomal activation package (MAP). Synthesis of the racemic GB analog (IV) and the racemic GD analog (V), along with the chemo-enzymatic preparation of the chiral analogs were prepared as described in Li et al. (Li et al., 2001). The VX analogs, ecothiophate iodide (VI), diethyl VX (VII), and tetriso (VIII), and were synthesized by modifications of procedures described in the literature (Ghosh, 1957)(Hoskin et al., 1969). All of these compounds are toxic and should be used with the appropriate safeguards.

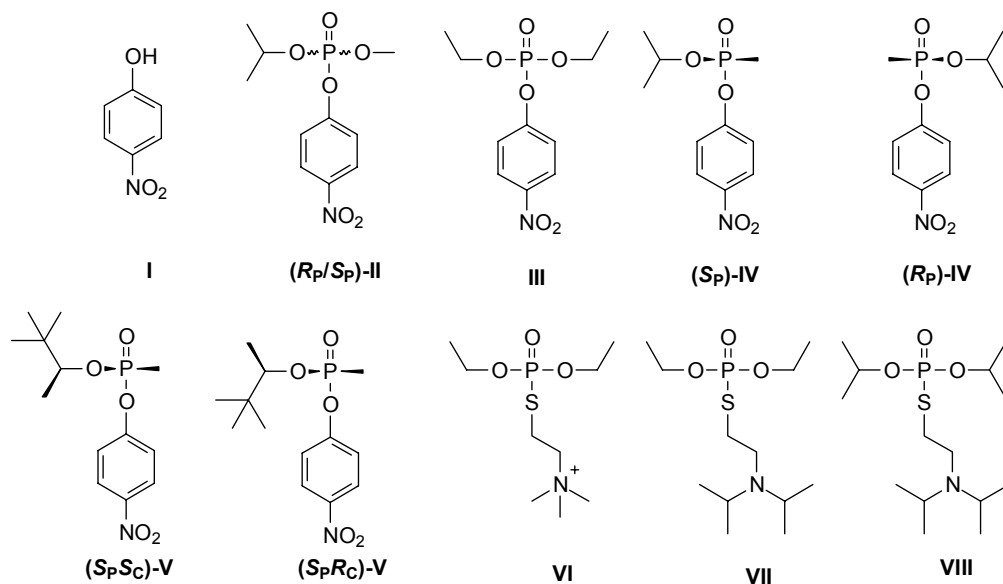
### *Structure Activity Analysis*

A model for each of the organophosphate compounds was made using ISIS/DRAW. The resulting files were imported into HyperChem Release 7 (Hyper Cube, Inc.), and various calculations were carried out. Properties, such as the octanol-water partition coefficient and polarizability, were obtained for each of the compounds tested. HyperChem calculations were made by a grid method assessment of van der Waals and solvent-accessible surfaces (Hasel et al., 1988). Determination of the octanol/water partition coefficients was based on implementation of an atom fragment method as described by Ghose et al. (Ghose et al, 1988). Polarizability information was deduced using an atom-based method as described by Miller (Miller, 1990). Geometry optimization data and molecular dynamics calculations were also determined after the structures of the compounds were modeled in Cerius<sup>2</sup> from Accelrys on a Silicon Graphics workstation.

## Results

### Chemical Compounds

A total of 10 different compounds were synthesized and analyzed for their toxicological properties using *Hydra* as the test system. Methyl isopropyl *p*-nitrophenyl phosphate (II) was utilized as a racemic mixture, while the sarin analog (IV) was prepared as individual enantiomers. The soman analog (V) was used as a mixture of 4 diastereomers, a mixture of the two possible  $S_p$  isomers, and as the single  $S_pS_c$  enantiomer. The three analogs of VX (VI, VII and VIII) are achiral. The structures of these compounds are presented in Scheme 1.



Scheme 1. The test substrates used in the *Hydra* Bioassay; *p*-nitrophenol (I), methyl isopropyl *p*-nitrophenyl phosphate (II), paraoxon (III), the GB analog, methyl isopropyl *p*-nitrophenyl phosphonate, methyl pinacolyl *p*-nitrophenyl phosphonate (IV), ecothiophate (V), diethyl VX (VII), and tetriso (VIII).

### *Hydra* Bioassay

*Hydra* were used to assess the toxicological properties of selected organophosphate nerve agents. In these tests, the *Hydra* were observed to undergo a series of morphological changes as a function of time and these physical changes are illustrated in Figure 5.1. The tentacles first begin to be “clubbed” at the end (Figure 5.1B) and then shorten in length (Figure 5.1C). The *Hydra* continue to shrink to a “tulip” stage (Figure 5.1D) and then eventually disintegrate (Figure 5.1E). The “tulip” stage is defined as the toxic endpoint. The minimum effective concentration was determined for each compound through a series of three tests. In the first test, the compound was assayed in increments of whole log concentrations. During the first stage of testing, the concentration at which the *Hydra* reached the toxic endpoint within 92 hours was used as the upper limit in the second phase of the assay. For example, the toxicity of paraoxon (III) on *Hydra* was first examined with a range from  $2.5 \times 10^{-4}$  to  $2.5 \times 10^2$  mg/L. From this initial assessment, the toxicity after 92 hours occurred from an exposure to paraoxon that was within the range from 2.5 to 25 mg/L. Representative data are presented in Figure 5.2. The second and third tests (data not shown) confirmed that the  $MEC_{92h}$  was 25 mg/L. Throughout each phase of testing, the culture solution was used in the absence of added nerve agent as a negative control to ensure the integrity of the *Hydra* throughout the assay. The  $MEC_{92h}$  values for the remaining 9 compounds were determined in exactly the same manner and the final values are summarized in Table 5.1.

Table 5.1. The MEC<sub>92h</sub> (mg/L) for each of the compounds administered are listed with the corresponding calculated log partition coefficient.

<b>Compound</b>	<b>MEC<sub>92h</sub> (mg/L)</b>	<b>log partition coefficient [octanol/water]</b>
<b>I</b>	9.4 x 10 <sup>1</sup>	-2.2
<b>(R<sub>P</sub>/S<sub>P</sub>)-II</b>	6.0 x 10 <sup>1</sup>	-0.92
<b>III</b>	2.5 x 10 <sup>1</sup>	-0.99
<b>(R<sub>P</sub>)-IV</b>	1.0 x 10 <sup>2</sup>	
<b>(R<sub>P</sub>/S<sub>P</sub>)-IV</b>	2.0 x 10 <sup>-2</sup>	-1.5
<b>(S<sub>P</sub>)-IV</b>	1.3 x 10 <sup>-2</sup>	
<b>(R<sub>P</sub>R<sub>C</sub>/R<sub>P</sub>S<sub>C</sub>/S<sub>P</sub>R<sub>C</sub>/S<sub>P</sub>S<sub>C</sub>)-V</b>	2.5 x 10 <sup>-4</sup>	-0.12
<b>(S<sub>P</sub>R<sub>C</sub>/S<sub>P</sub>S<sub>C</sub>)-V</b>	2.0 x 10 <sup>-4</sup>	
<b>(S<sub>P</sub>S<sub>C</sub>)-V</b>	8.0 x 10 <sup>-5</sup>	
<b>VI</b>	1.0 x 10 <sup>-4</sup>	2.0
<b>VII</b>	3.0 x 10 <sup>-6</sup>	3.1
<b>VIII</b>	3.0 x 10 <sup>-6</sup>	3.9



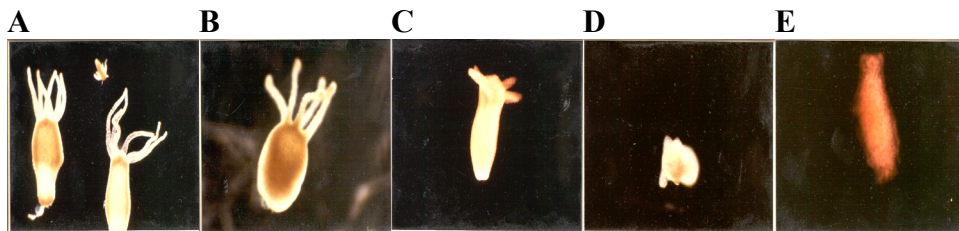


Figure 5.1. The physical stages of adult *Hydra attenuata*. The stages involve the following: (A) normal state; (B) clubbed tentacles; (C) shortened tentacles; and (D) the tulip stage, also defined as the toxic endpoint of the bioassay (E).

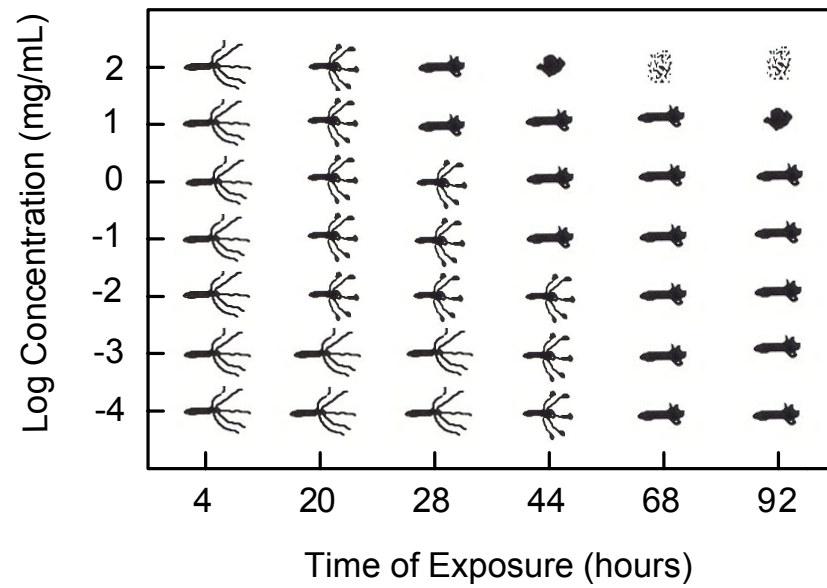


Figure 5.2. The time course for the toxic effect of various concentrations of paraoxon on *Hydra attenuata*. The symbols represent the morphologic changes as defined in Figure 5.1. Additional details are provided in the text.

Of the ten compounds tested for toxicity with *Hydra*, two of the VX analogs (VII and VIII) were the most toxic. The two  $S_p$  isomers of the GD analog (V) were approximately two orders of magnitude less toxic than the two most toxic analogs for VX. The most toxic enantiomer of the analog for GB ( $S_p$ -IV) was approximately 2 orders of magnitude less toxic than the most toxic analog for GD ( $S_pS_c$ -V). In contrast the  $R_p$  enantiomer of IV was approximately 4 orders of magnitude less toxic the corresponding  $S_p$  enantiomer. Overall, the compounds tested varied in toxicity by approximately 8 orders of magnitude. This order of toxic properties by the various analogs of GB, GD, and VX mirrors the toxicity of the nerve agents GB, GD, and VX (Scheme 2). Shown in Figure 5.3 is a plot of the  $MEC_{92h}$  values measured in this study for organophosphate nerve agent analogs IV, V, and VII versus the reference dosage (mg/kg/day) for GB ( $2 \times 10^{-5}$ ), GD ( $4 \times 10^{-6}$ ), and VX ( $6 \times 10^{-7}$ ), which estimates the daily exposure level that can be tolerated without harmful effects during a lifetime (Subcommittee on Chronic Reference Doses, 2000). The relative toxicity for the analogs is consistent with the relative toxicity displayed by the CW agents themselves.

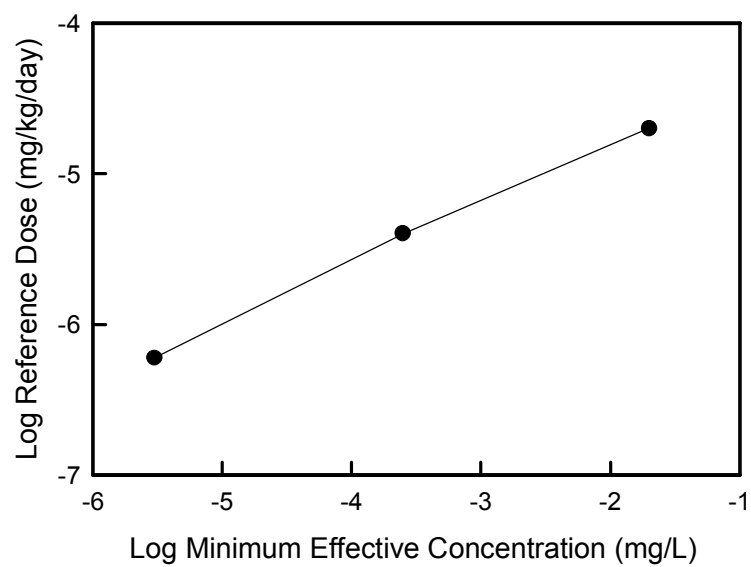
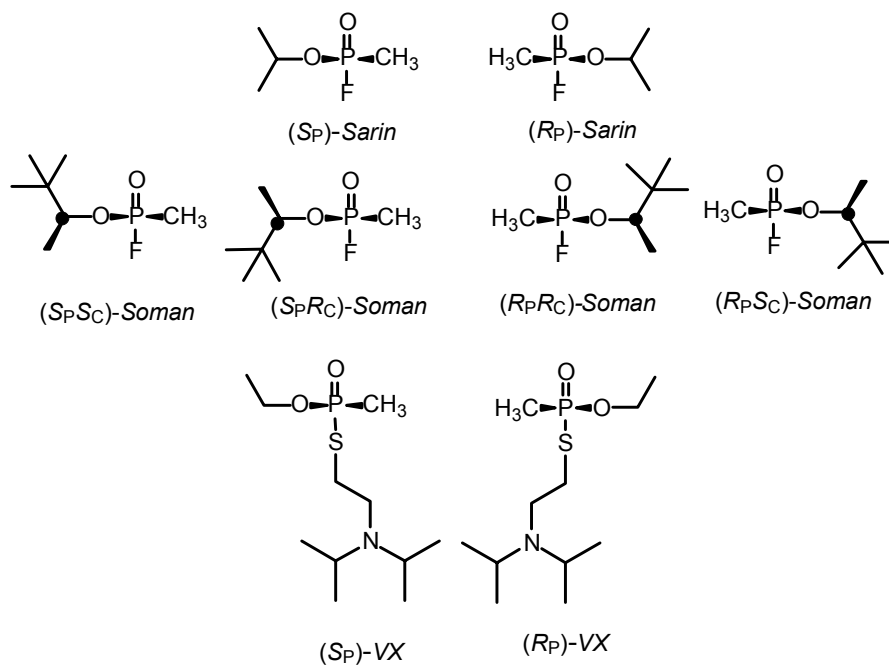


Figure 5.3. Comparison of the  $MEC_{92h}$  (mg/L) for the organophosphate nerve agent analogs IV, V, and VII determined in this investigation versus the reference dose (mg/kg/day) for the chemical warfare agents sarin (GB), soman (GD) and VX.



Scheme 2. The stereoisomers of sarin (GB), soman (GD), and VX.

The test compounds were modeled in ISIS/DRAW, and the resulting files were analyzed using HyperChem Release 7 (Hyper Cube, Inc.). Molecular dynamics calculations including geometry optimization energy, volume, and surface area were obtained for each compound, in addition to the polarizability and the partition coefficient for a mixture of 1-octanol and water (Figures 5.6 and 5.7). The lowest and highest geometry optimization energies were calculated for each of the compounds, as shown in Figure 5.4. The physical properties of volume, surface area, and mass for each of the compounds was also determined, as illustrated in Figure 5.5. Of these molecular properties the partition coefficient in octanol/water gave the best correlation relative to the MEC<sub>92h</sub> values determined here, as illustrated in Figure 5.8.

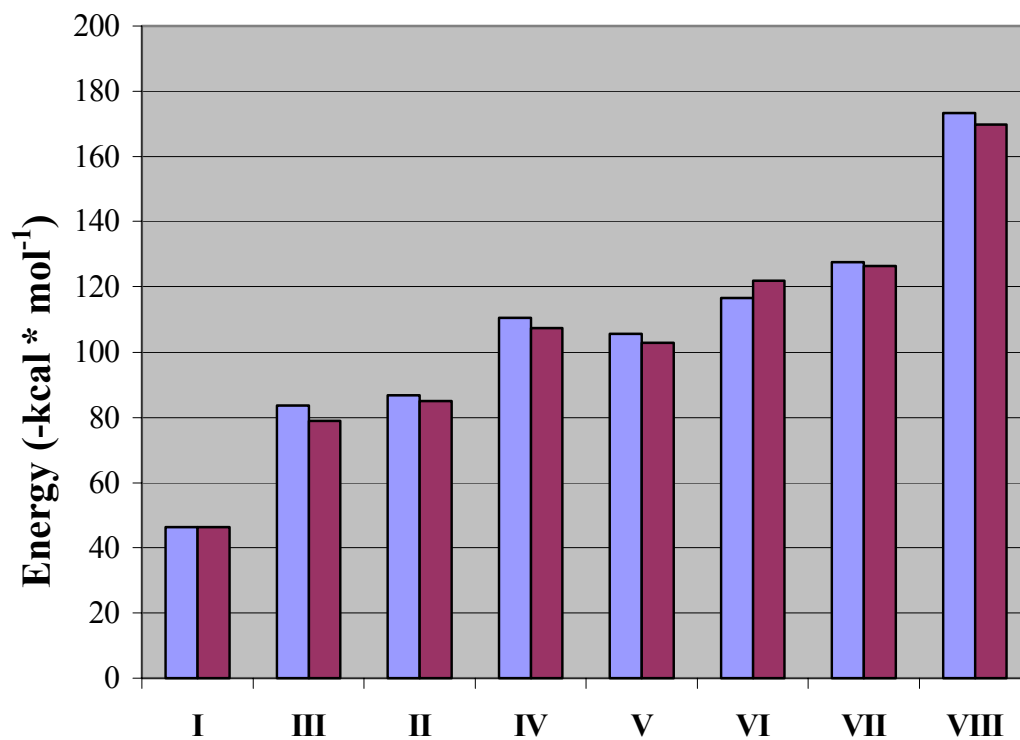


Figure 5.4. The lowest (blue) and highest energy (red) of the compounds as determined by the Boltzmann Conformer Search Method for each of the test compounds.

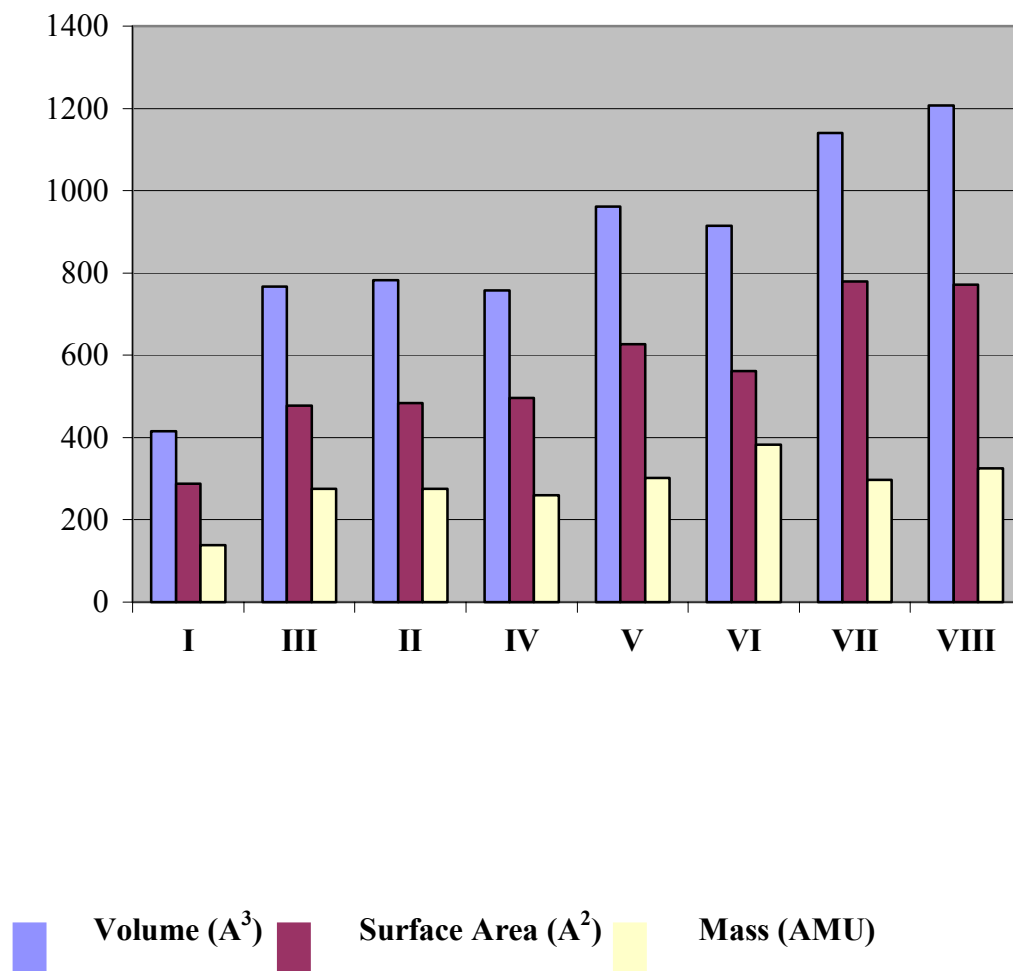


Figure 5.5. The physical properties of volume, surface area, and mass for each of the test compounds.

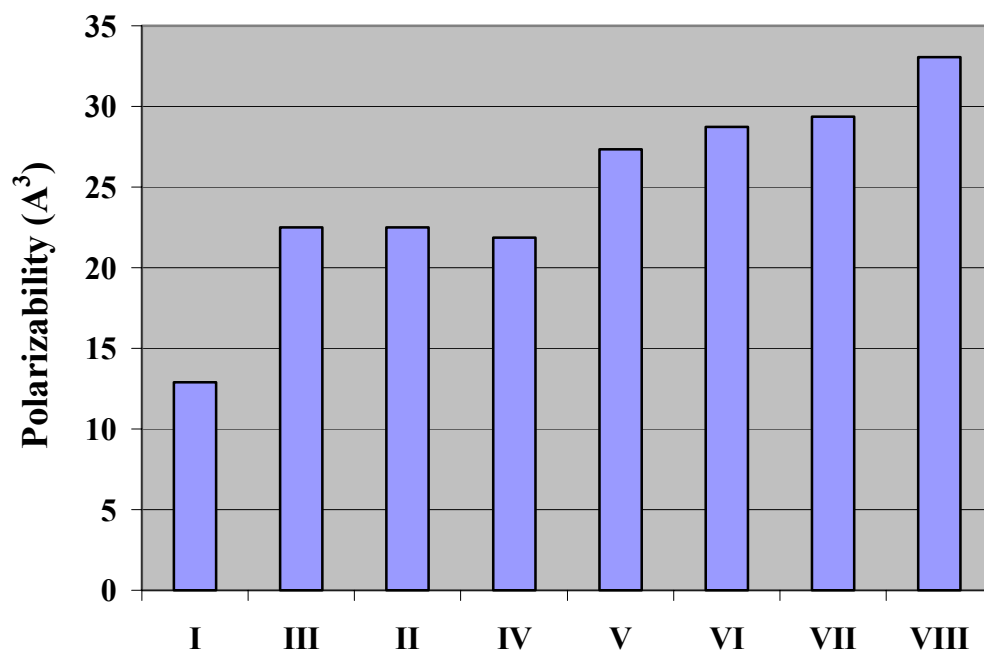


Figure 5.6. The polarizability for each of the compounds tested is expressed in  $\text{\AA}^3$ .



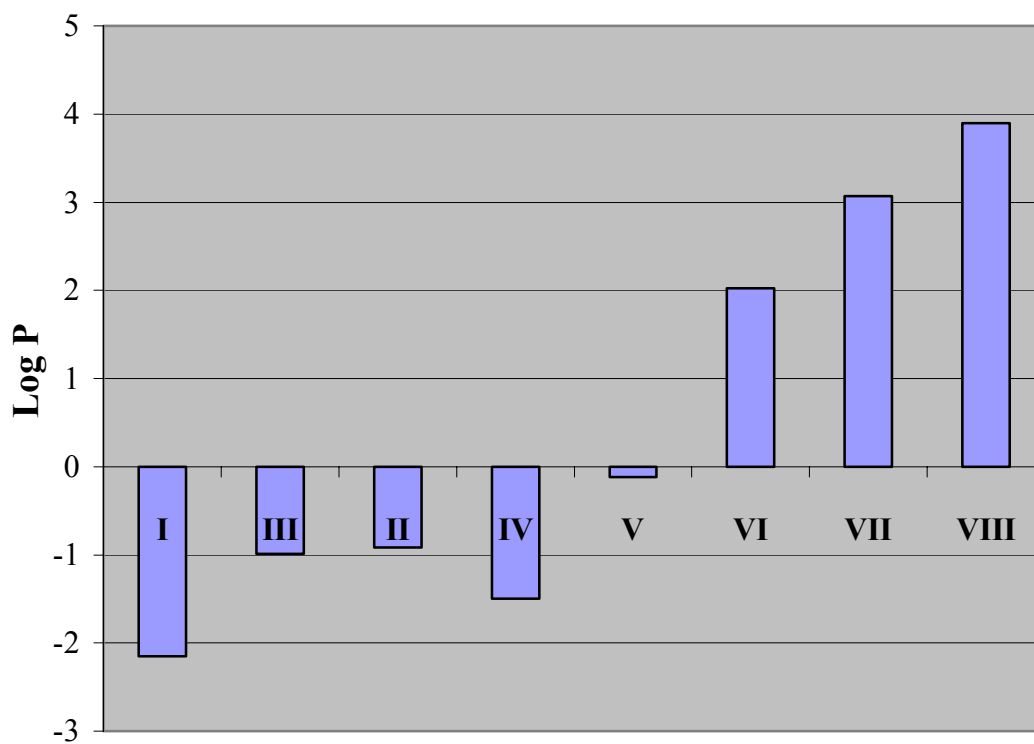


Figure 5.7. The molecular hydrophobicity is expressed as log P, the partition coefficient of octanol:water, for each test compound.

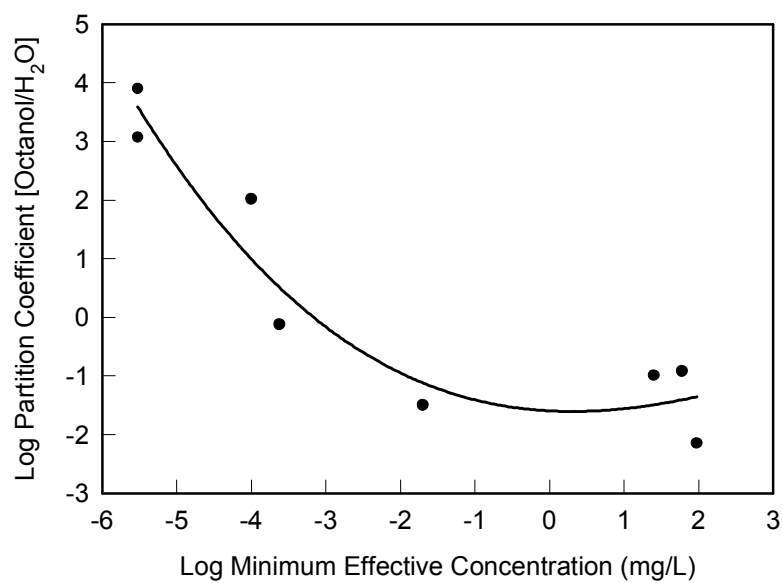


Figure 5.8. Correlation between the log of the partition coefficient for a mixture of octanol/water and the  $MEC_{92h}$  for the compounds assayed in this investigation. The solid line through the data is for comparison purposes only.

## Discussion

### *Hydra Bioassays*

Exposure to each organophosphate compound tested led to toxicity in *Hydra*. In terms of the MEC within 92 hours of exposure, the leaving group product, para-nitrophenol (I) was among the least toxic compound whereas two of the VX analogs, diethyl VX (VII) and tetriso (VIII), were the most toxic (Table 5.1). The toxicity elicited from *p*-nitrophenol was significantly lower than that of the various GB and GD analogs tested and thus it can be concluded that the lethality from exposure to these organophosphates was not due to the presence or accumulation of the leaving group product. However, the GB analog (II) and paraoxon (III) induced lethality only at relatively high concentrations. From this observation, it can be concluded that the organophosphate triesters have less of an inhibitory effect than the organophosphonate diesters on AChE *in vivo*, and are thus tolerated at higher concentrations. In contrast, organophosphonate diesters, containing a P-CH<sub>3</sub> substituent, cause significantly greater toxicity, which is supported by the data from exposure to the GB (IV) and GD (V) analogs. In comparing the two GB analogs (II and IV), the racemic phosphonate GB analog (IV) was significantly more toxic than that of the corresponding phosphate analog of GB (II), yielding a 3000-fold difference in MEC<sub>92h</sub>.

A notable effect on toxicity was observed on the stereochemistry at the phosphorus center for the two isomers of the GB analog (IV), and the stereoisomers of the GD analog (V). Exposure to the S<sub>p</sub> isomer of IV led to a 7,600-fold greater toxicity than that observed for the R<sub>p</sub> isomer. The differential toxicity has also been noted in studies with rodents exposed to individual nerve agent isomers of GB (Spruit et al., 2000). The rate constant for the inactivation of AChE for the S<sub>p</sub> isomer of GB was shown to be 5000-fold greater than

that of the R<sub>p</sub> isomer (Benschop and De Jong, 1988). The difference in the rate of inactivation of AChE is even greater between the most toxic S<sub>p</sub>S<sub>c</sub> isomer of GD and the relatively non-toxic R<sub>p</sub>R<sub>c</sub> isomer of GD (Benschop and De Jong, 1988).

The MEC for the GB analog (IV) is 100-fold greater than for the GD analog (V). From the literature it has been noted that GD is more toxic than GB, and that a differential toxicity occurs among the isomers of both nerve agents (Benschop and De Jong, 1988). The MEC in *Hydra* revealed that the most toxic isomer within the racemic GD analog (V) is of the S<sub>p</sub> configuration. The MEC of the isolated S<sub>p</sub>S<sub>c</sub> isomer is ~3 times lower than that of the racemic mixture. The results from this study are similar to those of Benschop et al., which indicate that the most toxic isomer in mouse studies is the S<sub>p</sub>S<sub>c</sub> isomer of GD (Benschop and De Jong, 1988). Experimental evidence also indicates that the S<sub>p</sub>S<sub>c</sub> isomer of GD is the most reactive with human AChE, and that the chirality at the phosphorus center is the most important element in determining the stereoselective toxicity (Ordentlich et al., 1999).

The compounds with the lowest values for MEC were the VX analogs, VI, VII, and VIII (Table 5.1). While the MEC for VI was only about half of that for the GD analog (V), the toxicity elicited from VII and VIII was ~100-fold greater than that for V. Both of these VX analogs caused lethality in *Hydra* at a concentration that was ~7 orders of magnitude less than that of paraoxon. However, the toxicity of diethyl VX (VII) was reduced by 10,000-fold (data not shown) in the presence of MAP, consisting of enzymes present within the S9 fraction from Aroclor 1254-induced male rats. From these data, it appears that the various enzymes present in MAP aid in the detoxification of diethyl VX, and perhaps structurally similar compounds as well. Overall, the VX analogs were more toxic than the GD analogs,

which in turn were more toxic than the GB analogs, as expected from the known order of toxicity (Munro, 1994).

### *Molecular Modeling*

All of the compounds used in the bioassays were modeled with HyperChem. In many studies, it has been reported that polarizability and hydrophobicity are significant factors in determining toxicity and drug reactivity (Hansch and Kurup, 2003)(Makhaeva et al., 1998). Polarizability for each compound was determined by van der waals (dispersion) forces, and has units of volume ( $\text{\AA}^3$ ). In order to calculate the electric dipole polarizability ( $\alpha$ ) in units of  $e^2 a_0^2 E_h^{-1}$ , energy in terms of hartrees ( $E_h = 4.3597E-18$  J) would have to be calculated. However from the bar graph in Figure 5.6 it is apparent that increased polarity is directly related to increased toxicity.

Molecular hydrophobicity was determined for each compound in terms of the partition coefficient for an octanol/water mixture. The leaving group for four of the compounds tested here, *p*-nitrophenol, was the most water soluble while tetriso was the most soluble in octanol. The most hydrophobic compounds exhibited greater toxicity as illustrated in Figures 5.7 and 5.8. These findings are in agreement with the hypothesis that hydrophobic organophosphorus compounds quickly enter the nervous system, and become readily available to attack multiple targets involved in organophosphate induced toxicity (Klaassen, 1996). It has been previously established that there is a good correlation between the partition coefficient for organophosphate compounds and NTE inhibition (Singh, 2001), and that an increase in OPIDN is observed as the hydrophobicity of a compound is increased (Makhaeva et al., 1998).

### *Potential Applications*

The *Hydra* bioassay may be incorporated into an array of other applications. The ability of this organism to detect *ppm* to *ppt* levels of organophosphate nerve agents enhances the degree of sensitivity demanded by biosensors. In addition, the cost, efficiency, and ease of this assay permit it to be run multiple times in a variety of formats. Because *Hydra attenuata* are sensitive to the organophosphates and organophosphonates tested here, it is assumed that the organism will be sensitive to related compounds. The bioassay used here could be applied as a pre-screening tool in determining the relative toxicity of related organophosphorus nerve agents, as well as individual stereoisomers, that have yet to be screened for toxicity.

## CHAPTER VI

### SUMMARY AND CONCLUSIONS

The stereoselectivity of sarin (GB) and soman (GD) analog hydrolysis is an important issue for assessing the use of PTE as an effective means of decontamination and detoxification of chemical warfare agents. It has been an underlying theme for the direction of experiments described throughout this dissertation. From Chapter II, it was established that wild type exerts stereoselectivity in the direction of  $R_p$  over  $S_p$  for both the GB and GD analogs. This is consistent with results from investigations probing structural determinants of substrate specificity (Chen-Goodspeed et al., 2001a,b). In such studies, it was concluded that wild type consistently preferred the  $S_p$  enantiomer over the corresponding  $R_p$  enantiomer from a variety of related organophosphate substrates, with factors ranging from 1-90 (Chen-Goodspeed et al., 2001a). With the  $S_p$  enantiomer, the larger substituent of the substrate fits in the *large subsite*, while the smaller substituent fits in the *small subsite*. The  $S_p$  enantiomer of phosphate substrates used in those studies corresponds to the  $R_p$  enantiomer(s) of the phosphonate substrates used throughout the experiments described in this dissertation.

Subtle modifications to the enzyme yielded variants with complementary stereoselectivities, as seen with G60A and the triple mutant I106A-F132A-H257Y. This illustrates the capabilities of effectively tailoring PTE to hydrolyze individual isomers of a substrate. A subtle modification in the *small subsite* yielded a mutant with enhanced activity for the  $R_p$  isomer, while maintaining the same stereoselectivity as wild type as seen with G60A. However, the  $R_p$  isomer for both GB and GD is not biologically relevant in terms of eliciting toxicity. It is believed that the  $R_p$  enantiomer serves as a substrate for other

enzymes similar to AChE, such as butyrylcholinesterase (Langenberg et al., 1998). The S<sub>p</sub> isomer of GB, and the S<sub>p</sub>S<sub>c</sub> and S<sub>p</sub>R<sub>c</sub> isomers of GD are responsible for toxicity, as indicated by results from both toxicity and toxicodynamics studies (Benschop and De Jong, 1988)(Spruit et al., 2000).

Modifications in the *small subsite*, *large subsite*, and *leaving group pocket* resulted in a triple mutant that was able to reverse the preference observed with wild type, such that the S<sub>p</sub> isomer was preferentially hydrolyzed over the R<sub>p</sub> isomer for both the GB and GD analogs. There was a substantial enhancement for S<sub>p</sub> isomer(s) hydrolysis, as there was a 50-fold increase with the  $k_{cat}$  and a 75-fold increase with the  $k_{cat}/K_m$  for hydrolysis of the S<sub>p</sub> isomers of the GD analog.

In Chapter III, directed evolutions studies of PTE combined with screen assays aided in the identification of other mutants with enhanced activity for GD analog hydrolysis. In particular, substitutions within the *large subsite* and *leaving group* region proved to be the most beneficial for hydrolysis of the toxic S<sub>p</sub> isomers of the analog. From the single substitution libraries, the mutants Y309F and Y309W showed a 53-fold and 88-fold enhancement for hydrolysis of the most toxic S<sub>p</sub>S<sub>c</sub> isomer. Aromatic amino acid substitution at position 257 also proved to be beneficial for S<sub>p</sub>R<sub>c</sub>/S<sub>p</sub>S<sub>c</sub> isomers hydrolysis, as observed with the identification of H257Y and H257W mutants. The H257Y mutation had the greatest enhancement for hydrolysis of the S<sub>p</sub>R<sub>c</sub>/S<sub>p</sub>S<sub>c</sub> isomers and the individual S<sub>p</sub>S<sub>c</sub> isomer of all the single mutations isolated. There was a 57-fold enhancement for the hydrolysis of the S<sub>p</sub> pair of isomers, with a  $k_{cat}/K_m$  of  $5.4 \times 10^3 \text{ M}^{-1} \text{ s}^{-1}$ , and a 88-fold enhancement for the hydrolysis of the individual S<sub>p</sub>S<sub>c</sub> isomer, with a  $k_{cat}/K_m$  of  $1.4 \times 10^3 \text{ M}^{-1} \text{ s}^{-1}$ .



An even greater degree of enhancement was seen with mutants obtained from the double substitution libraries. An overwhelmingly large population of enhanced mutants obtained from the screening of these libraries contained Arg and Gly mutations at position 254, while Tyr at position 257 also proved to be a beneficial modification for the hydrolysis of the toxic isomers of the GD analog. In addition, almost all of these mutants had reversed the order of stereoselectivity that was seen with wild type. They had preference for the  $S_p$  isomer over the  $R_p$  isomer. Among this description were H254G-H257R, H257Y-L303T, H254R-H257A-L303T, and H254R-H37S-L303T.

The best mutant for  $S_pR_c$  and  $S_pS_c$  isomer hydrolysis was H257Y-L303T. There was an 86- and 462-fold increase relative to wild type, respectively. Preferential hydrolysis was in the order of the  $S_pR_c$  isomer,  $S_pS_c$  isomer,  $R_pS_c$  isomer, and  $R_pR_c$  isomer. The triple mutant H254R-H257S-L303T also displayed a significant enhancement for hydrolysis of these isomers. There was a 89-fold increase for hydrolysis of the  $S_pR_c$  isomer, and a 194-fold increase for the hydrolysis of the  $S_pS_c$  isomer. Comparable results were seen with a similar mutant, H254R-H257A-L303T. For the respective isomers, there was a 34- and 150-fold enhancement relative to wild type. There was a 106-fold enhancement for hydrolysis of the  $S_pS_c$  isomer with the H254G-H257R mutant, and the screening of the same library led to the isolation of H257Y, which was initially obtained from the H257X single substitution library. The reappearance of this single mutation confirmed previous results.

The double substitution library was also screened for activity with the isomers of the GB analog. Many of these mutants had preference for the  $S_p$  isomer over the  $R_p$  isomer. However, there was a lesser degree of enhancement for hydrolysis of the GB analog. There was a 9-fold increase for hydrolysis of the  $S_p$  isomer for the H257Y-L303T mutant, which

was among the highest for the mutants obtained from the double substitution libraries. The H254G-H257W and H254G-H257R mutants had 8- and 5-fold increases for activity. The mutant with the highest activity for  $S_p$  isomer hydrolysis was the triple mutant I106A-F132A-H257W, and the mutant with the highest activity for  $R_p$  isomer hydrolysis was G60A. The  $k_{cat}/K_m$  for both was equal, with each being  $1.1 \times 10^7 \text{ M}^{-1} \text{ s}^{-1}$ . Both of these mutants were isolated by previous members of the Raushel group, and determined to have enhanced stereoselectivity for G60A and reversed stereoselectivity for the triple mutant (Chen-Goodspeed et al., 2001a,b).

In terms of stereoselectivity, many mutants obtained from the screen assays appeared to have reversed the order of preferential hydrolysis for both the GB and GD analogs. To confirm what was observed with the analogs, two triple mutants were tested with GB at Edgewood Chemical Biological Center. The I106A-F132A-H257Y and I106A-H257Y-S308A mutants were assayed with 0.5 mM GB at pH 7.72. With the later, there was a 33-fold difference between the rate constants obtained from the double exponential fit of hydrolysis. With the former, a 22-fold difference between the rate constants was observed. Assuming that the preference of both triple mutants is for the  $S_p$  isomer over the  $R_p$  isomer, as observed with comparable analogs, it is presumed that the  $S_p$  isomer of GB is hydrolyzed first, followed by the  $R_p$  isomer for these mutants. If this were true, such an enzyme would be desired for use in the detoxification of live nerve agent because of its ability to preferentially hydrolyze and detoxify the toxic isomer.

Prior to the work with the *Hydra* animal system, toxicity of the analog compounds was never established. The *Hydra* bioassay proved to be a convenient and sensitive method of determining toxicity of the 8 compounds. It was accurate enough to distinguish between

the isomers of the GB analog, as there was a 7600-fold difference between the minimal effective concentration ( $MEC_{92}$ ) of the  $S_p$  and  $R_p$  isomers. The difference observed with the *Hydra* was comparable to what was observed with AChE inhibition by the respective isomers, which yielded a 5000-fold difference in terms of inhibition rate constant (Benschop and De Jong, 1988). It was clear from the results that the  $S_p$  isomer was responsible for toxicity when the  $MEC_{92}$  values were compared to that of the  $R_p$ , as well as the racemic mixture.

Also as expected, differential toxicity was observed between the  $S_pS_c$  isomer of the GD analog and the racemic mixture. The difference was only 3-fold but it was clear from the  $MEC_{92}$  values that the  $S_pR_c/S_pS_c$  isomers were eliciting the toxicity within the racemic mixture. As presumed, the toxicity of the GD analog was greater than that of the GB analog. From the assay, there was a 100-fold difference between the  $MEC_{92}$  values for each. In turn, the GB analog was more toxic than the phosphate GB analog, paradoxes, and the *p*-nitro phenol compound. The range of  $MEC_{92}$  values spanned 7 orders of magnitude, such that the greatest toxicity was seen with the VX analogs, specifically the diethyl VX and tetriso compounds.

There was a distinct difference between the effects elicited by each compound tested, and as expected, the VX analogs were most toxic, followed by the GD analog, and the GB analog. In all animals tested, VX has been shown to be the most toxic when administered subcutaneously (Hartmann, 2002), and in most cases, GD is more toxic than GB in terms of inhalational toxicity (Spruit et al., 2000). Future use of this bioassay system with PTE could effectively demonstrate the ability of the enzyme to detoxify the nerve agents, GB, GD, and VX, as well as indicate the differential properties of individual variant proteins. This would

eventually lead to the formulation of an enzyme cocktail designed to combat the individual isomers of each nerve agent.

## REFERENCES

- Aspelin, A.L. and Grube, A.H. 1999. *Pesticides industry sales and usage: 1996 and 1997 market estimates*, United States Environmental Protection Agency Office of Pesticide Programs, Biological and Economic Analysis Division, Washington, DC.
- Bajgar, J. 1996. Present views on toxidynamics of soman poisoning, *Acta Medica*, **39(3)**: 101-105.
- Basu, M.K. 2001. SeWeR: A customizable and integrated dynamic HTML interface to bioinformatics services, *Bioinformatics*, **17(6)**: 577-578
- Benning, M.M., Hong, S.B., Raushel, F.M., Holden, H.M. 2000. The binding of substrate analogs to phosphotriesterase, *J. Biol. Chem.*, **275(39)**: 30556-30560.
- Benning, M.M., Kuo, J.M., Raushel, F.M., Holden, H.M. 1995 Three-dimensional structure of the binuclear metal center of phosphotriesterase, *Biochemistry*, **34(25)**: 7973-7978.
- Benning, M.M., Shim, H., Raushel, F.M., and Hoden, H.M. 2001. High resolution x-ray structures of different metal-substituted forms of phosphotriesterase from *Pseudomonas diminuta*, *Biochemistry*, **40(9)**: 2712-2722.
- Benschop, H.P. and De Jong, L.P.A. 1988. Nerve agent stereoisomers – analysis, isolation, and toxicology. *Acc. Chem. Res.*, **21**: 368-374.
- Benschop, H.P., Konings, C.A., Van Genderen, J., De Jong, L.P. 1984. Isolation, anticholinesterase properties, and acute toxicity in mice of the four stereoisomers of the nerve agent soman, *Toxicol. Appl. Pharmacol.*, **72(1)**: 61-74.
- Chaudhry, G.R., Ali, A.N., and Wheeler, W.B. 1988. Isolation of a methyl parathion-degrading *Pseudomonas* sp. that possesses DNA homologous to the opd gene from a *Flavobacterium* sp., *Appl. Environ. Microbiol.*, **54(2)**: 288-293.
- Chen-Goodspeed, M., Sogorb, M.A., Wu, F., and Raushel, F.M. 2001a. Enhancement, relaxation, and reversal of the stereoselectivity for phosphotriesterase by rational evolution of active site residues, *Biochemistry*, **40(5)**: 1332-1339.
- Chen-Goodspeed, M., Sogorb, M.A., Wu, F., Hong, S.B., and Raushel, F.M. 2001b. Structural determinants of the substrate and stereochemical specificity of phosphotriesterase, *Biochemistry*, **40(50)**: 1325-1331.
- Cheng, T.C., DeFrank, J.J., and Rastogi, V.K. 1999. *Alteromonas* prolidase for organophosphorus G-agent decontamination, *Chem. Biol. Interact.*, **119-120**: 455-462.

Chough, S.H., Mulchandani, A., Mulchandani, P., Chen, W., Wang, J., and Rogers, K.R. 2002. Organophosphorus hydrolase-based amperometric sensor: modulation of sensitivity and substrate selectivity, *Electroanalysis*, **14(4)**: 273-276.

Committee on Toxicology, National Research Council 1997. Review of acute human-toxicity estimates for selected chemical warfare agents, National Academy Press, Washington, DC.

Dan, Y., and Poo, M.M. 1992. Quantal transmitter secretion from myocytes loaded with acetylcholine, *Nature*, **359(6397)**: 733-736.

De Jong, L.P., van Dijk, C., and Benschop, H.P. 1988. Hydrolysis of the four stereoisomers of soman catalyzed by liver homogenate and plasma from rat, guinea pig and marmoset, and by human plasma, *Biochem. Pharmacol.*, **37(15)**: 2939-2948.

Diaz-Baez, M.C., Sanchez, W.A., Dutka, B.J., Ronco, A., Castillo, G., Pica-Granados, Y., Castillo, L.E., Ridal, J., Arkhipchuk, V., and Srivastava, R.C. 2002. Overview of results from the WaterTox intercalibration and environmental testing phase II program: part 2, ecotoxicological evaluation of drinking water supplies, *Environ. Toxicol.*, **17(3)**: 241-249.

Di Sioudi, B.D., Miller, C.E., Lai, K., Grimsley, J.K., and Wild, J.R. 1999. Rational design of organophosphorus hydrolase for altered substrate specificities, *Chem. Biol. Interact.*, **119-120**: 211-223.

Donaldson, D., Kiely, T., and Grube, A. 2002. 1998-1999 Pesticide market estimates, United States Environmental Protection Agency, Washington, DC.

Donarski, W.J., Dumas, D.P., Heitmeyer, D.P., Lewis, V.E., and Raushel, F.M. 1989. Structure-activity relationships in the hydrolysis of substrates by the phosphotriesterase from *Pseudomonas diminuta*, *Biochemistry*, **28(11)**: 4650-4655.

Dumas, D.P., Cladwell, S.R., Wild, J.R., and Raushel, F.M. 1989. Purification and properties of the phosphotriesterase from *Pseudomonas diminuta*, *J. Biol. Chem.* **264(33)**: 19659-19665.

Ecobichon, D.J. and Joy, R.M. 1994. Pesticides and Neurological Diseases, 2<sup>nd</sup> ed., CRC Press, Boca Raton, FL.

Eisenstadt, M. 1990. The sword of the Arabs: Iraq's strategic weapons, *Washington Institute Policy Papers*, **21**: 6.

Evison, D., Hinsley, D., and Rice, P. 2002. Chemical weapons, *BMJ*, **324(7333)**: 332-335.

Froede, H.C., and Wilson, I.B. 1984. Direct determination of acetyl-enzyme intermediate in the acetylcholinesterase-catalyzed hydrolysis of acetylcholine and acetylthiocholine, *J. Biol. Chem.*, **259(17)**: 11010-11013.

Furtado, M.C. and Chan, L. 2001. Toxicity, organophosphate, *eMedicine Journal*, **2(9)**: 1-10.

- Ghose, A.K., Pritchett, A., Crippen, G.M. 1988. Atomic physicochemical parameters for 3-dimensional structure directed quantitative structure-activity-relationships: 3. modeling hydrophobic interactions, *J. Comput. Chem.*, **9**: 80-90.
- Ghosh, R. 1957. Phosphorodithioates, Patent No. GB 783281.
- Glieder, A., Farinas, E.T., and Arnold, F.H. 2002. Laboratory evolution of a soluble, self-sufficient, highly active alkane hydrolyase, *Nat. Biotechnol.*, **20(11)**: 1135-1139.
- Grimsley, J.K., Scholtz, J.M., Pace, C.N., and Wild, J.R. (1997) Organophosphorus hydrolase is a remarkably stable enzyme that unfolds through a homodimeric intermediate, *Biochemistry*, **36(47)**: 14366-14374.
- Guilhermino, L., Diamantino, T., Silva, M.C., and Soares, A.M.V.M 2000. Acute toxicity test with *Daphnia magna*: an alternative to mammals in the prescreening of chemical toxicity, *Ecotoxicol. Environ. Saf.*, **46**: 357-362.
- Hansch, C. and Kurup, A. 2003. QSAR of chemical polarizability and nerve toxicity, *J. Chem. Inf. Comput. Sci.*, **43**: 1647-1651.
- Hartleib, J. and Rüterjans, H. 2001. High-yield expression, purification, and characterization of the recombinant diisopropylfluorophosphatase from *Loligo vulgaris*, *Protein Expr. Purif.*, **21(1)**: 210-219.
- Hartmann, H.M. 2002. Evaluation of risk assessment guideline levels for the chemical warfare agents mustard, GB, and VX, *Regul. Toxicol. Pharmacol.*, **35(3)**: 347-356.
- Hasel, W., Hendrickson, T.F., and Still, W.C., 1988. A rapid approximation to the solvent accessible surface areas of atoms, *Tet. Comput. Meth.*, **1**: 103.
- Hill, C.M., Li, W.S., Cheng, T.C., DeFrank, J.J., and Raushel, F.M. 2001. Stereochemical specificity of organophosphorus acid anhydrolase toward p-nitrophenyl analogs of soman and sarin, *Bioorg. Chem.*, **29(1)**: 27-35.
- Holm, L. and Sander, C. 1997. An evolutionary treasure: unification of a broad set of amidohydrolases related to urease, *Proteins*, **28(1)**: 72-82.
- Hong, S.B. and Raushel, F.M. 1999. Stereochemical constraints on the substrate specificity of phosphotriesterase, *Biochemistry*, **38(4)**: 1159-1165.
- Hoskin, F.C.G., Kremzner, L.T., and Rosenberg, P. 1969. Effects of some cholinesterase inhibitors on the squid giant axon. Their permeability, detoxication and effects on conduction and acetylcholinesterase activity, *Biochemical Pharmacology*, **18**: 1727-1737.
- Huff, R.A. and Abou-Donia, M.B. 1995. In vitro effect of chlorpyrifos oxon on muscarinic receptors and adenylate cyclase, *Neurotox.*, **16(2)**: 281-290.

- Jabri, E., Carr, M.B., Hausinger, R.P., and Karplus, P.A. 1995. The crystal structure of urease from *Klebsiella aerogenes*, *Science*, **268(5213)**: 998-1004.
- Johnson, E.M., Gorman, R.M., Gabel, B.E.G., and George, M.E. 1982. The *Hydra attenuata* system for detection of teratogenic hazards, *Teratogen.Carcinog. Mutagen.*, **2**: 263-276.
- Josse, D., Lockridge, O., Xie, W., Bartels, C.F., Schopfer, L.M., and Masson, P. 2001. The active site of human paraoxonase (PON1), *J. Appl. Toxicol.*, **21(S1)**: S7-S11.
- Kadar, T., Raveh, L., Cohen, G., Oz, N., Baranes, I., Balan, A., Ashani, Y., and Shapira, S. 1985. Distribution of 3H-soman in mice, *Arch. Toxicol.*, **58(1)**: 45-49.
- Karntanut, W. and Pascoe, D. 2000. A comparison of methods for measuring acute toxicity to *Hydra vulgaris*, *Chemosphere*, **41**: 1543-1548.
- Katz, E.J., Cortes, V.I., Eldefrawi, M.E., and Eldefrawi, A.T. 1997. Chlorpyrifos, parathion, and their oxons bind to and desensitize a nicotinic acetylcholine receptor: relevance to their toxicities, *Toxicol. Appl. Pharmacol.*, **146(2)**: 227-236.
- Klaassen, C.D. e.d. 1996. Casarett and Doull's Toxicology, 5<sup>th</sup> ed., McGraw-Hill, New York.
- Kuo, J.M., and Raushel, F.M. 1994. Identification of the histidine ligands to the binuclear metal center of phosphotriesterase by site-directed mutagenesis. *Biochemistry*, **33(14)**: 4265-4272.
- Lai, K. 1994. Modification and characterization of the neurotoxic substrate specificity of organophosphorus hydrolase, *Ph.D. Dissertation*, Texas A&M University.
- Langenberg, J.P., Spruit, H.E., van der Wiel, H.J., Trap, H.C., Helmich, R.B., Bergers, W.W., van Helden, H.P., and Benschop, H.P. 1998. Inhalation toxicokinetics of soman stereoisomers in the atropinized guinea pig with nose-only exposure to soman vapor, *Toxicol. Appl. Pharmacol.*, **151(1)**: 79-87.
- LeJeune, K.E., Dravis, B.C., Yang, F., Hetro, A.D., Doctor, B.P., and Russell, A.J. 1998. Fighting nerve agent chemical weapons with enzyme technology, *Ann. N.Y. Acad. Sci.*, **864**: 153-170.
- Lenhoff, H.M. (ed.) 1983. *Hydra: research methods*, Plenum Press, New York.
- Lewis, V.E., Donarski, W.J., Wild, J.R., and Raushel, F.M. 1988. Mechanism and stereochemical course at phosphorus of the reaction catalyzed by a bacterial phosphotriesterase, *Biochemistry*, **27(5)**: 1591-1597.
- Li, W.S., Lum, K.T., Chen-Goodspeed, M., Sogorb, M.A., and Raushel, F.M. 2001. Stereoselective detoxification of chiral sarin and soman analogues by phosphotriesterase, *Bioorg. Med. Chem.*, **9(8)**: 2083-2091.



- Makhaeva, G.F., Filomenko, I.V., Yankovskaya, V.L., Fomicheva, S.B., and Malygin, V.V. 1998. Comparative studies of O,O-dialkyl-O-chloromethylchloroformimino phosphates: interaction with neuropathy target esterase and acetylcholinesterase, *Neurotox.*, **19(4-5)**: 623-628.
- Marrs, T.C., Maynard, R.L., and Sidell, F.R., 1996. Chemical warfare agents, toxicology and treatment, John Wiley and Sons, New York.
- Matthews, G.G. 1991. Cellular physiology of nerve and muscle, Blackwell, Boston, M.A.
- Mayura, K., Smith, E.E., Clement, B.A., and Phillips, T.D. 1991. Evaluation of the developmental toxicity of chlorinated phenols utilizing *Hydra attenuata* and postimplantation rat embryos in culture, *Toxicol. Appl. Pharmacol.*, **108**: 253-266.
- Mileson, B.E., Chambers, J.E., Chen, W.L., Dettbarn, W., Ehrich, M., Eldefrawi, A.T., Gaylor, D.W., Hamernik, K., Hodgson, E., Karczmar, A.G., Padilla, S., Pope, C.N., Richardson, R.J., Saunders, D.R., Sheets, L.P., Sultatos, L.G., and Wallace, K.B. 1998. Common mechanism of toxicity: A case study of organophosphorus pesticides, *Toxicol. Sci.*, **41(1)**: 8-20.
- Millard, C.B, Kryger, G., Ordentlich, A., Greenblatt, H.M., Harel, M., Raves, M.L., Segall, Y., Barak, D., Shafferman, A., Silman, I., and Sussman, J.L. 1999. Crystal structures of aged phosphonylated acetylcholinesterase: nerve agent reaction products at the atomic level, *Biochemistry*, **38(22)**: 7032-7039.
- Miller, K.J. 1990. Additivity methods in molecular polarizability, *J. Am. Chem. Soc.*, **112(23)**: 8533-8542.
- Minton, N.A., and Murray, V.S. 1988. A review of organophosphate poisoning, *Med. Toxicol. Adverse Drug Exp.*, **3(5)**: 350-375.
- Moseley, V., and Snead, H.P. 1953. Poisoning due to the anticholinesterase, *J. S. C. Med. Assoc.*, **49(9)**: 227-232.
- Mulbry, W.W., Karns, J.S., Kearney, P.C., Nelson, J.O., McDaniel, C.S., and Wild, J.R.. 1986. Identification of a plasmid-borne parathion hydrolase gene from *Flavobacterium* sp. by southern hybridization with opd from *Pseudomonas diminuta*, *Appl. Environ. Microbiol.*, **51(5)**: 926-930.
- Munro, N. 1994. Toxicity of the organophosphate chemical warfare agents GA, GB, and VX: implications for public protection, *Environ. Health Perspect.*, **102(1)**: 18-37.
- Nagano, N., Orengo, C.A., and Thornton, J.M. 2002. One fold with many functions: the evolutionary relationships between TIM barrel families based on their sequences, structures and functions, *J. Mol. Biol.*, **321(5)**: 741-765.

- Olsen, M., Iverson, B., and Georgiou, G. 2000. High-throughput screening of enzyme libraries, *Curr. Opin. Biotechnol.*, **11(4)**: 331-337.
- Omburo, G.A., Kuo, J.M., Mullins, L.S., and Raushel, F.M. 1992. Characterization of the zinc binding site of bacterial phosphotriesterase, *J. Biol. Chem.*, **267(19)**: 13278-13283.
- Omburo, G.A., Mullins, L.S., Raushel, F.M. 1993. Structural characterization of the divalent cation sites of bacterial phosphotriesterase by <sup>113</sup>Cd NMR spectroscopy, *Biochemistry*, **32(35)**: 9148-9155.
- Ordentlich, A., Barak, D., Kronman, C., Benschop, H.P., De Jong, L.P., Ariel, N., Barak, R., Segall, Y., Velan, B., and Shafferman, A. 1999. Exploring the active center of human acetylcholinesterase with stereomers of an organophosphorus inhibitor with two chiral centers, *Biochemistry*, **38(10)**: 3055-3066.
- Pascoe, D., Carroll, K., Karntanut, W., and Watts, M.M. 2002. Toxicity of 17 alpha-ethinylestradiol and bisphenol A to the freshwater cnidarian *Hydra vulgaris*, *Arch. Environ. Contam. Toxicol.*, **43**: 56-63.
- Raushel, F.M. 2002. Bacterial detoxification of organophosphate nerve agents, *Curr. Opin. Microbiol.*, **5(3)**: 288-295.
- Raushel, F.M. and Holden, H.M. 2000. Phosphotriesterase: an enzyme in search of its natural substrate, *Adv. Enzymol. Relat. Areas Mol. Biol.*, **74**: 51-93.
- Reutter, S. 1999. Hazards of chemical weapons release during war: new perspectives, *Environ. Health Perspect.*, **107(12)**: 985-990.
- Ronco, A., Gagnon, P., Diaz-Baez, M.C., Arkhipchuk, V., Castillo, G., Castillo, L.E., Dutka, B.J., Pica-Granados, Y., Ridal, J., Srivastava, R.C., and Sanchez, A. 2002. Overview of results from the WaterTox intercalibration and environmental testing phase II program: part 1, statistical analysis of blind sample testing, *Environ. Toxicol.*, **17(3)**: 232-240.
- Scharff, E.I., Koepke, J., Fritsch, G., Luecke, C., and Rueterjans, H. 2001. Diisopropylfluorophosphatase from *Loligo Vulgaris*, *Structure*, **9(6)**: 493-502.
- Shim, H. and Raushel, F.M. 2000. Self-assembly of the binuclear metal center of phosphotriesterase, *Biochemistry*, **39(25)**: 7357-7364.
- Sidell, F.R. 1994. Clinical effects of organophosphorus cholinesterase inhibitors, *J. Appl. Toxicol.*, **14(2)**: 111-113.
- Silveira, C.L., Eldefrawi, A.T., Eldefrawi, M.E. 1990. Putative M2 muscarinic receptors of rat heart have high affinity for organophosphorus anticholinesterases, *Toxicol. Appl. Pharmacol.*, **103(3)**: 474-481.

Singh, A.K. 2001. QSAR for the organophosphate-induced inhibition and 'aging' of the enzyme neuropathy target esterase (NTE), *SAR QSAR Environ. Res.*, **12(3)**: 275-295.

Somani, S.M. 1992. *Chemical Warfare Agents*, Academic Press, Inc., New York.

Spruit, H.E., Langenberg, J.P., Trap, H.C., van der Wiel, H.J., Helmich, R.B., van Helden, H.P., and Benschop, H.P. 2000. Intravenous and inhalation toxicokinetics of sarin stereoisomers in atropinized guinea pigs, *Toxicol. Appl. Pharmacol.*, **169(3)**: 249-254.

Stewart, C.E., Aaron, C.K., and Burnstein, J.L. 2003. Chemical warfare agents: part II: nerve agents, blood agents, and protective gear, *Emerg. Med. Reports*, 1-12.

Subcommittee on Chronic Reference Doses 2000. Evaluation of reference doses for sarin (GB), soman (GD), and VX, *J. Toxicol. Environ. Health, Part A*, **59(5/6)**: 313-338.

Tuovinen, K., Kaliste-Korhonen, E., Raushel, F.M., and Hanninen, O. 1994. Phosphotriesterase - a promising candidate for use in detoxification of organophosphates, *Fundam. Appl. Toxicol.*, **23(4)**: 578-584.

Tuovinen, K., Kaliste-Korhonen, E., Raushel, F.M., and Hanninen, O. 1999. Success of pyridostigmine, physostigmine, eptastigmine and phosphotriesterase treatments in acute sarin intoxication, *Toxicology*, **134(2-3)**: 169-178.

United States Army Medical Research Institute of Chemical Defense (USAMRICD) 1995. *Medical management of chemical casualties handbook*, 2<sup>nd</sup> ed., U.S. Army Medical Research Institute of Chemical Defense, Aberdeen Proving Ground, MD.

United States Congress 1993. *Technologies underlying weapons of mass destruction*, Office of Technology Assessment, Washington, DC

United States Department of Defense, Office of the Under Secretary of Defense for Acquisition and Technology 1998. *The military critical technologies list part II: weapons of mass destruction technologies*, **4**: 1-37, Washington, DC.

United States Environmental Protection Agency 2001. *Preliminary cumulative risk assessment of the organophosphorus pesticides*, Office of Pesticide Programs, Washington, DC.

Vanhooke, J.L., Benning, M.M., Raushel, F.M., and Holden, H.M. 1996. Three-dimensional structure of the zinc-containing phosphotriesterase with the bound substrate analog diethyl 4-methylbenzylphosphonate, *Biochemistry*, **35(19)**: 6020-6025.

Veronesi, B., Ehrich, M., Blusztajn, J.K., Oortgiesen, M., and Durham, H. 1997. Cell culture models of interspecies selectivity to organophosphorous insecticides, *Neurotoxicology*, **18**: 283-298.

Yang, H., Carr, P.D., McLoughlin, S.Y., Liu, J.W., Horne, I., Qiu, X., Jeffries, C.M., Russell, R.J., Oakeshott, J.G., and Ollis, D.L. 2003. Evolution of an organophosphate-degrading enzyme: a comparison of natural and directed evolution, *ProteinEng.*, **16(2)**: 135-145.

**VITA**

Karin T. Lum

## Education:

Smith College  
Northampton, MA  
A.B. Biochemistry  
May, 1998

Texas A&M University  
College Station, TX  
Ph.D. Toxicology  
May, 2004

## Permanent Address:

1202 South Washington St.  
# 512  
Alexandria, VA 22314